ABSTRACT

COLLIER, JAMESON DREW. Utilization of Embedded Pressure Sensors in Smart Textile Applications.. (Under the direction of Dr. Abdel-Fattah Seyam and Dr. Jeffrey Joines.)

Many applications have benefited from the innovation of sensing technology in recent years. One such application that exists in the medical field is the ongoing task of preventing pressure ulcers in hospital patients. Advances in the technology of bed systems have been made in an attempt to mitigate the hazards that cause pressure ulcers, or "bedsores," to form in bedridden patients. However, little research exists that has attempted to improve the monitoring of the pressure point locations encountered by patients. The primary objective of this research was to develop a design of a "smart" textile device that will assist in the prevention of bedsores in such bedridden, or otherwise immobile, patients. Focusing this research on a bedsore prevention application will have a broader impact in the medical industry and may help save lives. In addition to assisting in bedsore prevention, other applications may potentially benefit from this research. Examples include rooms that can respond to the presence of people, which could be useful in security systems in buildings and, perhaps, for aesthetic purposes in interactive art galleries. The electronic industry could benefit by using the pressure sensors in a knob control mechanism in an application like audio volume control. After testing several commercially available pressure-sensing methods, a potentiometry-based sensor, the Spectra Symbol SoftPot, was chosen to be used in the makeup of a sensing bed sheet system prototype that would focus on pressure position, rather than pressure magnitude. An array layout of 35 sensors was determined based on common sites for bedsore formation. With this layout plan, a specialized woven fabric was designed and constructed with two alternating weave designs of a single-layer cloth (3x3

warp rib) and double cloth (face and back layers each made of 2x1 filling rib), which formed rows of tubes inside which the pressure sensors were housed. A computer detection system, in conjunction with a system of electrical circuits, was developed using LabVIEW software that manipulated the voltage data generated by the pressure sensors within the fabric. The prototype bed sheet was tested by placing a 165-pound mannequin on top of it and observed with both a hard surface beneath and a cushioned surface beneath the sheet. The sensors were successfully able to detect pressure points within their detection zones and the computer detection system was successfully able to keep track of the elapsed time of unrelieved pressure. The detection system was also successful in demonstrating the capability to activate an alarm when a prescribed time had elapsed with unrelieved pressure.

Utilization of Embedded Pressure Sensors in Smart Textile Applications

by
Jameson Drew Collier

A thesis submitted to the Graduate Faculty of
North Carolina State University
in partial fulfillment of the
requirements for the degree of
Master of Science

Textile Engineering

Raleigh, North Carolina

2011

APPROVED BY:

_____	_____
Dr. Jeffrey A. Joines Committee Co-chair	Dr. Abdel-Fattah M. Seyam Committee Co-chair
_____	_____
Dr. David Hinks	Dr. Ahmed El-Shafei

DEDICATION

To My Family and Friends

BIOGRAPHY

Jameson Drew Collier was born on February 28, 1984 in Wilson, North Carolina. He graduated from Ralph L. Fike High School in 2002. He studied Textile Engineering with a concentration in Product Engineering at NC State University's College of Textiles. In the summer of 2006, he participated in an internship with Milliken & Company in Bostic, NC. He graduated Magna Cum Laude with a Bachelor of Science Degree in 2007. From June 2007 through February 2009, he was employed by INVISTA™, in Waynesboro, Virginia, where he held the position of Technical Support to Operations for LYCRA® fiber manufacturing. In the fall of 2009, he began his Master of Science Degree in Textile Engineering.

ACKNOWLEDGEMENTS

It was a privilege to have assistance from the following individuals and organizations in the duration of this project.

I would like to thank Dr. Jeffrey Joines and Dr. Abdel-Fattah Seyam for their intimate support and encouragement and for serving as co-chairs of my research committee. I also express my gratitude to Dr. David Hinks and Dr. Ahmed El-Shafei for serving as members on my research committee and to Dr. Jon Rust for recruiting me to this project and for encouragement. Dzung Nguyen and William Barefoot were invaluable sources of help and encouragement during prototype fabrication. Thanks to Vicki Stocksdale for helping obtain necessary materials from suppliers. Thanks to Kevin Ross and the Thermal Protection and Comfort Center within the College of Textiles for lending testing components. Thanks to Jackie Jennings and Duke University for supplying me with materials essential to my research. Thanks to Dr. Jim Horton of Carolinas Medical Center and Dr. Taffy Williams of the Life Sciences Research Organization for their time and idea reflection. The project would not have been possible without the funding help from Dr. Harold Freeman, the National Textile Center and the State of North Carolina.

TABLE OF CONTENTS

LIST OF FIGURES

LIST OF TABLES

LIST OF EQUATIONS

1 Introduction

Many applications have benefited from the innovation of sensing technology in recent years. One such application that exists in the medical field is the ongoing task of preventing pressure ulcers, or "bedsores," in bedridden hospital patients. There exist technological advances in bed systems that actively attempt to mitigate the hazards that cause bedsores to form by performing the task of re-distributing pressure throughout the body-bed interface. Other, more traditional methods have involved giving a caregiver the responsibility of keeping a schedule of when a patient needs to be physically turned to relieve the pressure. However, there has been relatively little research acted upon to improve the monitoring of the collective locations of pressure points encountered by a patient, as well as the amount of time at which those pressures have been unrelieved, while they are laying on their bed. There exists a need to actively alert the caregiver when unrelieved pressure has built up for a prolonged amount of time, thus reducing the risk of bedsore formation due to caregiver negligence.

1.1 Background

The financial impact of bedsore treatment, in addition to adverse health results, is sizeable. In one study, the costs associated with bedsore care only trails oncological- and cardiovascular-related costs [1]. The cost associated with a single full-thickness bedsore can rise as high as $70,000 and, as of 2004, total bedsore treatment expenses in the United States had been estimated to be $11 billion annually [2, 3].

The legal ramifications of bedsores are apparent as well. Long-term care (LTC) facilities have industry standards that identify the techniques by which caretakers must abide in order to prevent or manage bedsores in LTC patients. In a 1999 study, it was found that 87% of judicial cases involving bedsores resulted in the plaintiff being rewarded some amount of recovery against the LTC facility [4]. However, the LTC facilities that have bedsore protocols in place have been shown to be less likely to have litigation suits brought against them or reduced recovery costs in the cases have been brought to court [5]. Clearly, facilities with bedsore prevention protocols are capable of taking appropriate measures to promote healing of bedsores that do form in patients.

The evidence of the benefits of reducing the occurrence and risk of bedsores has been demonstrated. Lawsuits can be avoided and the lives of bedridden hospital patients can be improved and, in many cases, prolonged. The following section will outline the specific objectives of the research performed in this project.

1.2 Specific Research Objectives

The primary objective of this research is to develop a design of a "smart" textile device that will assist in the prevention of bedsores in bedridden, or otherwise immobile, patients.

The specific research objectives (RO) are:

- RO1: To develop an understanding of the state of the art of commercially available pressure sensors and determine which of the potential candidates will best fit this project's needs
- RO2: To determine a method for integrating electrical pressure sensors into a textile substrate

- RO3: To develop a sensing bed sheet that detects an array of pressure over a period of time and alerts medical personnel at specified time limits

1.3 Research Outline

In order to accomplish the research objectives outlined in Section 1.2, the next chapter will present an overview of the dangers of bedsores. Chapter 2 will also illustrate the current state of technology of hospital bed systems, followed by an overview of several types of commercially available sensing methods that may be used in the research. Chapter 3 will provide an explanation for the determination of the appropriate pressure sensing method for the novel bedding system. This will include a description of the testing technique used, as well as a comparison of the results of several different commercially available pressure sensors. Chapter 4 will then describe how a layout of the sensors in a test fabric was realized. This will include details on the development of the design and construction of the fabric inside which the chosen pressure sensor will be embedded. Chapter 5 will present details on the design of the circuit and the computer detection system that will manipulate the sensors' data, including an explanation of the flow of logic. Conclusions made from the entire system will be collectively summarized to demonstrate how the problem of bedsore formation has been addressed. Finally, Chapter 6 will cover recommendations for potential future work and design adjustments.

2 Literature Review

The economical and physiological costs associated with the prevalence of bedsores encountered by bedridden patients are substantial. The benefits of lowering the occurrence of bedsores can be realized in the form of improved patient livelihood as well as reducing the number of litigation trials brought against caregivers.

The following sections will provide an overview of bedsores, including factors that influence their development. The health consequences due to bedsore formation will be described as well as current methods used to avoid such consequences. Then, the current bedding systems used in hospitals will be discussed. This will be followed by a description of several types of commercially available pressure sensing methods. The final section of Chapter 2 will describe the process of fabric formation as it relates to the implantation of sensors within a fabric's construction.

2.1 Overview of Bedsores

Bedsore formation is among the most common, but perhaps one of the most preventable conditions encountered by bedridden patients today. The development of bedsores can interfere with functional recovery, can contribute to longer hospital residence and may be complicated by infection and pain in the patient [6]. In some patients, the presence of bedsores has been shown to contribute to premature death [7].

The European Pressure Ulcer Advisory Panel (EPUAP) and the National Pressure Ulcer Advisory Panel (NPUAP) have developed an international pressure ulcer classification

system that identifies specific symptoms within four stages of increasing severity of damage. These stages, as the EPUAP and NPUAP have defined them, are provided in Appendix A as Table 8.1. The extremes of the classification system range from a least-serious “Stage I” to a potentially-lethal “Stage IV.”

In stage I bedsores, the patient experiences a non-blanchable erythema, which indicates a skin redness that does not fade out quickly. Warmth and swelling are also symptoms as seen in Figure 2.1. In stage II, shallow ulcers have formed with at least epidermal loss and, in some cases, even dermal loss. The affected area may resemble a blister or crater. Stage III bedsores involve skin loss of both the epidermis and dermis, as well as the underlying layers of skin tissue. Damage extends deep to the connective tissue of the body, known as the fascia. Stage IV bedsores are characterized by skin loss to both outer and underlying layers of skin tissue, as well as damage and dead tissue in the fascia, muscle, bone, tendon or joint capsule [8].

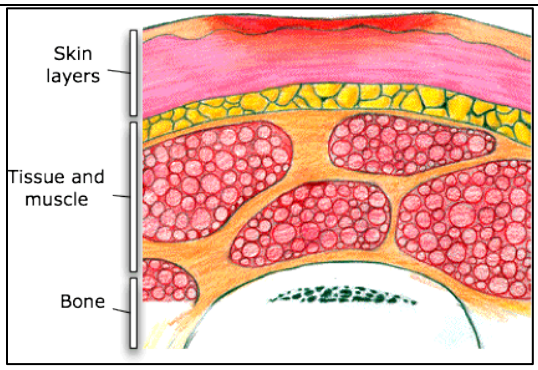

Stage I – Non-blanchable erythema

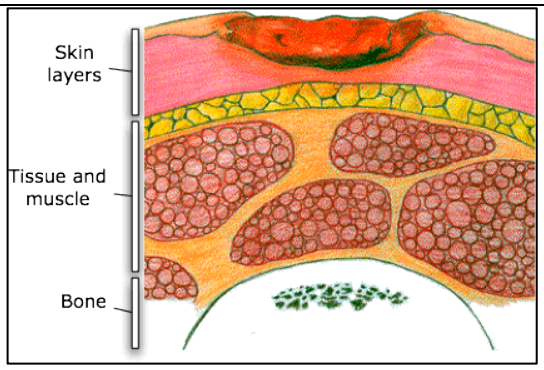

Stage II – Partial-thickness

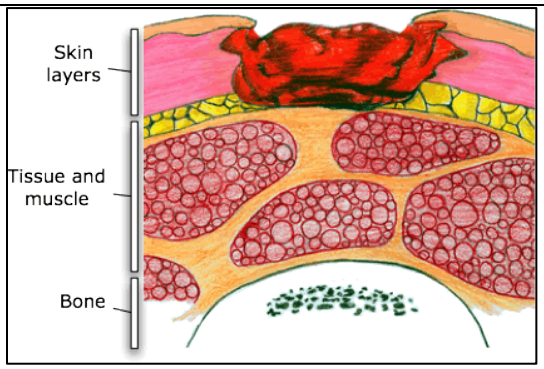

Stage III – Full thickness skin loss

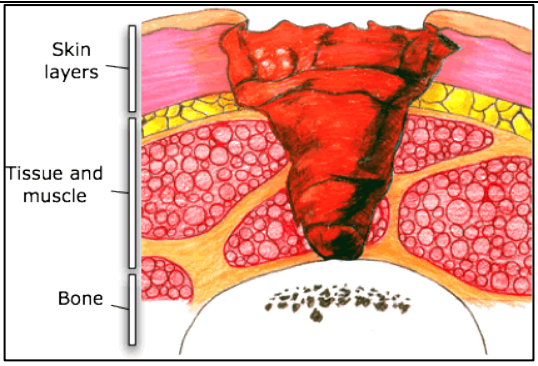

Stage IV – Full thickness tissue loss

(Taken from [8])

Figure 2.1: Four Stages of Bedsore Formation

2.1.1 Factors Influencing Bedsore Formation

To understand the factors that influence the formation of bedsores in patients one must first understand the risk factors that may be present. Two types of risk factors have been identified as "local" and "systemic." Examples of these types of risk factors may include, but are not limited to the following, as defined by Nayak *et al.* [9] in Table 2.1.

Table 2.1: Risk Factors Influencing Bedsore Formation

Local Risk Factors	o "Unrelieved pressure (lying in the same position for more than 2 hours) o Capillary occlusion and disruption of lymphatic drainage o Shearing force (aggravated by head-end elevation of greater than 45°) o Increased temperature and moisture (bed-soiling due to incontinence, poor nursing care, poor ventilation)"
Systemic Risk Factors	o "Aging o Decreased mobility (fractures, paraplegia, coma, major surgery) o Poor nutrition (hypoproteinemia, poor oral intake) o Arterial disease and hypotension" (Taken from [9])

Bedsores typically form due to a combination of pressure, shear and frictional forces acting on skin tissue. These are considered to bring upon the onset of the ulcer formation while other factors have been shown to catalyze or aggravate the condition. Skin wetness is one example of such a catalyst because it promotes bacterial colonization and skin-softening, which decreases the skin's resistance to pressure points [10].

The formation of a bedsore is directly proportional to the amount of time that the unrelieved pressure has been present in a patient. A stage I bedsore can degenerate into a stage IV bedsore within a day's time [11]. The caretaker has the responsibility of taking the appropriate measures to prevent any bedsores from forming by turning the patient's body to relieve built-up pressure.

2.1.2 Potential Dangers of Bedsores

The effects on the body from bedsores can range in severity, depending on the factors outlined in Table 2.1. In precarious cases, advanced formation of bedsores has led to

amputation and even death. Bedsores may promote the systemic spread of infection, which can cause other health problems in patients. Bedsores may form more frequently in patients that are paralyzed or bedridden because they are unable to shift their positions in bed. Also, the paralyzed patients cannot feel the onset of bedsore formation, so their caretaker must be diligent in scheduling body-turning for them. The changing of body position allows blood circulation in areas that an applied pressure may inhibit such circulation. Able-bodied individuals begin to feel uncomfortable in areas that have had an applied pressure—resting one's head on their hand, causing pressure on at an elbow-to-table interface, for instance—and eventually the person will remove the pressure and blood circulation will be restored. Patients with spinal injuries, for example, cannot transmit the neural messages that are generated in areas of low blood circulation and the affected area of tissue will become increasingly jeopardized regarding bedsore formation.

Bedsores tend to form over projections of bone where pressure on the skin can be concentrated. Some of these common spots on the body include the hip bones, tailbone, shoulder blades, back of the head, heels, ankles and elbows [12]. These spots are highlighted in Figure 2.2. If the surface on which the body is laying provides pressure points, then other areas of contact can form bedsores as well. Some examples of external pressure points include contact with wheelchairs, casts, splints and other hard objects.

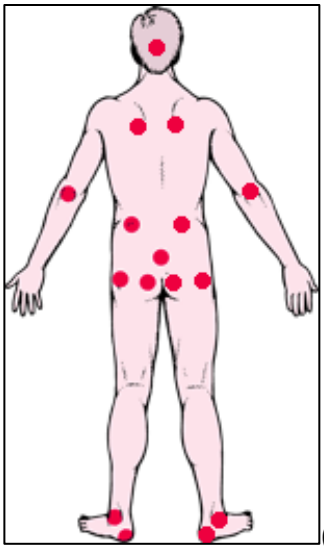 (Adapted from [12])

Figure 2.2: Common Sites for Bedsore Formation

2.1.3 Current Methods for Preventing Bedsores

Facilities that serve as homes for bedridden residents must abide by federal regulations that address the issue of bedsores. One specific regulation was created in the Omnibus Budget Reconciliation Act of 1987, which specifies that "based on the comprehensive assessment of a resident, the facility must ensure that: (1) a resident who enters the facility without pressure sores does not develop pressure sores unless the individual's clinical condition demonstrates that they were unavoidable; and (2) a resident having pressure sores receives necessary treatment and services to promote healing, prevent infection and prevent new sores from developing" [13].

Tools are available that help assess whether a patient may be at risk for forming bedsores. One such tool that exists is the Braden Scale, a universally-accepted method that helps hospital and nursing home workers evaluate these risks. The Braden Scale helps evaluate

residents in areas including sensory perception, degree to which the skin is exposed to moisture, individual's activity level, their ability to change positions, their nutrition and also their exposure to situations that may result in friction and/or shear to the skin [14]. Table 8.2, in Appendix A, outlines the details of the Braden Scale and scoring system. The lower the score calculated for the patient, the higher the risk that patient is determined to have for bedsore formation. The completed Braden Scales for each patient are kept as part of their medical chart for reference to address medical needs.

There are several steps that caretakers take to minimize the risk of bedsores in patients that are broadly accepted by the medical community. A turning schedule for the at-risk patients is maintained. The staff is educated on skin integrity and is encouraged to communicate concerns on skin issues during changes in employee shifts. Special lifting devices are used to reduce the friction on skin areas prone to breakdown. Other steps may apply to any hospital or nursing home residents and include keeping them clean and dry and ensuring appropriate nutrition and hydration is maintained. The use of pressure-relieving devices is encouraged if available, which include items like pillows, heel boots or pressure-relieving mattresses. The latter will be defined in more detail in Section 2.2.2.

2.2 Overview of Bedding Systems

The dangers associated with bedsores have been described. Several of the local risk factors previously outlined in Table 2.1 relate to the environment in which the patient resides. The immediate environment for the patient is the hospital bed on which they spend most of their time. These beds have, traditionally, been designed in a way that is convenient for the

caregiver to perform his or her duties while tending to patients. As the number of bedsore incidents has increased, adjustments have been made to some bed designs so that the incident rate is minimized. The following sections will describe the state of current technology of some commercially available hospital beds as well as illustrate recent developments in several types of commercially available pressure-relief bedding systems.

2.2.1 Hospital Beds

Hospital beds are functionally designed for patients or other individuals that are in need of various forms of health care. The architecture of the beds has evolved throughout history with improvements made regarding comfort for the patient, as well as convenience for health care workers. In terms of comfort for the patient, one can proclaim that the mattress is the most important component of the bed. The mattress, in conjunction with bed sheets, represents the interface between the patient and the bed itself. Any movement or vibration that comes in contact with the bed will be transferred to the patient through the mattress, unless the mattress can effectively dampen the shock.

The functionality of the hospital bed requires that the mattress has special capability. A normal mattress found in a home does not typically have the flexibility found in hospital beds. Bending is important for hospital beds, so the accompanying mattress should not only have the capability to bend along with the bed frame, but also have long-term stability for performing such actions. The types of mattresses found in hospital beds may typically be either inner-spring or foam mattresses [15]. These types differ in price, with the more economical mattress being the inner-spring type. The inner-spring mattress is the less

comfortable of the two types, with the foam mattresses typically being more expensive. According to Preferred Health Choice, a vendor of hospital bed mattresses, the foam mattress' surface softness may hide the firmer foundation of the mattress. They also proclaim that a foam mattress does not break down as easily as an inner-spring mattress [16].

The dimensions of hospital bed mattresses currently available are more flexible in the length direction compared to the width direction. The length may range from 193 centimeters (cm) (76 inches, in) to 213 cm (84 in) while the width typically remains at 91.4 cm (36 in). Depending on the type of mattress, the thickness may average around 15.2 cm (6 in) [17].

Another type of mattress, which is substantially more expensive than inner-spring and foam mattresses, is the air mattress. These mattresses are more customizable so that the amount of air in the mattress can be inflated or deflated to the level that makes the patient more comfortable. Advanced air mattress systems, described in more detail in Section 2.2.2, are available that actively guard against build-up of pressure.

Also available are mattress overlays, which are often used to combat bedsore formation at a lower price than higher-quality hospital bed mattresses. These overlays are placed between the patient and the existing mattress and can help to distribute pressure over larger areas, reducing the chance of bedsores. One particular type of mattress overlay, the Völkner® Turning System, is designed to automatically turn the patient every 4-6 minutes, eliminating the need for manual turning. A double-row of air cells divide in the center to give pressure relief along the body's central axis, thus removing pressure from the spinal area. A control unit contains microprocessors that are connected to the air cells via hoses. The actual turning

of the patient was achieved by the air cells alternating between inflation and deflation phases at rates slow enough to feel gentle to the patient [18].

2.2.2 Current Pressure-Relief Systems

Most patients who are known to be at high risk for bedsores are placed on mattress beds that have a constant flow of air into the mattress. These air-bladder systems may range from $750 to $5,500 [17]. The most common mattress width among air-bladder systems is 91.4 cm (36 in), although some vendors provide options for larger widths at increased prices. The length of these mattresses is typically no shorter than 203 cm (80 in) while some are offered in lengths up to 213 cm (84 in). The weight capacity of these mattress systems is no lower than 114 kilograms (kg) (250 pounds, lb), however many systems provide support for patients up to 159 kg (350 lb) on the standard width varieties [17].

There are two main technologies for bedsore prevention and healing that involve the use of air mattresses. These two categories of mattresses are known as “alternating pressure” and “low air-loss” systems. Both are composed of a mattress pad with air cells and tubes. They both also utilize software-based controllers that command an air pump to perform its functions [19]. Alternating pressure systems have the air cells alternating between inflation and deflation so that the pressure is not applied to the same spots on the patient all of the time, but instead distributed throughout their entire body. Low air-loss systems have the pressure of different parts of the mattress manipulated so that it is confined with the patient’s body surface and the pressure is evenly distributed. Some air-based pressure relief systems are capable of providing both of these technologies within the same mattress [19].

2.3 Sensing Methods

The previously reported bedding systems that utilize air bladder pressure distribution are useful in removing pressure concentrations on the patient's body surface. The design does not guarantee that bedsores will be prevented because the pressure still exists and as time is prolonged, the risk of forming a bedsore increases. A better bedding system will have the ability to automatically detect conditions of the microenvironment of the patient that are known to be factors in bedsore formation. Such a system requires sensor technology to monitor these conditions, which includes pressure due to the patient's body-weight. Potentially, the system may also provide detection of moisture due to temperature (sweating) and accidental release of bodily fluid. Descriptions of potential sensor technologies to be used in this research will be provided in subsequent sections.

2.3.1 Pressure Sensing

Pressure sensors are used to measure presence of pressure at a certain area and, in many cases, the level of pressure being applied. It should be clarified that these "pressure" sensors actually only detect the presence of an applied force, which is only one component of pressure. Engineering pressure refers to the amount of force applied over an area. Nevertheless, the trade usage of "pressure" will be used for the remainder of this thesis. These sensors typically act as transducers, which convert one type of energy into another type of energy. In the case of most pressure sensors, the energy is converted from mechanical to electrical energy—energy which can be gauge-reported. There are several

different types of technology used in different types of pressure sensors including resistance-based, capacitance-based, piezoresistance-based and linear potentiometry-based systems.

2.3.1.1 Piezoresistance-Based Pressure Sensing

Piezoresistance-based pressure sensors utilize the piezoresistive effect of strain gauges to detect a strain upon an applied pressure. One common device with this technology is the strain gauge pressure transducer. The strain gauge is a length of conducting material that is arranged in a zigzag pattern on a membrane. When stretched, the resistance increases. The gauges are mounted in the same direction as the strain direction. When mounted in groups of four, a full "Wheatstone bridge" is formed [20].

A Wheatstone bridge is used to measure an unknown electrical resistance by balancing two legs of a bridge circuit, where one of the legs is home to the unknown component [21]. If the transducer is bent in a direction, the gauges on one side of it will stretch while the other side's gauges will compress. Therefore, the resistance measured in the stretched gauges will be greater than the resistance measured in the compressed gauges. The presence of the Wheatstone bridge maximizes the output of the pressure sensor. The pressure is detected as a proportional differential voltage across the bridge [22]. A schematic of a Wheatstone bridge is illustrated in Figure 2.3.

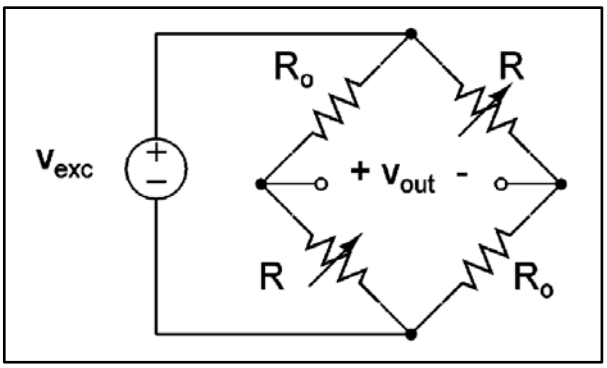

(Taken from [23])

Figure 2.3: Schematic of Wheatstone Bridge

One of the widely-used types of piezoresistance-based pressure sensors involves the use of monocrystalline silicon, which is actually manufactured with semiconductor technology. It operates on the resistive principle previously described and the resistance change is higher than that measured in standard strain gauges. The conductivity in a doped semiconductor is influenced by a deviation that can be produced by very small mechanical deformation. This allows the monocrystalline sensors to be more sensitive than many other types of sensors. There are advantages and disadvantages of monocrystalline sensors. The advantages include high sensitivity, good linearity at a constant temperature and the ability to track pressure variations without signal hysteresis (up to its destructive limit). The disadvantages involve a strong, nonlinear dependence on the full-scale signal on temperature, a large initial offset and a strong drift of offset with temperature [22]. There are several types of piezoresistive pressure sensors commercially available. Some of these will be discussed in the following sections.

2.3.1.1.1 Images Scientific Instruments

Images Scientific offers several different models of resistance-based pressure sensors. Two basic types offered are the two-directional bi-flex sensor and the one-directional flex sensor, and each of these types has options within themselves. One type of two-directional bi-flex sensor is the FLX-01, which is designed to decrease its resistance from the nominal value when it is being bent in either direction (see Figure 2.4). These sensors are 114.3 millimeters (mm) (4.5 in) long by 9.5 mm (0.375 in) wide and 0.9 mm (0.038 in) thick. They are available in three nominal resistance ranges including 1-20 kilo-ohms (kΩ), 20-50 kΩ and 50-200 kΩ and are priced at approximately $10 each, as of 2011 [24].

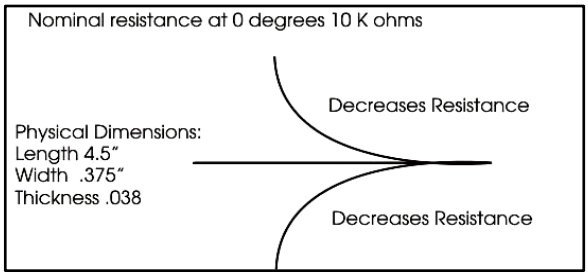

(Taken from [24])

Figure 2.4: Images Scientific Instruments FLX-01

The FLX-02 flex sensor is similar to the FLX-01 in that it changes resistance when it is bent in either direction. However, in one direction the resistance will increase and in the other direction the resistance will decrease upon bending (see Figure 2.5). These have similar dimensions to the FLX-01 sensors, but with a 50% narrower width of 6.4 mm (0.25 in) and less thickness of 0.5 mm (0.02 in).

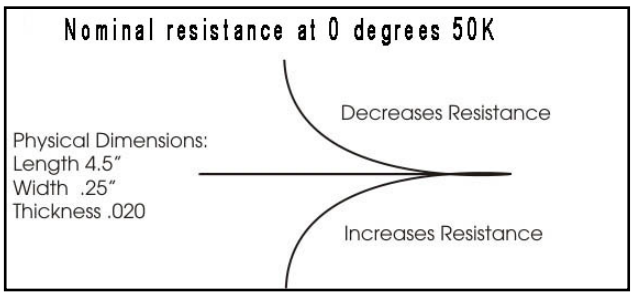

(Taken from [24])

Figure 2.5: Images Scientific Instruments FLX-02

The FLX-03 flex sensor is bendable in just one direction. When bent, the resistance will increase gradually from a nominal resistance of 10 kΩ and up to 40 kΩ, depending on the degree of the bend. The diagram in Figure 2.6 provides a visual demonstration of the behavior upon bending.

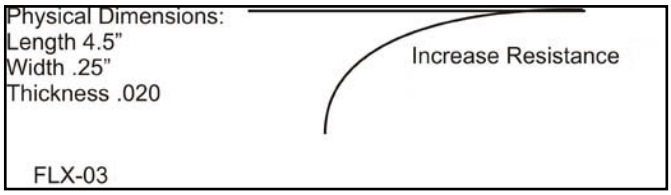

(Taken from [24])

Figure 2.6: Images Scientific Instruments FLX-03

Initial concerns regarding the sensors developed by Images Scientific include the length of the sensors being less than 13 cm (5 in). The implications on the total cost of a system are influenced by the fact that many of these sensors would be required for a single bedding system. The sensors themselves also have an inherent stiffness, so there is a potential problem with creating pressure points for the body, which can actually increase the chance for bedsore formation.

2.3.1.1.2 Tekscan, Incorporated – FlexiForce®

Another commercially available piezoresistive pressure sensor was developed by Tekscan. The FlexiForce® sensor is another example of a product that uses piezoresistive technology to determine applied pressures, both statically and dynamically. As force is applied to the sensor, the resistance is decreased [25]. The resistor can be monitored by connecting a multimeter to the outer two pins. See Figure 2.7 and Figure 2.8 for a diagram of the anatomy of the sensor and a sample graph of force-applied versus detected resistance, respectively.

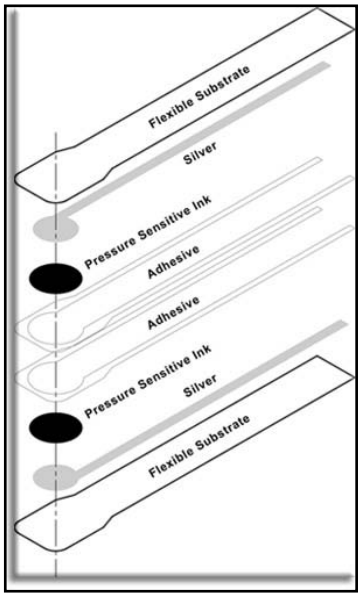

(Taken from [25])

Figure 2.7: Anatomy of FlexiForce Sensor

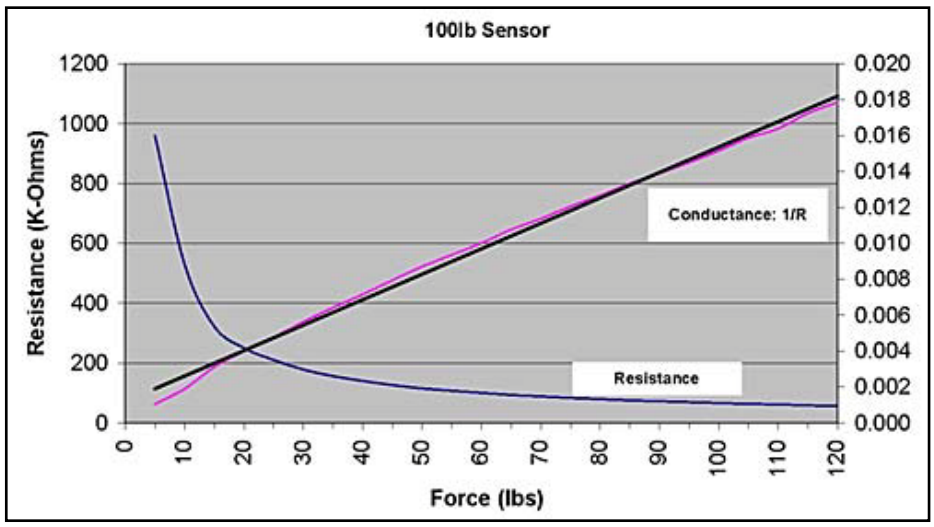

(Taken from [25])

Figure 2.8: Force vs. Resistance of 100-lb FlexiForce Sensor

The sensors are very thin at 0.1 mm (0.005 in) thickness. There is a maximum length of 20.3 cm (8 in) for the sensors, but they can be custom-trimmed to a shorter length if desired. The sensor can withstand temperatures up to 68.3 degrees Celsius (155 degrees Fahrenheit), but may be damaged at higher temperatures. Water-submersion may degrade the adhesive that holds the sensors' layers together and may cause the layers to separate. Also damaging to the sensors are sharp objects, shear forces, creasing and loads greater than 68.9 megapascals (10,000 lb/in^2, psi). There are three types of sensors that differ in the optimal force range for each. These ranges are 0-0.45 kg (0-1 lb), 0-11.36 kg (0-25 lb) and 0-45.45 kg (0-100 lb). Each type of sensor costs approximately $20 and is used in conjunction with an op-amp, which costs approximately $30, as of 2011 [26].

A disadvantage of the FlexiForce sensor is that it can only detect pressure at the tip end of the sensor strip. In other words, if a pressure is applied anywhere other than the tip, then either no detection or an inaccurate detection will occur. In order for a large area to be fitted

with this type of pressure sensor, an array of hundreds of this sensor-type would be required to detect all pressure points for, say, a human body laying on a mattress.

2.3.1.2 Capacitance-Based Pressure Sensing

Capacitance-based pressure sensors obtain readings from variable capacitors created from a metal diaphragm and pressure cavity. Applied pressure causes the cavity to collapse, thus resulting in a different capacitance value. These sensors are considered to be in the strain-based category of sensing techniques. Typically, a spring member exists to maintain a constant space between the capacitance plates, consequently keeping capacitance at a constant value when no pressure is loaded [27]. The diaphragm is exposed to a variable pressure on one side and a reference pressure on the other side. As pressure increases, the capacitance is not necessarily linear with respect to the applied pressure [28]. A sample schematic of a capacitive pressure sensor is seen in Figure 2.9.

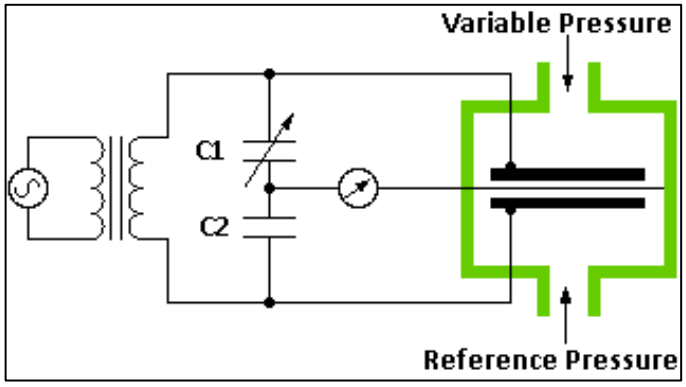

(Taken from [28])

Figure 2.9: Schematic Capacitive Pressure Sensor

One specific company that uses capacitance in their pressure sensors is Pressure Profile Systems, based in Los Angeles, California. The products they developed, named "ConTacts," are available in three types, depending on end use. The three types are

conformable tactile pads, industrial tactile pads and hybrid tactile pads. A technical comparison between the three types is demonstrated in Appendix B in Table 8.3.

The conformable type can conform to most any surface and is manufactured in sizes of small (10x10 mm^2), medium (25x25 mm^2) and large (50x50 mm^2). The large pads include "relief cuts" to allow for additional conformability around curved surfaces, such as knees and elbows if interfacing the human body. The conformable sensors are capable of detecting pressure up to 345 kilopascals (50 psi) and are made of a flexible, conductive cloth. These pads are sold in conjunction with the ConTacts C500 signal conditioning system, which drives a single tactile sensor with a 0-4.5 VDC output. The price for a C500 system with a single sensor is estimated to be approximately $1000, as of 2011 [29].

The industrial type of ConTacts sensor is designed to be more durable and capable of withstanding high-temperature and high-pressure applications. They are available in the same sizes given in the previous paragraph. Compared to the conformable sensors, the industrial type can measure pressures up to 13.8 megapascals (2000 psi) and withstand temperatures up to 200 degrees Celsius. The minimum detectable pressure range is at 345 kilopascals (50 psi). This is outside of the realm of the human physiology and such capability is unnecessary for the bedding system that this research aims to develop. The aforementioned hybrid type has similar capabilities as it is somewhat conformable and also durable. They provide the same sensitivity as the conformable pads, but sacrifice some flexibility for curved surfaces [29].

2.3.1.3 Potentiometry-Based Pressure Sensing

These sensors operate with an arm mechanically attached to an elastic pressure-sensing element. As pressure varies, there is deformation in the elastic element and the arm is forced to move backwards or forwards across a potentiometer and a resistance measurement is recorded. Potentiometric pressure sensors are considered to have limited resolution and also to be "low end" sensors with few applications. There is low sensitivity and limited working range, so this type of sensor is suitable for evaluating coarse processes [30].

The SoftPot, developed by Spectra Symbol, is a linear potentiometer that detects position upon application of a force [31]. The sensor lengths range from 2 to 2000 mm. These sensors are sealed and therefore better-protected against harsh environments, which may include areas with condensed moisture, such as bodily fluids. A disadvantage of this sensor may be that it can only detect one position along its length per gauge; this position being the location of the applied force. A diagram of the cross-section of the sensor is shown in Figure 2.10.

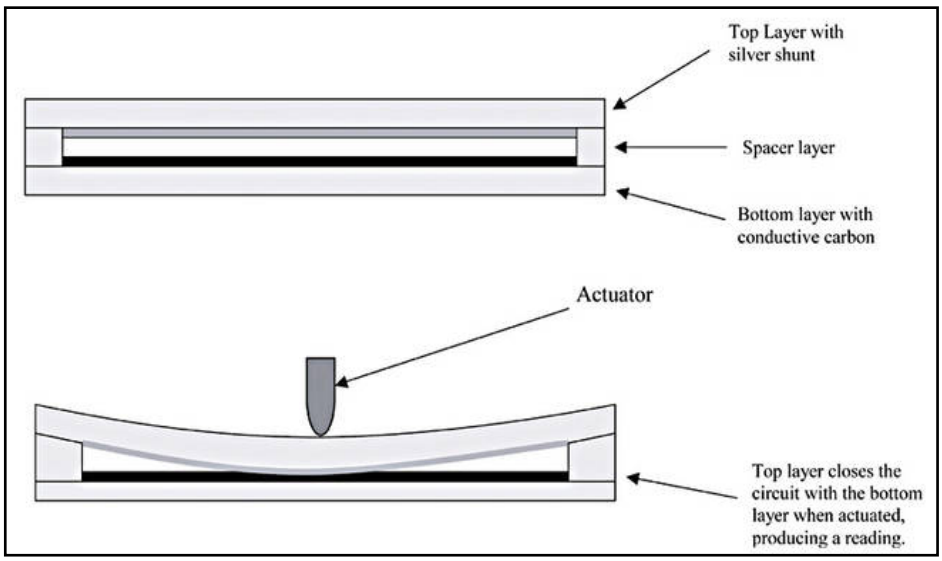

(Taken from [31])

Figure 2.10: Schematic of SoftPot Potentiometer

With the use of two gauges, however, two positions of pressure application can be detected using the SoftPot. The output of the sensor allows for up to two gauges to be attached. Based on the readings, the points of outermost pressure—outermost meaning the pressure points closest to each end of the sensor—can be detected and the distance of the pressures points from each end can be determined.

2.3.1.4 Piezoelectric-Based Pressure Sensing

Piezoelectric sensors have rapid response times to constant pressure variations. They use a crystal sensor and when pressure is applied, the crystal deforms and a small electric charge is generated. The magnitude of this electric charge is directly related to the amount of pressure that was introduced to create the charge [30]. These types of sensors are best suited for dynamic pressure applications, such as shock absorbers, where discrete changes in pressure are monitored.

2.3.1.5 Current Applications of Pressure Sensing in Textiles

Many applications with diverse motivations have benefited from research in textile-based pressure sensing. A great deal of existing research has been focused on "wearable" smart textiles, which are integrated into the clothing that its users wear for the appropriate application. Although a bedding system with pressure sensors embedded in its sheets would not be considered a "wearable" garment, the fact that the sheet will be in constant contact with the bedridden patient creates a similar situation. In any case, comfort is of great importance to the user, even if the user cannot actually feel the comfort. Comfort represents more than a physically-pleasant state of mind. It also represents an optimal level of blood-flow through the body. Without this blood-flow, cells cannot obtain the necessary nutrients and they will begin to degrade or die in the localized pressure region. Therefore, the guidelines that govern comfortability of wearable smart textiles may also be applicable to the bedding system that this research aims to develop.

One recent study involved placement of an array of pressure sensors into the insole of shoes. The purpose of the research was to determine the viability of an in-shoe plantar pressure measurement and analysis system that was textile-sensor-based. Using a strain-gauge method, the group developed a knitted fabric coated with carbon-black-filled silicon, which was used as the strain sensing element. The sensor was soft so that comfort for the wearer of the shoe was not compromised by the design. Six sensors were placed at strategic locations in the insole where pressure points in the foot could provide the most useful data. During the test, as more pressure was applied, the resistance measurement increased. This

allowed the pressure values to be converted into electrical signals and eventually plotted on a remote computer [32].

2.3.2 Moisture Sensing

The influence of unrelieved pressure on the formation of bedsores has been described. There are other factors, however, which can expedite the process of ulcer development. The introduction of moisture to the skin's microenvironment, in sufficient amounts, can cause the skin to change its properties. The skin becomes softer and more prone to bedsore growth due to localized pressure. Therefore, there is value for the bedding system to have the capability to detect events that introduce unsafe moisture levels, such as incontinence in those that cannot feel a sensation of wetness themselves.

One research group has developed a system that involves a smart wireless continence management system for individuals with dementia [33]. Their process utilizes an instantaneous wireless communication between moisture sensors in diapers with sensor nodes nearby to detect broadcasted signals. The current method for monitoring the continence of patients involves workers manually conducting periodic checks, which can be time consuming and also lead to a delayed response if an incontinence event occurs just after a check is performed. The system showed signs of success in that no false-alarms were detected. However, the system was only able to detect 50% of actual incontinence events, due to low sensitivity settings and sensor positional mistakes by workers in the diapers.

2.4 Fabric Formation Methods

The pressure sensors that have been described have relatively flat dimensions that provide the feasibility for them to be inserted into a fabric used for bedding material on which patients may rest. The fabric must not have significant concentrations of pressure points added into it because the local risk factors would negatively affect the prevention of bedsores in the patient. There is a need for embedding the sensors into the fabric on which the patient will lay. This helps to provide an intimate contact that improves the ability for the patient-to-bed pressure interface to be monitored. A typical fabric formation method used for typical hospital bed sheets is weaving. The following sections will describe the weaving process and provide examples of different types of woven constructions that may be used to develop the sheet that will be used in this research.

Three basic weave constructions span a vast majority of bed sheets that are currently manufactured. These three weaves are plain weave, twill weave and sateen weave types. A fourth weave—the pattern weave—exists, but requires the use of a Jacquard loom, which has a design complexity that makes the product very expensive to manufacture. A sample bed sheet was obtained from Duke University and its weaving construction parameters were analyzed. The warp and filling densities were found to be 114 ends/in and 70 picks/in, respectively. The warp yarns were found to have a cotton count of approximately 40 hanks/lb (130 denier) and the filling yarns were found to be about 36 hanks/lb (145 denier). Both the warp and filling yarns were ring spun and made of a 50% cotton to 50% polyester blend. The weave pattern in the sheet was determined to be a plain weave. Hospital bed

sheets are usually made with plain weaves because the robust weaving process is the least expensive and easiest method. In fact, most household bed sheets are made using a plain weave or plain weave derivatives, even though twill weaves may provide a softer drape compared to plain weaves. Sateen weaves or plain weave derivatives produce a fabric that is smoother to the touch and more lustrous in appearance compared to plain woven sheets.

2.4.1 Weaving Overview

The process of weaving involves the interlacing of two sets of yarns that are orthogonal to one another. The weaving machine, or loom, consists of several components used to accomplish the process. The warp beam is a metal cylinder onto which the warp yarns, or "ends," are wrapped. The other source of yarn that is used in weaving is the filling yarn, which may also be referred to as weft yarns or picks. Figure 2.11 illustrates the weaving process, with the direction of the flow of warp ends going from left to right.

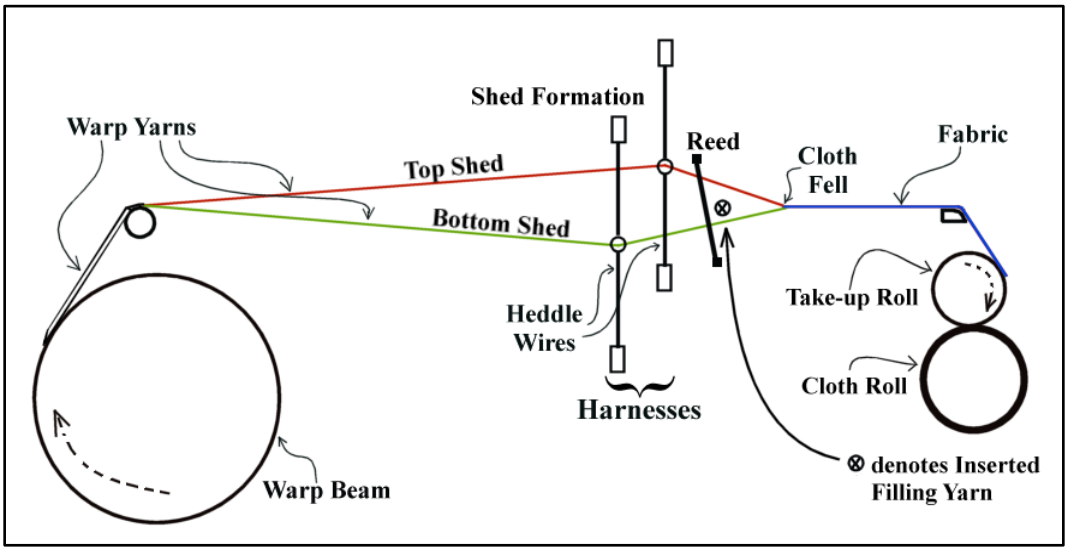

Figure 2.11: Schematic of the Weaving Process

Ends are drawn from the warp beam through heddle wires that are mounted in harnesses. These harnesses are what create the ability for the shed formation to occur. The shed refers to the open space between separated warp ends. The filling insertion, or pick insertion, takes place inside the shed. There are several commercial methods for accomplishing filling insertion, including rigid or flexible rapiers, air jets, water jets, projectiles and shuttles. The shuttle actually houses a bobbin of filling yarn and passes through the shed back and forth leaving the pick behind in the process. The other filling insertion methods mentioned are all examples of shuttleless weaving. After the filling yarn passes through the shed, it must be forced into the "fell" of the cloth, which is the point where the top shed and bottom shed meet at the fabric, by the beat up motion. The component that applies this required "beat-up" force is the reed. The reed is formed from two metal bars with vertical wires mounted between the bars, seen in Figure 2.12. The spaces between the wires are known as "dents." Each warp yarn is threaded through a dent. Depending on the number of dents per unit length of the reed and the required warp density, the number of ends in each dent is decided. Beside the beat up force, the reed controls the warp density and the in-loom fabric width.

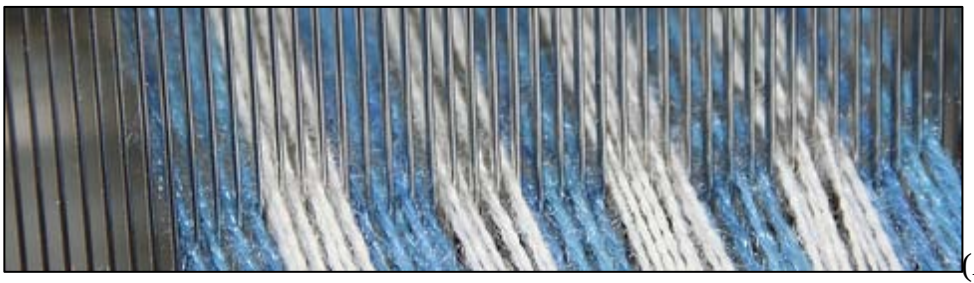

(Adapted from [34])

Figure 2.12: Reed with warp yarns drawn in dents

The beat-up motion may occur before or after formation of a new shed. The fabric is taken up on a roll at a specified rate that matches the speed at which the ends are drawn from the warp beam. In addition to forming the shed, the harnesses also allow for different weave constructions to be developed. The harnesses can be programmed to be raised or lowered for a given shed depending on the weave construction. Different weave constructions will be described in the next section.

2.4.2 Weave Construction Overview

The plain weave is the simplest of the basic weaves and has only one construction iteration. There are derivatives of plain weave, however, which include basket, warp rip and filling rib weaves. The plain weave involves an interlacement for every thread. Examples of the repeat units of the plain weave and its derivatives are shown in Figure 2.13. In the figures depicting repeat units, a black-filled square indicates that the end is on top of a pick. Consecutive painted squares (more than one) represent floats, which indicate that the end passes over two picks, as seen in the 2x2 warp rib example. The longer the float in a woven structure, the looser is the fabric produced. Thus, plain weave is the tightest construction.

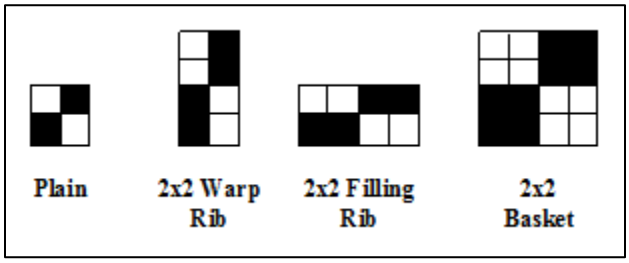

Figure 2.13: Repeat Units of Plain Weave and Several Derivatives

The twill weave has a characteristic that causes its resulting fabric to have a diagonal-line appearance. One common example of fabric that is made from twill weave construction is denim, which is the fabric from which blue jeans are manufactured. Examples of the repeat units of twill weaves are shown in Figure 2.14.

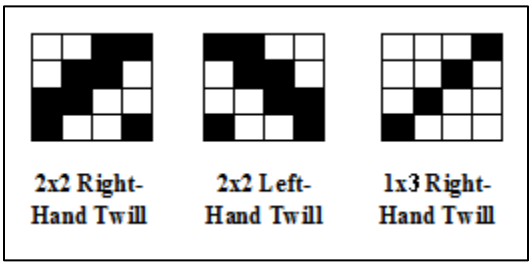

Figure 2.14: Repeat Units of Twill Weaves

The sateen weave is often used to develop fabrics that will have an inherent lustrous appearance to them. The characteristic sheen that is seen in these fabrics comes from the floats of continuous lack of interlacement between ends and picks, which promote more light reflection, as opposed to light scatter [35]. Examples of the repeat units of the sateen weave and a satin weave are shown in Figure 2.15.

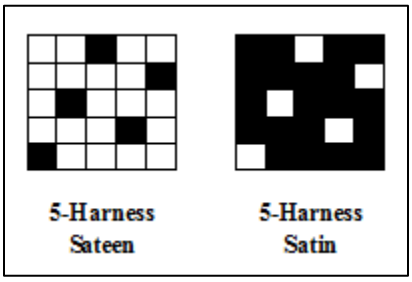

Figure 2.15: Repeat Units of Sateen and Satin Weave Examples

The aforementioned weave structures can be woven into a single layer of fabric or into multiple layers of fabric. Multiple-layered fabric is termed as “double-cloth” for two layers, “triple-cloth” for three layers, and so on. These layers can either be held together by stitches

to serve as anchors or they can be unstitched to keep the layers separate from one another. The stitching is inserted as part of the weave repeat pattern and is usually placed so that the stitches are somewhat hidden from view for aesthetic purposes. An advantage of unstitched double cloth involves the ability for a tubular structure that allows for materials to be held within the fabric if desired. Such materials may include the electronic pressure sensors described in Section 2.3.1.

2.5 Summary

The purpose of this literature review has been to investigate the current state of technology used for the prevention of bedsores in bedridden patients caused by prolonged periods of unrelieved pressure on the human body. An overview of the nature of bedsore formation was provided, with an in depth review of formation factors, potential dangers of bedsores and current tactics for prevention. The current prevention methods, while they help relieve and distribute pressure, do not provide a map of the location of pressure points on the body nor do they keep track of the time between moments of pressure relief. Also reviewed were several commercially available pressure sensing methods that may be applicable to the following research. These systems' characteristics were described and compared based on how they may be useful in a new hospital bedding system that will assist in the detection of unrelieved pressure in bedridden patients. Lastly, an overview of the weaving process has been outlined as well as examples of various weave structures that may be used in the development of the test bed sheet. There is evidence that research on inserting sensing elements into bed sheets can potentially yield results that will assist in the prevention of

bedsores. Other applications could also benefit from the insertion of sensors into textile substrates. Some examples include rooms that can respond to the presence of people, which could be useful for security purposes in buildings and, perhaps, for aesthetic purposes in interactive art galleries. This would involve sensors being inserted into carpeting on the floor, and systems would be activated when someone stepped onto the carpet. The electronic industry could potentially benefit by using the pressure sensors in a knob control mechanism in an application like audio volume control. In such a case, the end user would touch a part of the volume bar to indicate the amount of volume they desired for their audio application. There are many textile product areas that could use this technology to enhance the systems that already exist today.

3 Pressure Sensing

The previous chapter described the technology of several types of commercially available pressure sensors. This chapter will test the aforementioned sensors for applicability in a bed sheet sensing system. The procedure by which the sensors were test analyzed will be discussed. Each of the types of sensors has advantages and disadvantages with respect to one another based on their viability for implementation in the project.

3.1 Images Scientific Instruments Sensors

The first type of sensor tested was part of the FLX series by Images Scientific, utilizing a piezoresistive-based sensing technology. Four sensor samples of this type were obtained from Images Scientific Instruments that varied only in resistance rating. Three of the four samples were of type FLX-01-L, FLX-01-M and FLX-01-L with the resistance ratings being in the ranges of 1-20 kΩ, 20-50 kΩ and 50-200 kΩ, respectively, while the fourth sample was the FLX-03.

An initial examination of the sensors' behavior was performed. In this case, a multimeter (METEX® M-3890D USB) was connected to the sensor by two wirings as seen in Figure 3.1 with the schematic for the connection shown in Figure 3.2.

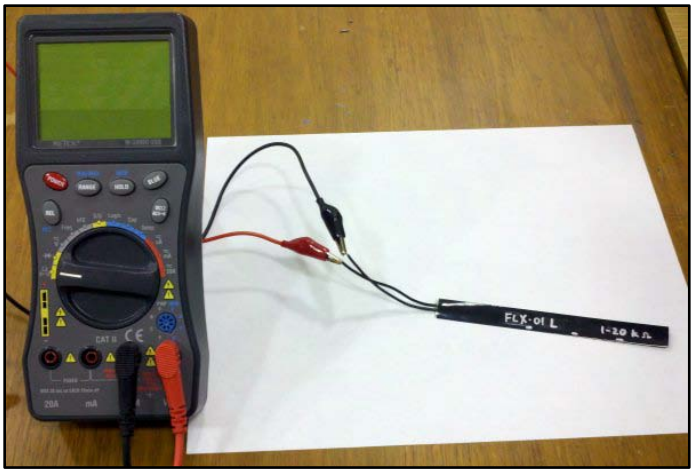

Figure 3.1: Experimental setup of FLX-01 Series Sensor (Cushion not shown)

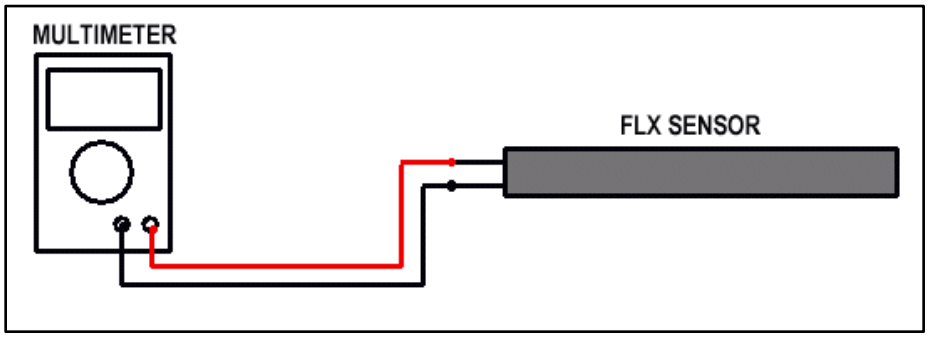

Figure 3.2: Schematic of FLX-01 Series Sensor Connection with Multimeter

Two stranded copper conductor wires extend from each of the FLX-01 sensors, as seen in Figure 3.3. Using the multimeter, the resting (unstressed) measurements of resistance values, in kΩ, were recorded for each of the three sensors. While some quantitative behavior was examined, such as resistance values, qualitative behavior was scrutinized more intently in this preliminary analysis of the sensors. These qualitative behaviors include basic operating performances and characteristics.

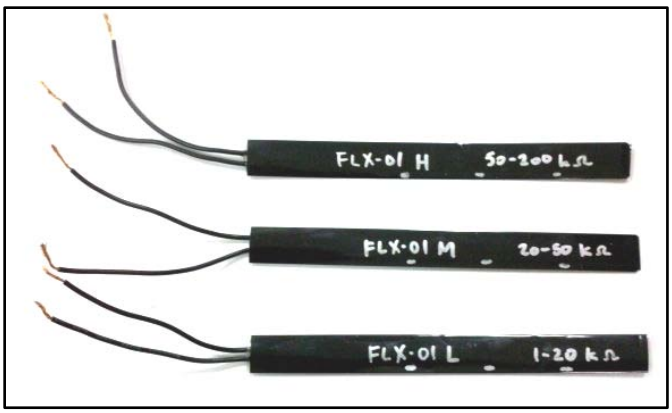

Figure 3.3: FLX-01 Series (Sample Sensors)

The sensors were each placed on a cushioned surface for the first iteration of unstressed testing, as shown in Figure 3.4. The material used for cushioning was a thick, spongy, folded woven fabric where four layers of the fabric separated the sensors from the table top surface. The purpose of the cushioned surface was to mimic a hospital bed mattress, which is the target end use surface for the project. The sensors were tested individually, as opposed to simultaneously.

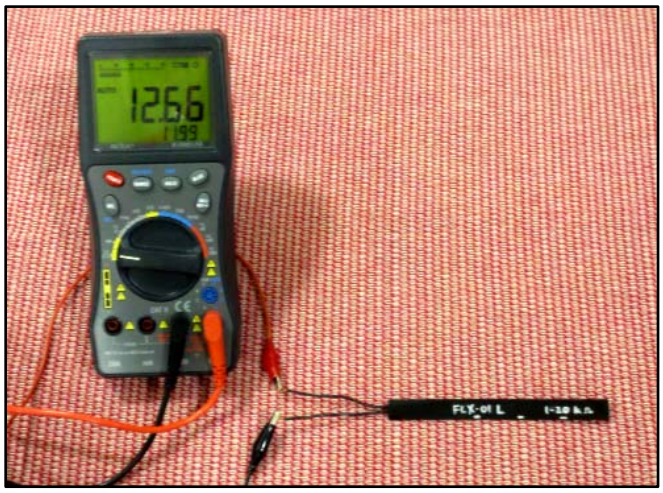

Figure 3.4: FLX-01 Sensor Unstressed Flat on Cushioned Surface

Upon initialization of the multimeter, very erratic resistance readings were observed for each of the three unstressed sensors. Due to the unstable readings, an estimate was subjectively determined for the starting resistance upon multimeter initialization. After the estimate was recorded, a simple test was performed to confirm that the resistance measurement decreased upon bending of the sensor, as the manufacturer declared. The observations of unstressed and stressed states of the sensors are listed in Table 3.1.

Table 3.1: Subjective Observations of Unstressed and Stressed FLX-01 Series Sensors

State	FLX-01-L (1-20 kΩ)	FLX-01-M (20-50 kΩ)	FLX-01-H (50-200 kΩ)
Unstressed (laying flat)	• Very erratic readings on multimeter • Resistance started at approximately 17 kΩ and slowly decreases without user instigation • Resistance never settled after 20 seconds	• Very erratic readings on multimeter • Resistance started at approximately 165 kΩ and slowly decreases without user instigation • Resistance settled near 60 kΩ after 20 seconds	• Very erratic readings on multimeter • Resistance started at approximately 152 kΩ and slowly decreases without user instigation • Resistance never settled after 20 seconds
Stressed (pressed)	• Resistance decreased when an unmeasured force was applied (finger pressed down onto unspecified points along the length of the sensor)	• Resistance decreased when an unmeasured force was applied (finger pressed down onto unspecified points along the length of the sensor)	• Resistance decreased when an unmeasured force was applied (finger pressed down onto unspecified points along the length of the sensor)
Stressed (bent)	• Resistance was confirmed to decrease while bending the sensor • Resistance reading was unstable while bent	• Resistance was confirmed to decrease while bending the sensor • Resistance reading was unstable while bent	• Resistance was confirmed to decrease while bending the sensor • Resistance reading was unstable while bent

The FLX-03 sensor, shown in Figure 3.5, operated with a different mechanism. As discussed in Section 2.3.1.1.1, the sensor is bendable in only one direction. The connection with a multimeter had the same type of setup as previously shown in Figure 3.2. Unlike the sensors in the FLX-01 series, the FLX-03 did not change its resistance upon a normal force being applied to its surface. The resistance only changed upon bending. The nominal resistance maintained a relatively steady value of 9.8 kΩ in the unstressed state. Upon bending, the resistance increased with increasing bend angle. Upon bending this sensor, a slow recovery was noticed for the sensor to return to its lay-flat state. This delay was reflected in the resistance reading. Multiple runs of the same experiment yielded different results. Similar to the FLX-01 sensors, the FLX-03 resistance readings would not stabilize while specific bend angles were held constant.

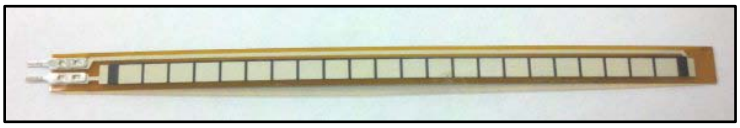

Figure 3.5: FLX-03 Sensor

Another type of piezoresistance-based pressure sensor was obtained from Images Scientific Instruments that uses Velostat™, a carbon-impregnated polyolefin conductive film developed by 3M™ [36]. The film is sandwiched between two layers of neoprene and sewn in place by conductive thread. Instructions for the fabrication of the neoprene bend sensor are included in Appendix C. Much like the FLX-01 series sensors, the neoprene bend sensor will change its resistance upon either bending or application of a normal force. The neoprene bend sensor is shown in Figure 3.6. The leads are located at opposite ends of the sensor (see Figure 3.7), unlike the sensors in the FLX-01 and -03, which have leads on the same end.

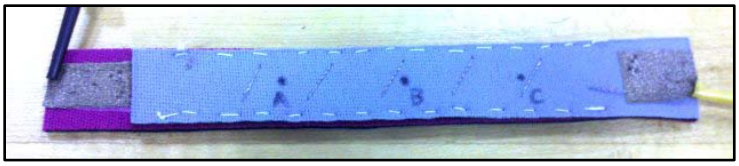

Figure 3.6: Neoprene Bend Sensor

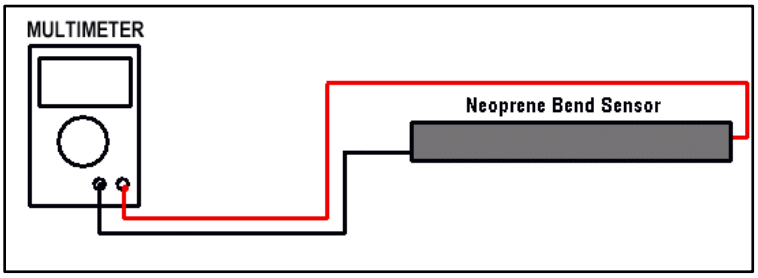

Figure 3.7: Neoprene Bend Sensor Schematic

Similar to the FLX-01 sensors' behavior in an unstressed state, the neoprene bend sensor exhibited a resistance value that slowly decreased after the multimeter was first initialized. The initial value was approximately 30 kΩ before slowly decreasing to approximately 25 kΩ after 20 seconds of sitting unstressed. Upon stressing the sensor with normal forces and bending, the resistance decreased. To reiterate, these first sensor examinations were not focusing on specific values, rather the general behavior of the sensors when unstressed and stressed.

3.2 Spectra Symbol Sensor

Only one type of sensor was tested based on Spectra Symbol's potentiometry-based pressure sensing technology. Instead of detecting a resistance based on a magnitude of pressure, the SoftPot sensor detects the presence of pressure along its length at the two outermost pressure points. In other words, a point of pressure that exists on the sensor between two other

pressure points is undetectable. Therefore, each sensor can detect no more than two pressure points simultaneously. The schematic of the SoftPot connection with two multimeters (both being METEX® M-3890D USB models) is shown in Figure 3.8.

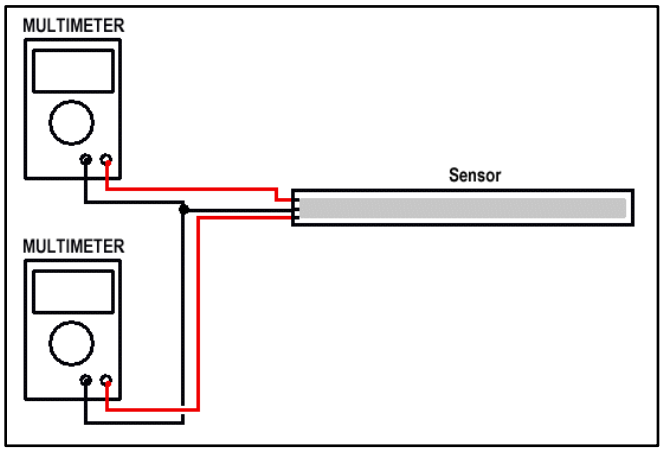

Figure 3.8: SoftPot Potentiometer Schematic

The sensor obtained from distributor Digi-Key® Corporation was a 1-meter length SoftPot potentiometer with three connections on one end. The electrical schematic is demonstrated in Figure 3.9. *Pin 3* allows a resistance to be measured from the left direction and *Pin 1* allows the same from the right direction.

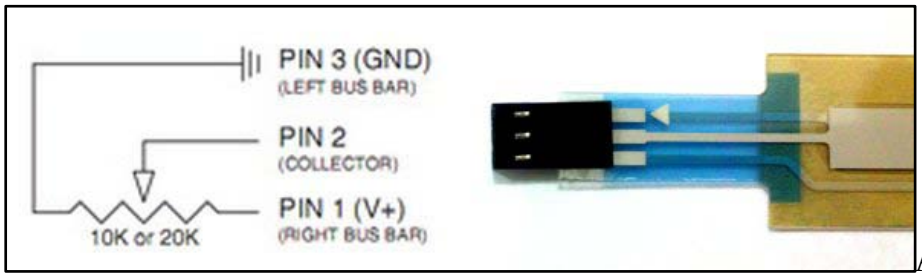

Adapted from [31]

Figure 3.9: SoftPot Potentiometer Electrical Schematic

The sensor contains a top circuit, which serves as a collector, and a bottom circuit, which is the resistor. These two circuits are separated by a circuit spacer. Pressing down onto the top circuit produces the desired potentiometric electrical output.

The pilot test that was performed with the SoftPot involved placing pressure points at various locations along the length of the sensing element. The unstressed sensor yielded a resistance measurement of 18 kΩ, which corresponds to the rating for the sensor advertised as 20 kΩ. When one pressure point was applied, the two multimeters' readings summed to 18 kΩ. At a point near the halfway point of the sensing element's length, the two multimeters both reported approximately 9 kΩ. At points relatively equidistant from each respective end of the sensor, the resistances reported by both multimeters were shown to be approximately equal at 4 kΩ, as shown in Figure 3.10. At different locations, the pressure yielded different resistance values consistently (see Figure 3.11). Finally, Figure 3.12 shows that the two outer pressure points remain the same when a third pressure is introduced between the original two pressure locations.

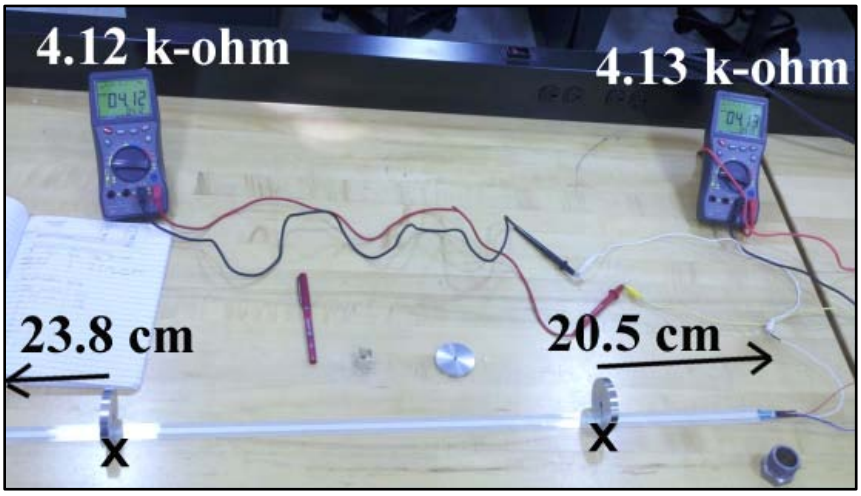

Figure 3.10: SoftPot Setup with 2 Pressure Points – Equal Resistances

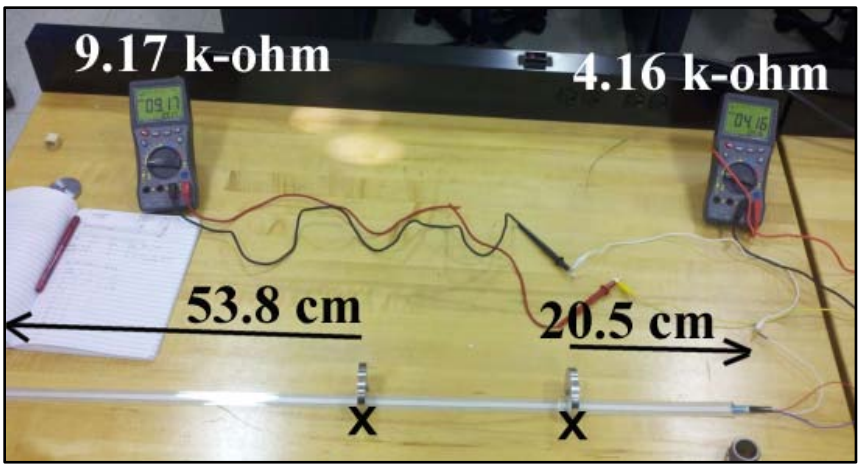

Figure 3.11: SoftPot Setup with 2 Pressure Points – Unequal Resistances

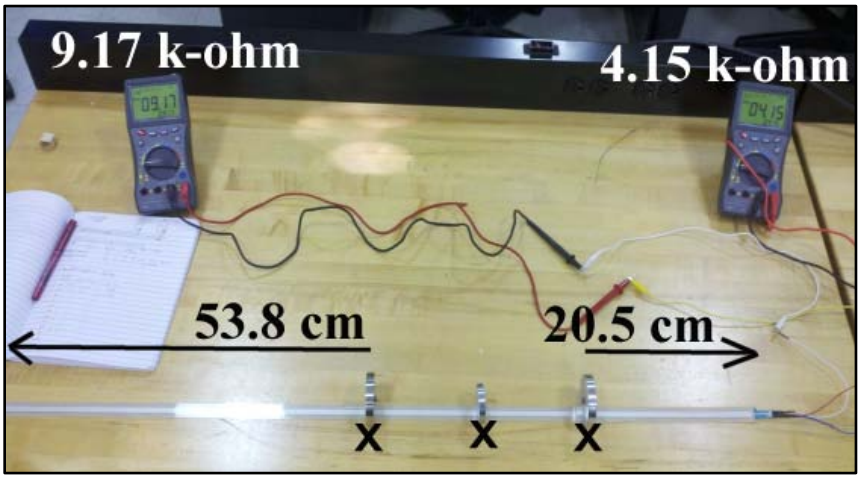

Figure 3.12: SoftPot Setup with 3 Pressure Points

Initial assessment of these results indicates that the position(s) of up to two pressure points can be determined by manipulating the resistance readings and converting them to lengths along the sensor.

3.3 Weight vs. Resistance Test – Piezoresistance-Based Sensors

After the preliminary examination of the FLX-01 series of sensors was completed, a quantitative behavior analysis needed to be performed in order to understand the relationship between the force applied to the sensors and the resulting resistance that they would yield. A simple test was developed that involved applying various forces and recording the resistance. Recall the observation that the resistance continued to decrease without settling after the multimeter was initialized. Due to the instability of the resistance reading seen in the FLX-01 sensors, a factor of variability needed to be removed. Therefore, for each reading, the resistance was recorded as the value displayed on the multimeter after ten seconds had passed upon placing the weight on the sensor.

Three different locations on each sensor were labeled as A, B and C in order to measure the resistance at more than one pressure point. This helped determine whether there was any relationship between the pressure location and the resistance measured. The locations of pressure points A, B and C can be seen in Figure 3.13 and the same locations were used on sensor type FLX-01-H, as well.

Figure 3.13: Location of Tested Pressure Points on FLX-01 Sensors

Four different weights measuring 0.25, 0.5, 1.0 and 1.5 lb were selected to be used as pressure points. These four weights were used to run the test using a hard surface that was a

table top. A small, plastic cube measuring 19 mm (mm) x 19 mm x 19 mm (0.75 in x 0.75 in x 0.75 in), of negligible inherent weight compared to the weights applied, was used to concentrate the test weight onto a constant area for each measurement (see Figure 3.14). The weights were balanced on top of the cube as seen in Figure 3.15.

Figure 3.14: Cube Used to Concentrate Pressure on FLX Sensors

Figure 3.15: Demonstration of Balanced Weight on FLX-01 Sensors

Five measurements for each test pressure point and each weight were recorded, for a total of 60 measurements for each sensor. This includes testing the FLX-01-L, FLX-01-H and the neoprene bend sensors. Also identified was the measurement of the resistance while unstressed.

The results of the test show the relationship between the weight applied and the resistance measured for each of the sensor types. Figure 3.16 shows the average resistance values for the FLX-01-L sensor's test and the numerical values are given in Table 3.2. There is a general inverse relationship between weight and resistance. As the weight is increased, the

resistance value decreases. This is true for each of the weight positions A, B and C. There is an anomaly within the dataset for point C, however, because the resistance is increased when the weight increases from 1.0 to 1.5 lb. The reason for this wayward behavior was undeterminable, and can be attributed to a possible defect within the sensor.

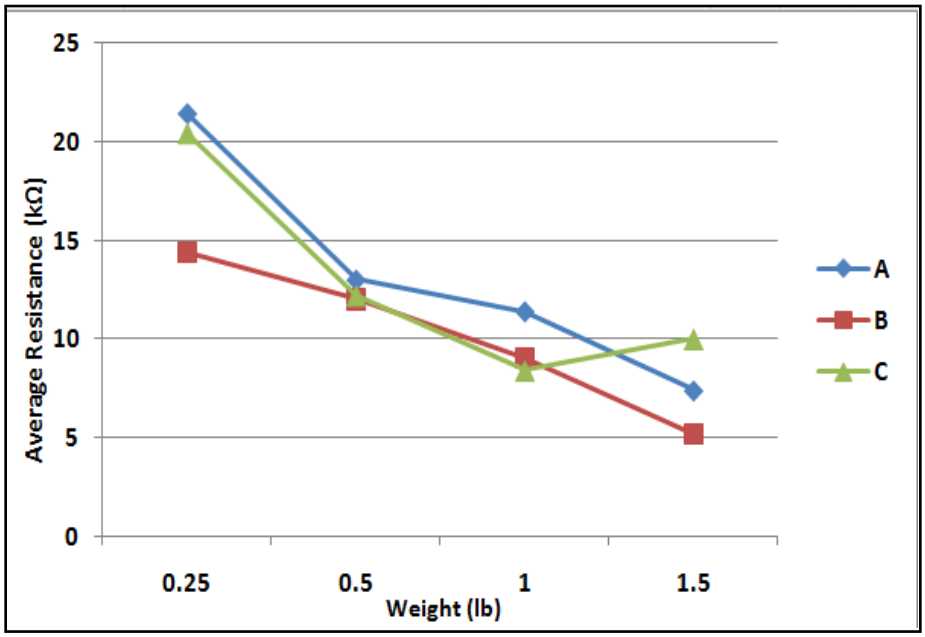

Figure 3.16: Weight vs. Average Resistance for FLX-01-L Sensor

Table 3.2: Resistance Values for FLX-01-L Sensor

		Repetition					
Weight (lb)	**Pressure Point**	**1 (kΩ)**	**2 (kΩ)**	**3 (kΩ)**	**4 (kΩ)**	**5 (kΩ)**	**Average (kΩ)**
0.25	A	20	20	28	20	19	21.4
	B	13	15	13	16	15	14.4
	C	21	19	19	18	25	20.4
0.5	A	12	15	10	15	13	13.0
	B	14	8	13	16	9	12.0
	C	13	10	11	15	12	12.2
1.0	A	12	12	11	11	11	11.4
	B	9	14	9	7	6	9.0
	C	7	11	10	7	7	8.4
1.5	A	7	9	7	7	7	7.4
	B	5	5	5	6	5	5.2
	C	10	10	10	9	11	10.0
Unstressed resistance value: 95 kΩ							

A graph of the average resistance values of the test on the FLX-01-H sensor is shown in Figure 3.17 and the numerical results are given in Table 3.3. A similar trend for each of the pressure point locations was seen, which involves the uncharacteristic increase in resistance at the C location when increasing the weight from 1.0 to 1.5 lb. Again, this may be due to a defect in the sensor. Another difference seen in this sensor's results compared to the FLX-01-L's results is the vast decrease in measured resistance for the C location as a whole compared to the results for points A and B, which are closer to overlapping data. This difference may be due to a potential defect in the sensor near the C location. The drop in overall magnitude of the resistance is due to the fact that the FLX-01-L is rated from 1-20 kΩ and the FLX-01-H is rated from 50-200 kΩ.

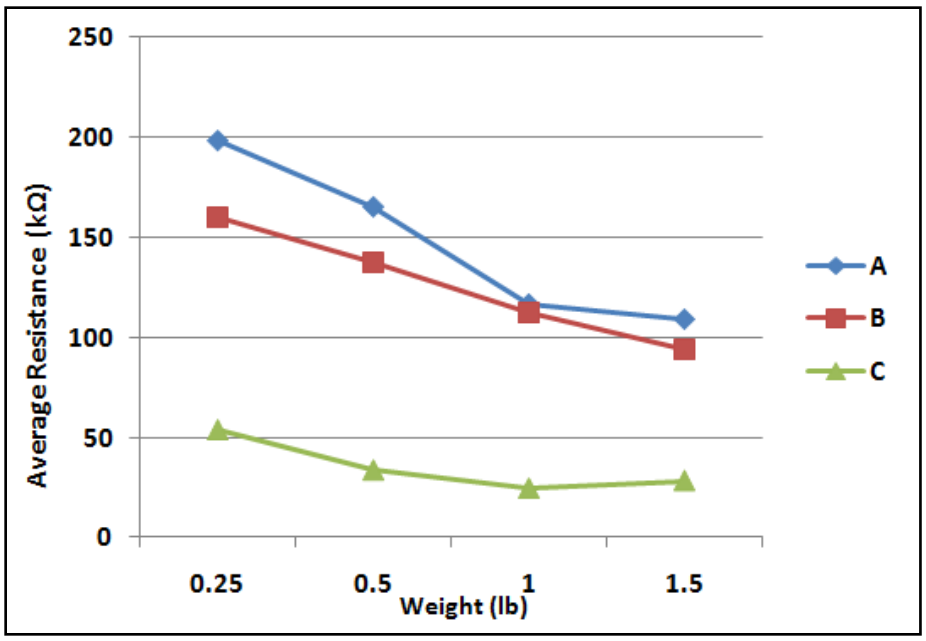

Figure 3.17: Weight vs. Average Resistance for FLX-01-H Sensor

Table 3.3: Resistance Values for FLX-01-H Sensor

		Repetition					
Weight (lb)	**Pressure Point**	**1 (kΩ)**	**2 (kΩ)**	**3 (kΩ)**	**4 (kΩ)**	**5 (kΩ)**	**Average (kΩ)**
0.25	A	188	189	204	197	213	198.2
	B	184	161	139	162	153	159.8
	C	47	37	73	36	76	53.80
0.5	A	183	187	154	148	154	165.2
	B	142	139	130	137	139	137.4
	C	41	28	39	30	29	33.40
1.0	A	134	109	110	113	118	116.8
	B	106	127	118	109	101	112.2
	C	25	24	22	25	25	24.20
1.5	A	95	107	114	122	108	109.2
	B	75	92	92	109	101	93.80
	C	22	27	38	26	28	28.20
Unstressed resistance value: 320 (kΩ)							

The locations of the test pressure points A, B and C used in the test of the neoprene bend sensor are shown in Figure 3.18. A graph of the average resistance values for the test on the

neoprene bend sensor is shown in Figure 3.19 and the numerical values are given in Table 3.4. This sensor did not have an advertised rating, as compared to the FLX series sensors. These resistance results also show an inverse relationship between weight and resistance. Unlike the FLX-01 sensors, all of the pressure points have overlapping data with a continuous decreasing trend with increasing weight. The relationship provides a glimpse of a possible asymptotic lower limit that the resistance may approach with increased weight application. In such a case, the slope of decreasing resistance at a much larger weight may be less discernable in terms of converting a resistance to an applied force. This would likely result in inaccurate conversions of analog signals into usable data.

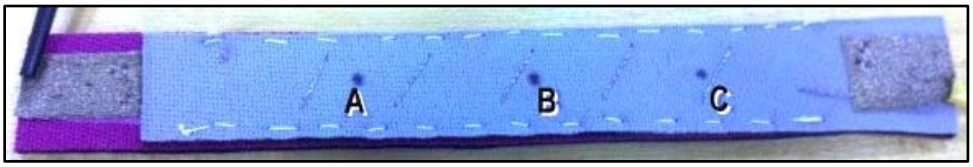

Figure 3.18: Location of Tested Pressure Points on Neoprene Bend Sensor

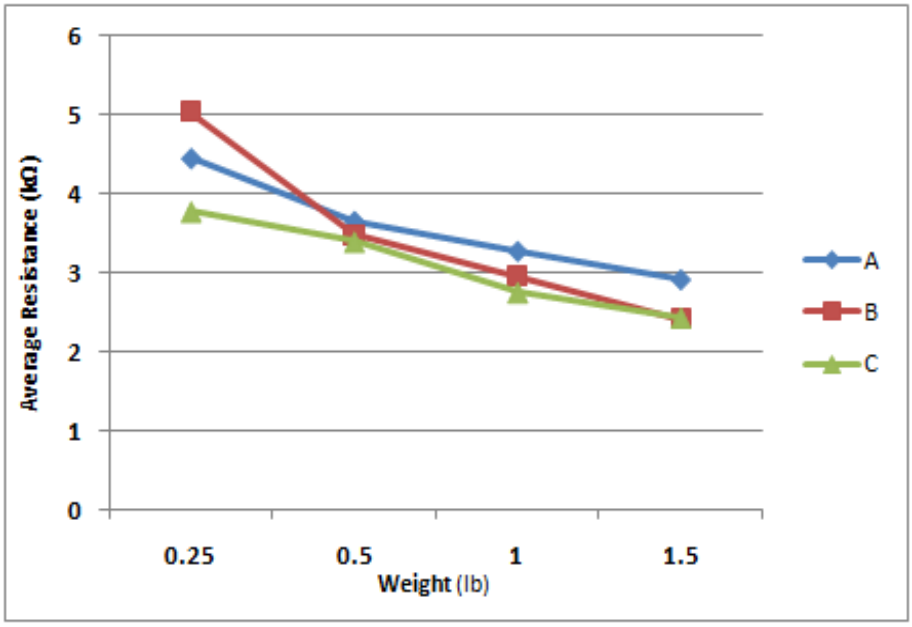

Figure 3.19: Weight vs. Resistance for Neoprene Bend Sensor

Table 3.4: Resistance Values for Neoprene Bend Sensor

		Repetition					
Weight (lb)	**Pressure Point**	**1 (kΩ)**	**2 (kΩ)**	**3 (kΩ)**	**4 (kΩ)**	**5 (kΩ)**	**Average (kΩ)**
0.25	A	4.7	5.0	4.8	3.8	4.0	4.5
	B	5.4	4.7	5.0	5.4	4.7	5.0
	C	3.7	3.7	3.7	4.2	3.6	3.8
0.5	A	3.6	4.1	3.6	3.6	3.4	3.7
	B	3.9	3.7	3.2	3.3	3.3	3.5
	C	3.0	4.2	3.6	3.1	3.1	3.4
1.0	A	3.9	3.3	3.1	3.1	3.0	3.3
	B	2.9	2.8	3.2	2.9	3.0	3.0
	C	2.6	2.7	2.8	2.7	3.0	2.8
1.5	A	2.8	2.9	3.0	3.0	2.9	2.9
	B	2.5	2.5	2.4	2.4	2.3	2.4
	C	2.5	2.4	2.5	2.4	2.4	2.4
Unstressed resistance value: 18 (kΩ)							

All of the results described so far have been based on the sensors' testing while on a hard, firm surface. The following results will be based on the same sensors being tested on a

cushioned surface, which more closely mimics a hospital mattress. This setup required a different method for applying the weight to the sensors because the weights were unable to balance on the cube on top of the sensors without toppling. In this test, only two weights were measured—0.5- and 1-lb weights. Just as in the previously-reported test, each of three locations of pressure points was tested for each sensor. The setup can be seen in Figure 3.20 along with the simple schematic in Figure 3.21. The cushion used was a fabric with 16 layers of folded cloth. The rope holding the weights was lowered down onto the cube until just before it began to topple and the resistance was recorded ten seconds after the weight was applied.

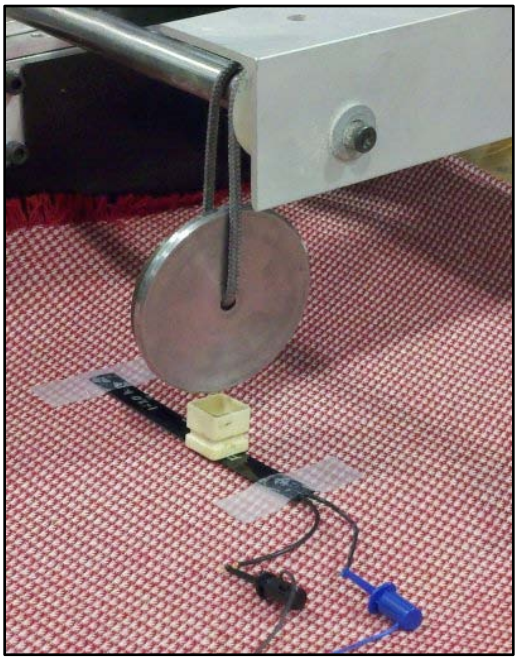

Figure 3.20: Setup for On-Cushion Testing of FLX Sensors

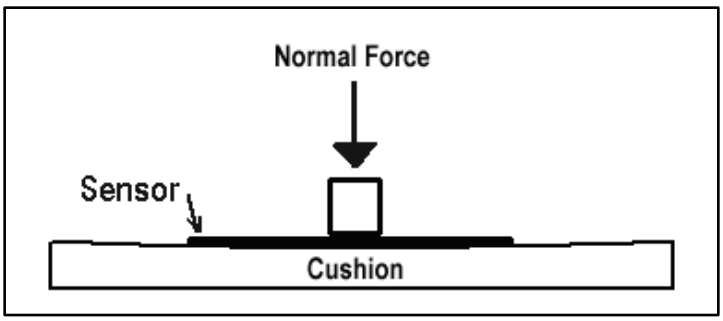

Figure 3.21: Schematic of On-Cushion Weight vs. Resistance Testing of FLX Sensors

Graphs of the average resistance values measured in each of the tests for the FLX-01-L, the FLX-01-H and the neoprene bend sensor are shown in Figure 3.22, Figure 3.23 and Figure 3.24, respectively. The numerical values are provided in Table 3.5, Table 3.6 and Table 3.7, respectively. The limitation of using of only two different weights caused the usefulness of the data to be somewhat bound. There is a separation between the data when comparing the three pressure point locations' results. No overlap is observed, which indicates that the location of the pressure point has a significant impact on the resistance measurement. The data shown for FLX-01-L indicates that the reduction in resistance between the weights on cushion was inconsistent with the data shown for the same points of data on a hard surface. This further supports the conclusion that the FLX-01 sensors were too inconsistent to demonstrate success in this project.

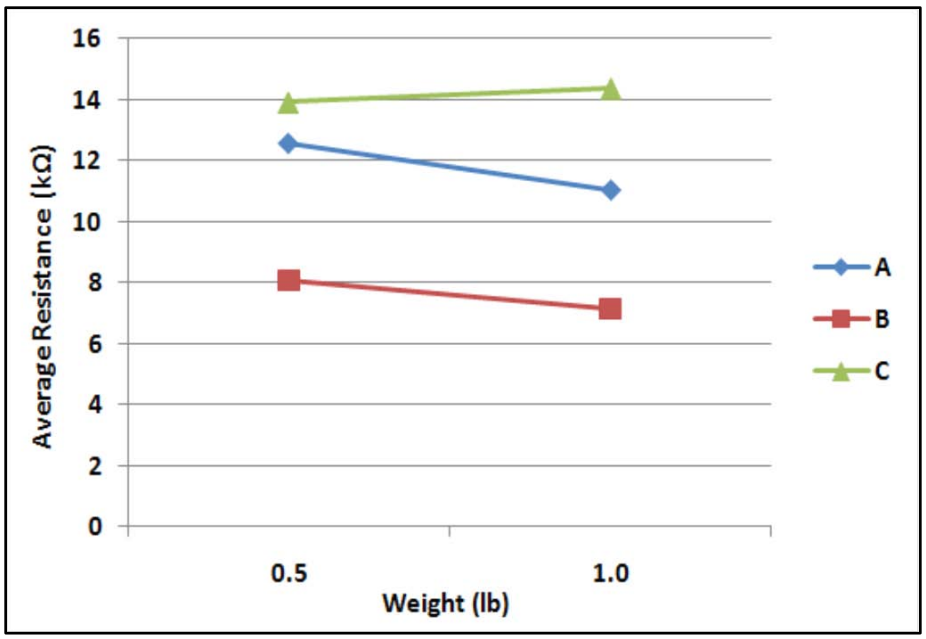

Figure 3.22: On-Cushion Weight vs. Average Resistance for FLX-01-L

Table 3.5: Resistance Values for FLX-01-L Sensor on Cushion

		Repetition					
Weight (lb)	**Pressure Point**	**1 (kΩ)**	**2 (kΩ)**	**3 (kΩ)**	**4 (kΩ)**	**5 (kΩ)**	**Average (kΩ)**
0.5	A	14.1	12.1	12.3	11.8	12.4	12.5
	B	8.2	8.3	7.8	8.2	7.7	8.0
	C	14.4	12.9	13.4	13.0	15.8	13.9
1.0	A	10.5	11.7	11.3	10.4	11.1	11.0
	B	6.4	7.1	7.0	7.8	7.4	7.1
	C	16.0	11.2	15.0	15.1	14.4	14.3
Unstressed resistance value: 160 (kΩ)							

The results of the cushion testing of FLX-01-H shown in Figure 3.23 are in slight agreement with the results from the hard surface testing in that the average resistance values for point C are far less than the values shown for points A and B. This further indicates that there may have been a defect in the sensor.

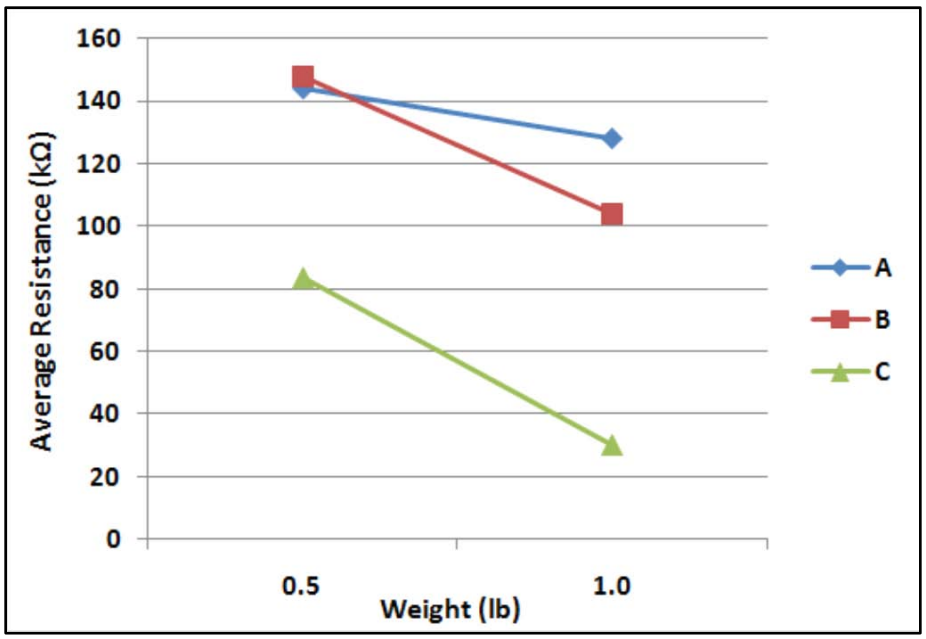

Figure 3.23: On-Cushion Weight vs. Resistance for FLX-01-H

Table 3.6: Resistance Values for FLX-01-H Sensor on Cushion

		Repetition					
Weight (lb)	**Pressure Point**	**1 (kΩ)**	**2 (kΩ)**	**3 (kΩ)**	**4 (kΩ)**	**5 (kΩ)**	**Average (kΩ)**
0.5	A	157	142	131	144	145	143.8
	B	151	153	153	144	137	147.6
	C	78	90	87	73	89	83.4
1.0	A	125	132	133	128	122	128.0
	B	121	107	94	106	91	103.8
	C	29	30	33	28	29	29.8
Unstressed resistance value: 320 (kΩ)							

Results shown in Figure 3.24 represent the data collected for the neoprene bend sensor during the on-cushion testing. Curiously, there is a gap in magnitude of resistance between pressure points C compared with A and B. One possible cause for this was operator error while taking the reading from point C. Analysis of the hard surface test results did not provide any indication that there was a difference between points A, B and C. Each of the

point locations shows a decrease from the 0.5-lb to the 1-lb force application, which is consistent behavior compared to the hard surface testing results.

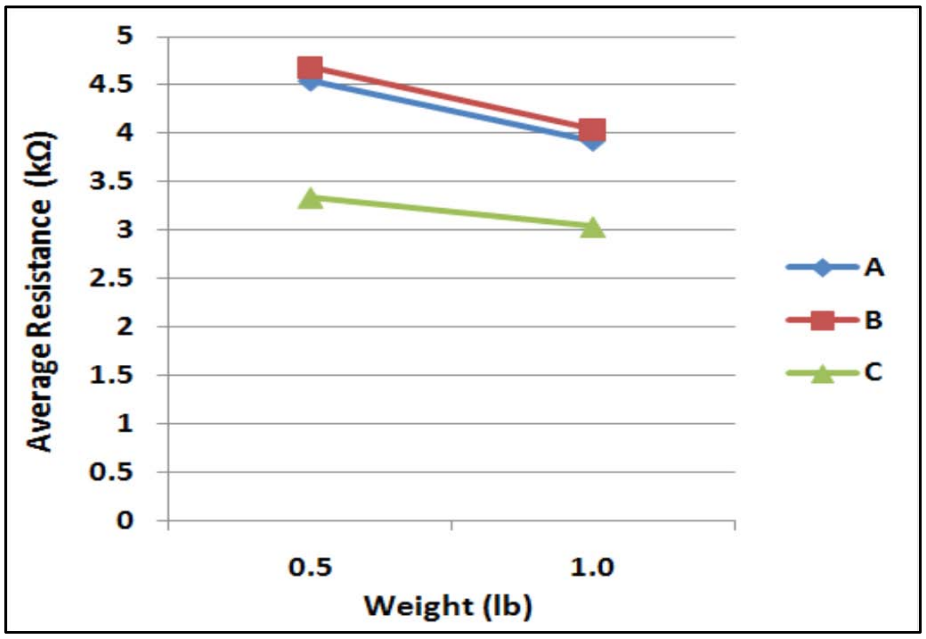

Figure 3.24: On-Cushion Weight vs. Resistance for Neoprene Bend Sensor

Table 3.7: Resistance Values for Neoprene Bend Sensor on Cushion

		Repetition					
Weight (lb)	**Pressure Point**	**1 (kΩ)**	**2 (kΩ)**	**3 (kΩ)**	**4 (kΩ)**	**5 (kΩ)**	**Average (kΩ)**
0.5	A	4.6	4.6	4.6	4.4	4.5	4.5
	B	4.8	4.8	4.8	4.5	4.5	4.7
	C	3.5	3.3	3.4	3.3	3.2	3.3
1.0	A	4.2	4.0	3.9	3.8	3.7	3.9
	B	5.1	3.9	4.0	3.6	3.6	4.0
	C	3.3	3.1	3.0	3.0	2.8	3.0
Unstressed resistance value: 12 (kΩ)							

3.4 Choosing Appropriate Sensor

Based on the tests performed, the results have led to the decision to use the SoftPot as a position-focused pressure sensor. With a thickness at less than 0.5 mm, the SoftPot potentiometer is very thin, which promotes its viability for being embedded into a fabric without creating a dangerous pressure point for patients at-risk for bedsore formation. The method for measuring the resistance in the SoftPot creates consistent results because a stationary pressure point results in a single resistance output that remains static unless the pressure point moves to a new location or removed altogether as compared to the flex sensors, which demonstrate erratic readings with stationary pressure points.

The piezoresistance-based sensors, in ideal conditions, may have the capability of being used to determine force values at pressure points. Empirical formulae may be developed from tests in such ideal conditions, which may include stable force application, no slippage at the force-sensor interface and absence of defects within the sensors themselves. The preliminary results from the pilot test do not provide strong evidence that these sensors can be used in this application in non-ideal conditions. The SoftPot sensor provided precise measurement readings that can be used to determine a force location, rather than force magnitude.

For the application on which this project is focused, the amount of time that an applied force's location is unchanged can be used to signal an alarm event. This alarm event can be used to alert a caregiver to tend to a patient to relieve the buildup of pressure, thus reducing the risk of a bedsore. It is important to reinforce the suggestion that other applications could

also benefit from embedding sensors into their existing textile products to enhance their functionality. This research is only focusing on one application (bedsore risk mitigation) known to potentially have a broad impact in improved healthcare and livelihood of patients. The next chapter will describe the development of the sensor layout plan as well as provide an overview on the construction of the fabric inside which the sensors will be embedded.

4 Sensor Layout and Fabric Design

Based on the findings, an acceptable sensor type was selected. The next step in the development of the design of the prototype involved a focus on determining the appropriate sensor layout. The feasible number of iterations for the layout was dependent on the capabilities of the fabric formation system. The following section will provide insight on the factors taken into consideration while designing the layout of the sensors in the test area of the prototype.

4.1 Layout of Sensors on Prototype

In order to effectively capture the critical pressure points exerted on the body while a patient is laying down, several dimensions needed to be identified regarding the human physique. Anthropometric data was used to determine an appropriate test area size as well as the actual placement of the array of sensors into the test area.

4.1.1 Anthropometry

Due to the vast range of humans' body dimensions, an estimate needed to be made based on anthropometric data. The Federal Aviation Administration (FAA) prepared a collection of body dimension percentiles in the "Human Factors Design Standard" (HFDS) for use in the design and testing of FAA systems, equipment and facilities [37]. The HFDS was used in this research to determine the appropriate length dimension for which an assumption could be made on a patient's height.

For the purpose of proof of concept, the entire length of a laying body was not deemed necessary for the development of the prototype. Recalled from Section 2.1.2, the common sites for bedsore formation on the human body can be seen in Figure 4.1.

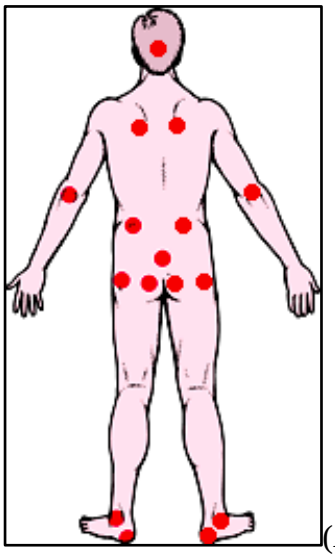
(Adapted from [12])

Figure 4.1: Common Sites for Bedsore Formation

A majority of the pressure point locations reside between the top of the head and just above the thighs. According to the HFDS, the "vertical distance from the sitting surface to the top of the head" is referred to as the subject's "sitting height," as seen in Figure 4.2 [37].

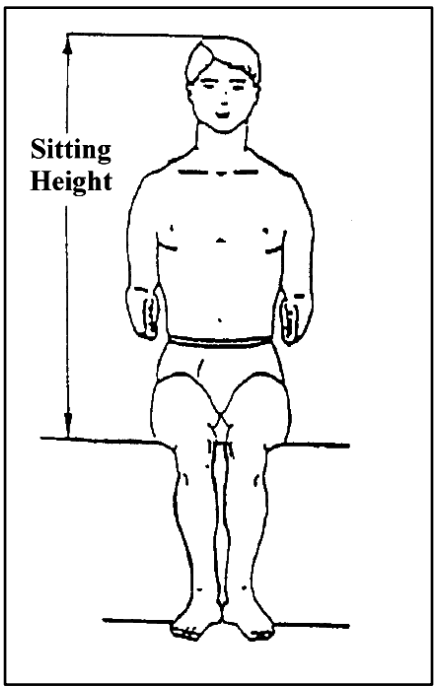

(Adapted from [37])

Figure 4.2: Diagram of Sitting Height Dimension

A sensor layout of this height measurement captures 12 of the 16 bedsore pressure points shown in Figure 4.1. Only the pressure points located on the ankles and heels were untested according to the sensor layout. Therefore, the sitting height characteristic was used as the height dimension of the test area for the prototype. The sitting height data for men and women collected in the HFDS is given in Table 4.1. Based on the 50^{th} percentile for men and the 95^{th} percentile of women, the target sitting height used in the prototype was set as 91.4 cm (36 in). With this measurement providing the test area length, the next step was to determine the test area width.

Table 4.1: Percentiles of Human Sitting Height Measurement

		Percentiles				
Gender		**1st**	**5th**	**50th**	**95th**	**99th**
Male	(in)	32.4	33.7	36.0	38.3	39.0
	(cm)	82.3	85.6	91.4	97.3	99.1
Female	(in)	30.5	31.3	33.5	35.8	36.7
	(cm)	77.5	79.5	85.1	90.9	93.2
(Adapted from [37])						

4.1.2 Test Area Dimensions

The previous section described the human limitations of the test bed design based on anthropometric data gathered by the FAA. Also present were limitations of the test area due to the hospital bed itself. From Section 2.2.1, the width of a hospital bed typically remains at 91.4 cm (36 in) while the length and thickness may vary. This dimension conveniently, although coincidentally, matched the sitting height dimension. Therefore, the resulting test area was a perfect square shape of 91.4 cm by 91.4 cm (36 in by 36 in). The next step in developing a sensor arrangement involves the determination of the location of the sensors' placement on the test area.

4.1.3 Placement of Array of Sensors

With the test area dimensions identified, the actual placement of sensors within the test area needed to be resolved. This decision relied on several different factors. One, and perhaps the most obvious, influence was the location of common pressure points that have been shown to result in bedsores (recall Figure 4.1). The area of sensing needed to capture each of these pressure points and their immediate surrounding areas. The surrounding area of

sensing permitted the detection of pressure points that might have been slightly off target due to human physique variability. Another factor that affected the sensor layout plan was the list of commercially available lengths of sensors. The lengths offered by Digi-Key® Corporation of the Spectra Symbol SoftPot potentiometer are listed in Table 4.2.

Table 4.2: Commercially Available SoftPot Sensor Detection Lengths

Detection Length	
(mm)	**(in)**
12.5	0.49
25	0.98
50	1.97
100	3.94
150	5.91
170	6.69
200	7.87
300	11.81
400	15.75
500	19.96
750	29.53
1000	39.37
(Adapted from [38])	

These lengths identify the range of detection location on the sensors. The sensors' total lengths are the sum of the wiring component, detection length and a small boundary length. The wire connection and the boundary have fixed lengths each of 38.1 mm (1.5 in) and 6.4 mm (0.25 in), respectively, as shown in Figure 4.3. However, the detection length varies depending on the rated length provided by the distributor, which were listed in Table 4.2.

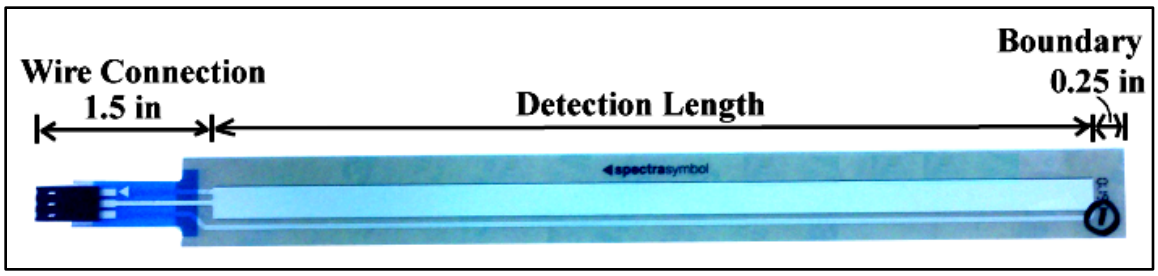

Figure 4.3: SoftPot Sensor Length Diagram

The weaving machine's capabilities would also prove to create limitations on the sensor layout plan. Due to the nature of an 8-harness weaving machine, the required unstitched pockets, or "tubes," into which the sensors would be embedded would have to span the entire width of the woven fabric. It should be noted that there were actually only six harnesses available for weave design because two harnesses are dedicated to "leno" selvage, which is needed to prevent warp yarns from fraying in shuttleless weaving. The tubes spanned the entire fabric width, which resulted in the sensors only having the capability to be mounted within the tube parallel to the direction of the fabric width. However, multiple tubes were capable of being woven into the same fabric, at different locations. These characteristics will be described further in Section 4.2.

Based on the aforementioned constraints, a preliminary design was developed for which sensors of varying length were placed onto a 91.4-cm by 91.4-cm (36-in by 36-in) square area. Sensors were grouped together at spots of common bedsore formation, noted by blue dots on Figure 4.4. The sensors are represented as numbered red rectangles in the figure. The lengths corresponding to the sensors' identification numbers are listed in Table 4.3.

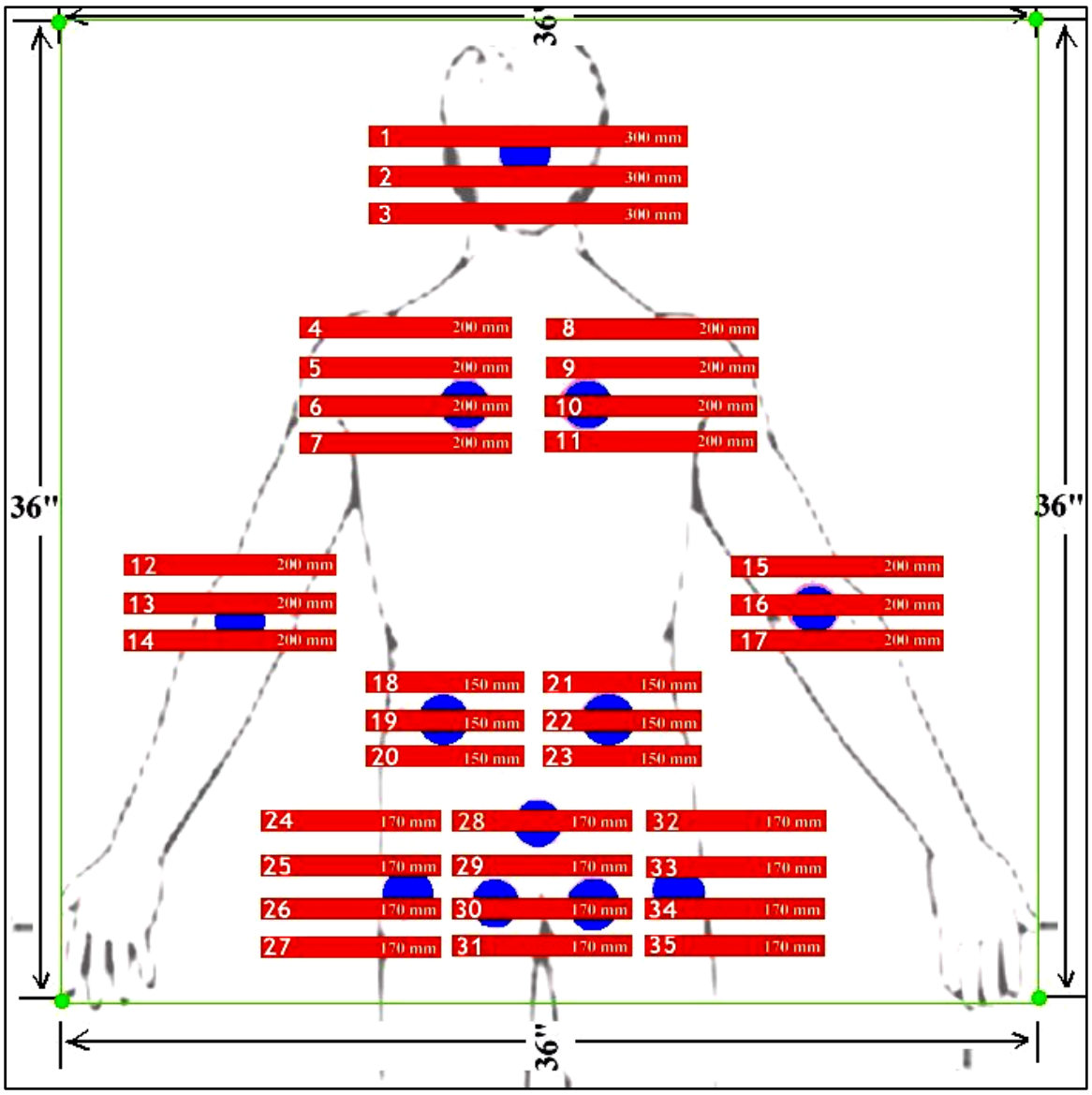

Figure 4.4: Preliminary Sensor Layout Plan

Table 4.3: Preliminary Layout Plan Sensor Lengths

Sensor ID#	Quantity	Detection Length (mm)
1-3	3	300
4-17	14	200
18-23	6	150
24-35	12	170

Several design adjustments were made regarding the preliminary layout plan based on factors such as human shoulder and torso width variability as well as cost efficiency. Patients vary in their shoulder breadth, which is the "horizontal distance across the upper arms between the maximum bulges of the deltoid muscles" according to the HFDS [37]. For men, the 99th percentile of shoulder breadth is about 55.1 cm (21.7 in). The preliminary design of the sensors in the shoulder breadth area consisting of 200-mm (7.9-in) sensors resulted in 39.9 cm (15.7 in) of detection length and a 5.1-cm (2-in) gap between sensors in line with one another (for example, sensors *4* and *8* in Figure 4.4 are in line with one another). The lengths to be used for sensors *4* through *11* were each increased to 300 mm (11.8 in). This increase resulted in a shoulder breadth detection range of 59.9 cm (23.6 in), which is greater than 55.1 cm (21.7 in), the 99th percentile of that measurement as stated by the HFDS. Another benefit of changing the sensor length in the shoulder breadth area was the price break offered by the distributer of the sensors, Digi-Key® Corporation. The change resulted in 11 of the 300-mm sensors being purchased, with the price break being applied once the quantity reached ten sensors. The lengths of sensors *18* through *35* were also increased to create a larger pressure detection area. Each of the sensors numbered *18* through *23* were increased from 150 mm to 200 mm. Each of sensors numbered *24* through *35* were increased from 170 mm to 200 mm. This brought the total quantity of 200-mm sensors required to 24 units. A price break was realized at a quantity of 25 sensors, and a cost savings resulted in a spare 200-mm sensor available if needed. The updated sensor layout plan is shown in Figure 4.5 and the updated list of sensor lengths is provided in Table 4.4.

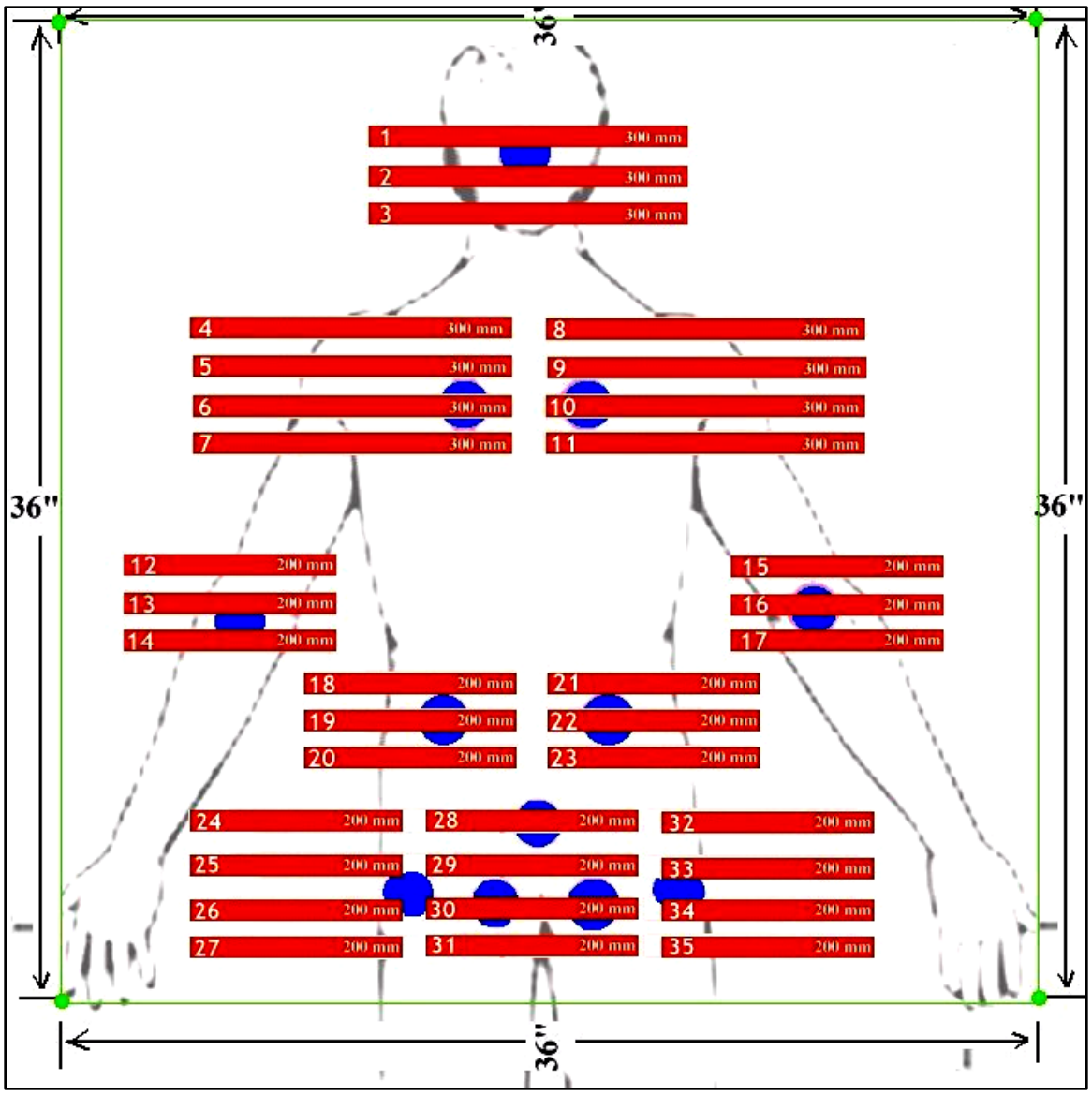

Figure 4.5: Final Sensor Layout Plan

Table 4.4: Final Layout Plan Sensor Lengths

Sensor ID#	Quantity	Detection Length (mm)
1-11	11	300
12-35	24	200

Next, a set of distances from the respective edges of the test area needed to be defined for the sensors. The sensors inside the fabric were constrained vertically in the test area due to the tubes, but were free to slide within their tubes. The level of freedom at which the sensors were to slide was dependent on the rigidity of the flat cable wiring by which the sensors were connected to the circuit board. For the purpose of testing, temporary "anchors" for the sensors were constructed by taping down the flat cable wiring outside of the test area to the table on which the prototype sheet resided with heavy duty tape, as shown in Figure 4.6. This minimized the freedom for the sensors to slide within their respective tubes.

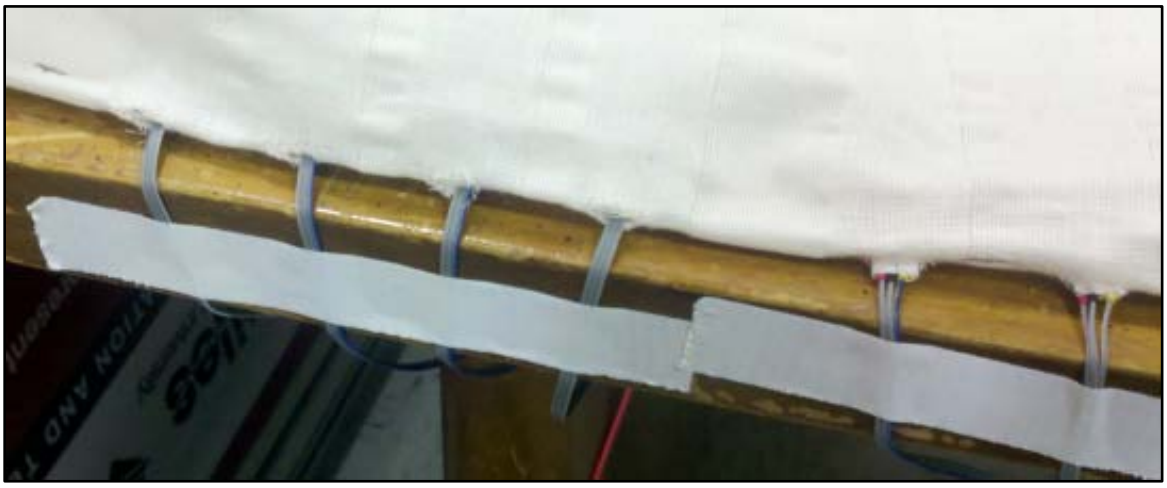

Figure 4.6: Anchoring Flat Cable to Maintain Horizontal Sensor Spacing in Tubes

The actual distances from each sensor-cluster's reference edge to a test area edge are shown in Figure 4.7. It must be clarified that the figure's focus is on the horizontal spacing, rather than the vertical spacing. While it appears in the figure that the sensors (green rectangles) touch within their clusters, they are actually separated by 3.8 cm (1.5 in) from each other's center.

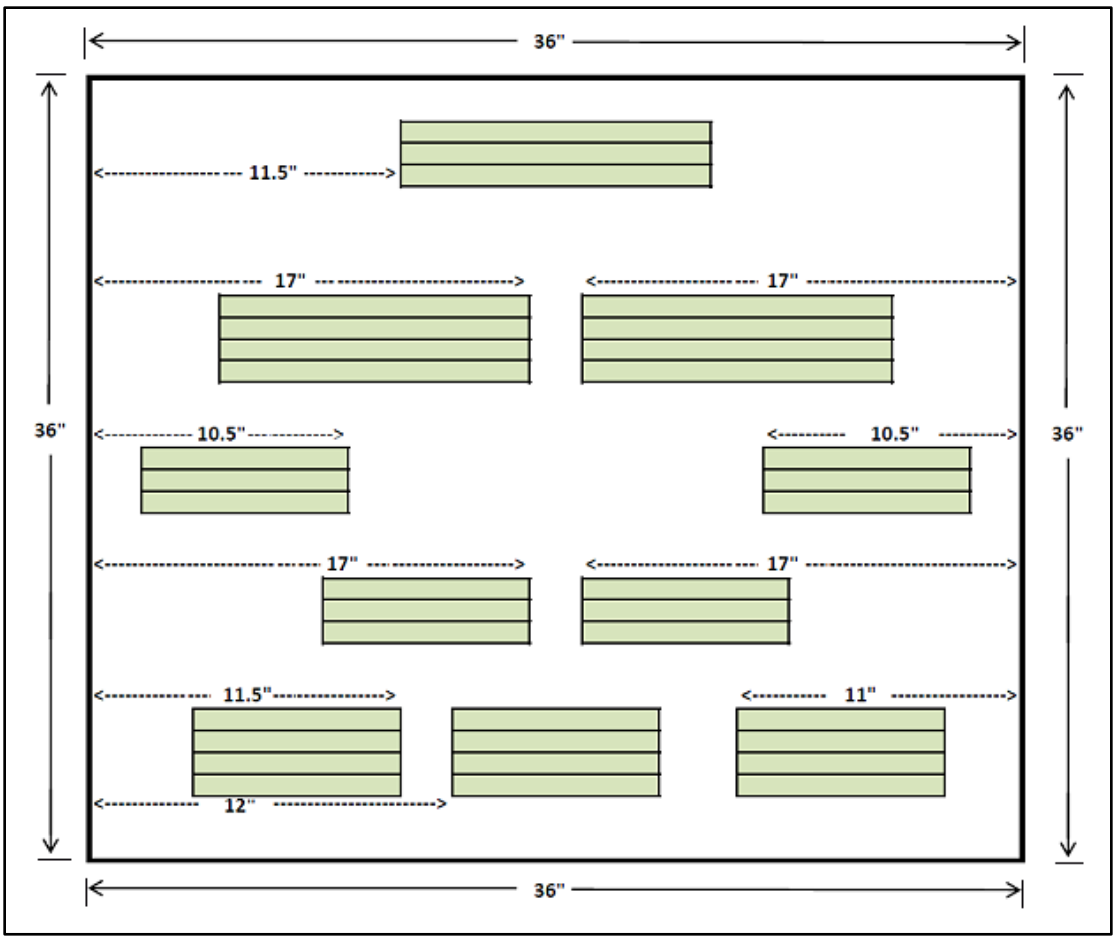

Figure 4.7: Diagram of Sensors' Horizontal Arrangement

Note that there are 17 rows of sensors in the layout. Each of these rows represents a tube woven into the test fabric where the sensors are embedded inside these tubes. The construction of these tubes is the topic of discussion in the next section.

4.2 Design of Fabric for Sensor Embedment

The next stage of research involved the design of the smart textile inside which the sensors would be embedded. The fabric would consist of two patterns of fabric construction woven together seamlessly. The resulting sheet would contain alternating sections of single-layer

fabric and double cloth. The double cloth sections served as the pockets inside which the sensors would reside.

4.2.1 Fabric Parameters

The fabric parameters for any woven fabric depend on characteristics of the loom on which the fabric is woven as well as characteristics of the yarn from which it is made. The loom settings control what type of woven structure is yielded and the yarn characteristics control how the fabric will feel and appear. The mechanical performance of the fabric may depend on both the loom settings and the yarn parameters. However, this research was not focused on testing tensile or compressive stress tests on the fabric, only the ability to implant pressure sensors.

4.2.1.1 Yarn Parameters

Two types of yarns were used in the construction of the woven fabric. The parameters for both the warp and filling yarns are listed in Table 4.5.

Table 4.5: Yarn Parameters

Direction	Yarn Count (Cotton Hanks/lb)	Fiber Type	Thread Density
Warp	20	50/50 Polyester/Cotton	37 ends/cm (93 ends/in)
Filling	24	100% Pima Cotton	32 picks/cm (79 picks/in)

4.2.1.2 Loom Settings

A Picanol PAT-A Airjet weaving machine with an Electronic Staubli Dobby was used in the College of Textiles at North Carolina State University to weave the fabric for the prototype.

The pick density was dependent on the gearing setup on the loom. The reed used to keep the ends parallel was identified as No. 46.52 with a grouping of two ends-per-dent.

There exist looms that can change the pick density electronically without the need to change gears. The Picanol PAT-A Airjet loom, however, requires changes to the gear setup to alter pick density within a fabric. Therefore, an individual program for each of the weave repeat patterns had to be created before weaving so that the loom could automatically change between single layer fabric and double cloth without machine interruption. As stated in Section 4.1.3, there were 17 rows of tubes in the test area, which means that the pattern had to be alternated 34 times to complete the 91.4 cm (36 in) of fabric. The individual programs increased the productivity of the loom and ensured that the woven tubes' sizes would be consistent.

4.2.1.3 Weave Construction

Two different weave repeat patterns were used to create the fabric. For the single layer portion of the test area, a pattern of 3x3 warp rib was used. This repeat pattern is shown in Figure 4.8. The plain weave on the left of the 3x3 warp rib is the leno weave design presentation.

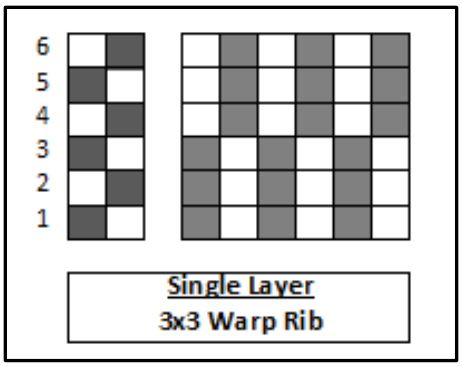

Figure 4.8: Single Layer Repeat Pattern, 3x3 Warp Rib Weave

A constraint of this particular loom involved the need for the repeat to fit into a 6-harness design. The 3x3 warp rib is identified by the 6x6-sized repeat on the right side of Figure 4.8 while the leno selvage is identified by the 6x2-sized repeat on the left side. The double cloth portion of the weave utilized a 2x1 filling rib weave for both the face and the back layers of the fabric. An individual 2x1 filling rib weave repeat pattern is shown in part A of Figure 4.9.

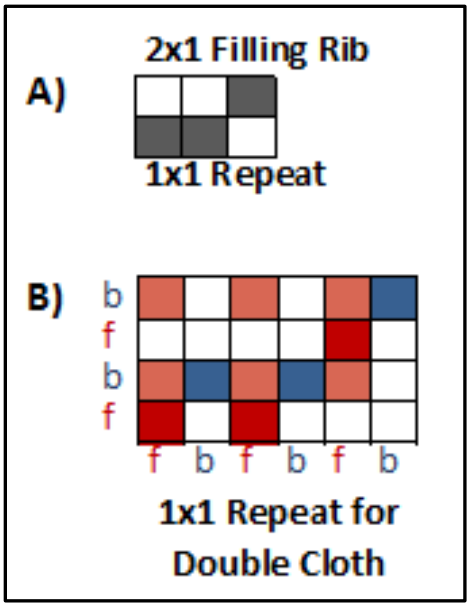

Figure 4.9: Progression of 2x1 Filling Rib Repeat into Double Cloth

In part B of Figure 4.9, the repeat pattern for the double cloth portion of the fabric is shown. Each colored square can still be interpreted to represent the warp end being above the filling yarn. The darker shade of red, corresponding to the risers of the "f" ends and "f" picks, show the pattern that creates the 2x1 filling rib for the face layer. The blue color represents the risers of the back layer weave. In order to create the blue 2x1 filling rib pattern, corresponding to the "b" ends and "b" picks for the back layer, the face ends must be lifted up. These lifts are represented by the lighter shade of red at intersections of "f" ends and "b" picks. The chain plan and draw-in draft, for the overall design of the test area, are included in Appendix E.

In order to ensure that the loom was capable of handling the aforementioned weave structures, calculations for maximum-weavability were performed. Seyam derived a formula that is applicable to fabrics woven in any weave pattern from any yarns spun from any fiber or fiber blend, shown as Equation 4.1 [39]. The equation was used to determine the value of K_2, which is the filling cover factor. The variables of Equation 4.1 are explained in Table 4.6.

$$\sqrt{1-\left\{\frac{\left(\left({}^{28M_1}/_{K_1}\right)-\left({}^{\pi}/_{4}\right)(M_1-1)\right)}{(1+\beta)}\right\}^2}+\sqrt{1-\left[\frac{\left\{\left(\left({}^{28M_2}/_{K_2}\right)-\left({}^{\pi}/_{4}\right)(M_2-1)\right\}\beta\right]}{(1+\beta)}\right]^2}=1$$

(Taken from [39])

Equation 4.1: General Maximum-Weavability Equation

Table 4.6: Description of Variables in General Maximum-Weavability Equation

Variable	Description
$\boldsymbol{M_1}$	Warp weave factor $M_1 = N_1/i_1$ Where: N_1 = number of ends per repeat i_1 = number of filling intersections per repeat
$\boldsymbol{M_2}$	Filling weave factor $M_2 = N_2/i_2$ Where: N_2 = number of picks per repeat i_2 = number of warp intersections per repeat
$\boldsymbol{K_1}$	Warp cover factor $K_1 = 28 d_1 t_1$ Where: d_1=end diameter t_1=warp density
$\boldsymbol{K_2}$	Filling cover factor $K_2 = 28 d_2 t_2$ Where: d_2=pick diameter t_2=pick density
$\boldsymbol{\beta}$	Ratio of pick diameter to end diameter $\beta = d_2/d_1$

The warp cover factor, K_1, due to the fixed warp density on the loom being 37 ends/cm (93 ends/in), was calculated to be 21.3. The ratio of pick diameter to end diameter, β, was calculated to be 0.89. M_1 and M_2 for the single-layer, 3x3 warp rib weave were calculated to be 1 and 3, respectively. Finally, solving for K_2 yielded a value of approximately 24. The need for determining K_2 was due to the flexibility of pick density on the loom. By changing

the pick gear in the loom gear setup, different pick densities can be achieved. By using the equation for filling cover factor in Table 4.6 and solving for t_2, the maximum pick density was determined to be about 47 picks/cm (117 picks/in). A safety factor of 85% was applied to t_2 to improve the insurance that the loom could handle the weave design, which resulted in a value of about 39 picks/cm (99 picks/in). The highest available pick gear setup for the loom, however, would only yield a pick density of about 32 picks/cm (80 picks/in). This value was acceptable and was chosen to be used for the weaving process. The gearing diagram is shown in Figure 8.13 in Appendix D.

By alternating between the single layer and double cloth repeat patterns, a structure was formed that contained portions of both patterns woven together seamlessly to form unstitched tubes between single layer fabric portions. A model was created with the computer program "EAT DesignScope Victor" to demonstrate a three-dimensional preview of this structure. This model is shown in Figure 4.10.

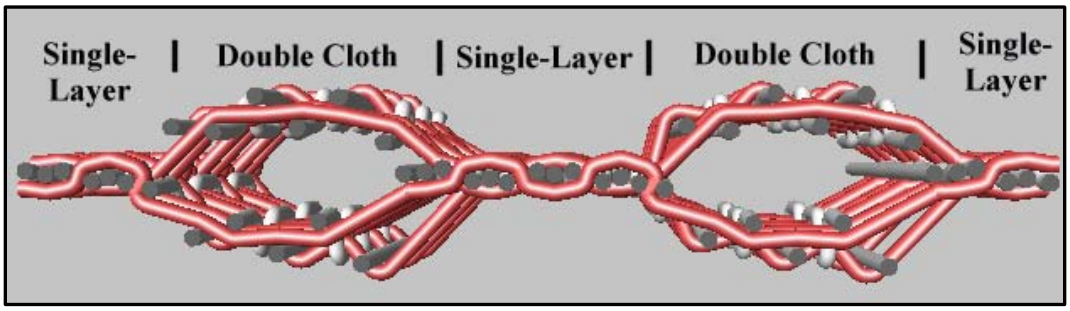

Figure 4.10: 3D Model of Alternating Single-Layer and Double Cloth in Fabric

It must be noted that the model shown does not depict the actual number of repeats to create the fabric for the prototype, but only enough to provide an example of the seamless

joining of the two weave types. The following section will describe how the sensors were embedded into the fabric's tubes.

4.2.2 Sensor Implementation

The pressure-sensing potentiometers could be inserted into the tubes by removing the selvage from the tubes or by cutting slits into the tubes near the selvages, as shown in Figure 4.11. The figure is not to-scale and should only be interpreted as how the sensor is capable of being embedded into the tube.

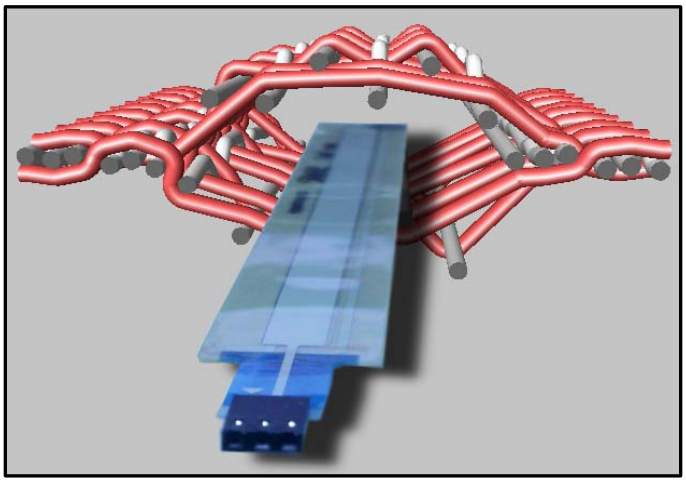

Figure 4.11: 3D Depiction of Sensor Insertion into Fabric Tube

The photographs in Figure 4.12 and Figure 4.13 show the act of inserting an individual sensor into a tube and a sensor partially inserted, minus the wire connection, respectively.

Figure 4.12: Sensor Being Inserted into Open Selvage of Tube

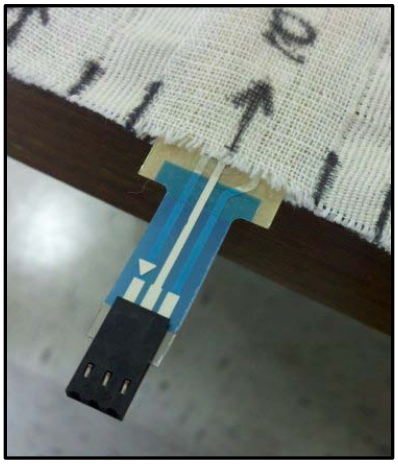

Figure 4.13: Sensor with Majority of Length inside Tube

The sensors were slid completely into their respective tubes to their respective locations according to the layout plan previously described in Section 4.1.3. A photograph of the entire system is seen in Figure 4.14. Once the sensors were set in place, the next stage of the process involved the creation of the wires by which the sensors would be connected to the electrical circuit. This would allow the computer hardware to be connected to the sensors and the software to communicate with the sensors for pressure detection. The next chapter will describe the design of the circuit and the development of the computer program needed to create a pressure sensing system.

Figure 4.14: Prototype View with Sensors Embedded

5 Circuit Design and LabVIEW Programming

The next phase of the research involved the creation of a circuit and computer detection system that could be used to manipulate analog signals from the pressure-sensing potentiometers. In order to convert an array of applied pressure points to a graphical user interface (GUI) and perform functions to create an alarm event after a set period of time of unrelieved pressure, a software package known as LabVIEW version 9.0.1, developed by National Instruments™, was used to build the programming code. This chapter will focus on describing the details of the circuit design and the development of the computer detection system.

5.1 Voltage Divider Circuit Design

The computer hardware-software bundle that was available for use for data acquisition (DAQ) in the prototype development was incapable of taking direct measurements of electrical resistance from the sensors. Therefore, the variable resistors—another way to describe the sensors—needed to have their readings converted into voltages that could be detected and manipulated by the DAQ tools. These sensors were used as voltage dividers.

A voltage divider is a circuit that produces a predicted fraction of the input voltage as the output voltage, given a known voltage input [40]. In other words, a specified input voltage could be used to determine the output voltage at various pressure points along the length of the sensor. A static resistor was required to build the voltage divider circuit as opposed to a variable resistor (i.e. potentiometer). This static resistor can be referred to as a “shunt”

resistor (R_{Shunt}) and is placed in series with the sensor (i.e. a variable resistor (R_{Var})) as seen in Figure 5.1. A list of variables and their respective definitions are seen in Table 5.1.

Table 5.1: List of Variables and their Descriptions

Variable	Description
R_{var}	Sensor Resistance (measured in ohms, Ω)
R_{shunt}	Static Resistance (measured in ohms, Ω)
I	Current (measured in amperes, commonly referred to as amps)
V_{in}	Input Voltage (measured in volts)
V_{out}	Output Voltage (measured in volts)

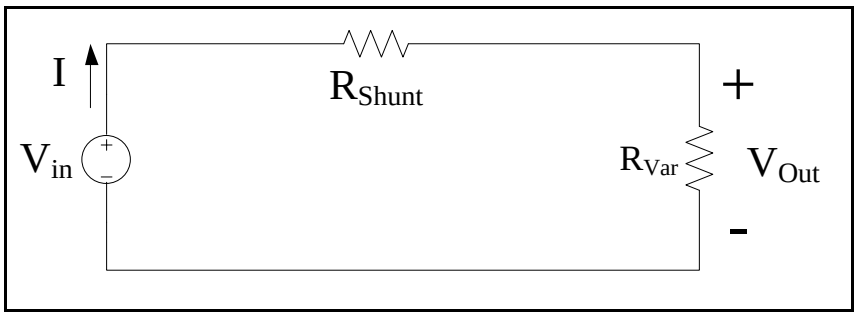

Figure 5.1: Circuit Showing Shunt Resistor in Series with Variable Resistor

The current (I) of the circuit is constant throughout the loop in Figure 5.1 which is the definition of resistors in series. Therefore, using the fact that resistors add in series (see Equation 5.1), the circuit can be reduced to an equivalent circuit with respect to the voltage source (V_{in}) as shown in Figure 5.2.

$$R = R_{var} + R_{shunt}$$

Equation 5.1: Sum of Resistors in Series

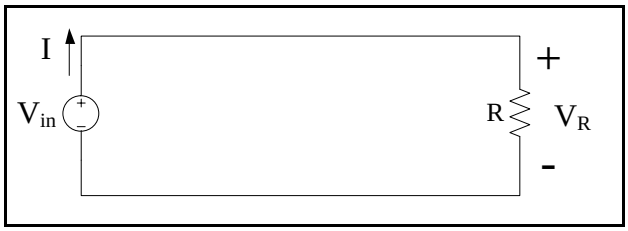

Figure 5.2: Circuit Showing Equivalent Resistance

Using Kirchoff's Voltage Law (KVL), the voltage across the equivalent resistor (*R*) is equal to the input voltage (V_{in}). Using Ohm's Law (see Equation 5.2), the current in the equivalent circuit can be determined with regard to the input voltage and equivalent resistance.

$$V_R = IR \qquad I = \frac{V_R}{R} = \frac{V_{in}}{R}$$

Equation 5.2: Ohm's Law

Replacing *R* in Equation 5.2 with the definition given in Equation 5.1 yields the current (*I*) of the circuit in both the original and equivalent circuit, as seen in Equation 5.3.

$$I = \frac{V_{in}}{R_{var} + R_{shunt}}$$

Equation 5.3: Ohm's Law with Resistance Component Extended

Therefore, given a particular R_{var} and knowing the current (*I*) through the resistor, the output voltage is defined by the voltage divider of Equation 5.4.

$$V_{out} = IR_{var} = \frac{R_{var}}{R_{shunt} + R_{var}} V_{in}$$

Equation 5.4: Output Voltage for Voltage Divider Circuit

The output voltage will always be less than or equal to the input voltage. This is why it is called a voltage divider. The base circuit developed in this research is shown in Figure 5.3.

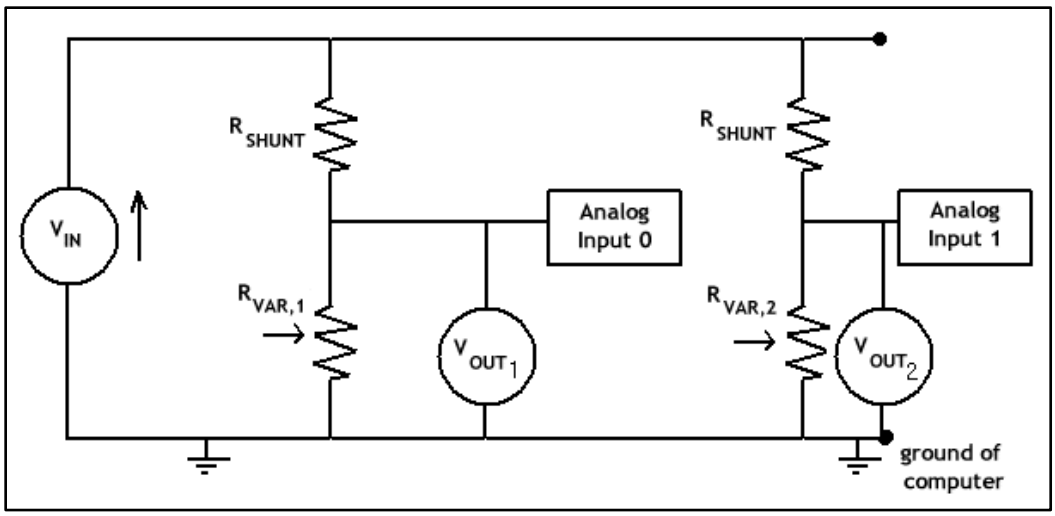

Figure 5.3: Voltage Divider Sensor Circuit Connected to DAQ Hardware

Each of the sensors will be connected to one of these circuits on a bread board connected to the DAQ hardware. The blocks identified as "Analog Input 0" and "Analog Input 1" demonstrate consecutive numbers of 0 and 1 to indicate that two connections to the hardware connector block are required for each sensor to obtain two different pressure point detections. The arrows pointing at the $R_{var,1}$ and $R_{var,2}$ resistors indicate that the resistors are potentiometers, while the R_{shunt} resistors have fixed resistance values. The V_{out1} and V_{out2} components indicate that the voltage can be measured at each respective node, which is actually what the analog input connections make the DAQ hardware capable of doing.

A spreadsheet (see Appendix F, Figure 8.19 and Figure 8.20) was developed to help determine the shunt resistance value previously mentioned. Each of the sensors used were rated at 10 kΩ of resistance. Therefore, intervals of values ranging from 0 to 10 kΩ were plotted on a graph versus the output voltage of the voltage divider circuit. With the input voltage set as five volts, the first shunt resistance tested was 10 kΩ. The success of the test depended on how close the R^2 value of a linear model predicted by Microsoft® Excel came

to a value of 1. The graph for the resistance versus the output voltage is shown in Figure 5.4 for the 10 kΩ shunt resistor.

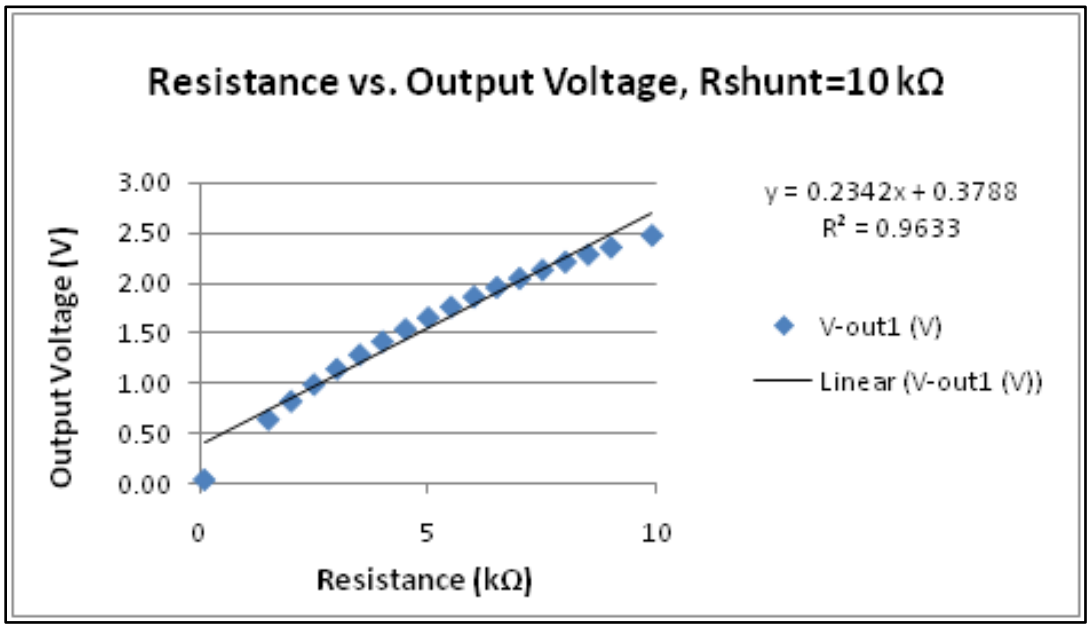

Figure 5.4: Resistance vs. Output Voltage (10 kΩ Shunt Resistance)

The R^2 value for the linear model was found to be 0.9633. A second graph was formulated to predict the output voltage if the shunt resistance was set to 100 kΩ. This graph is shown in Figure 5.5 and the resulting R^2 value calculated by Excel was 0.9993.

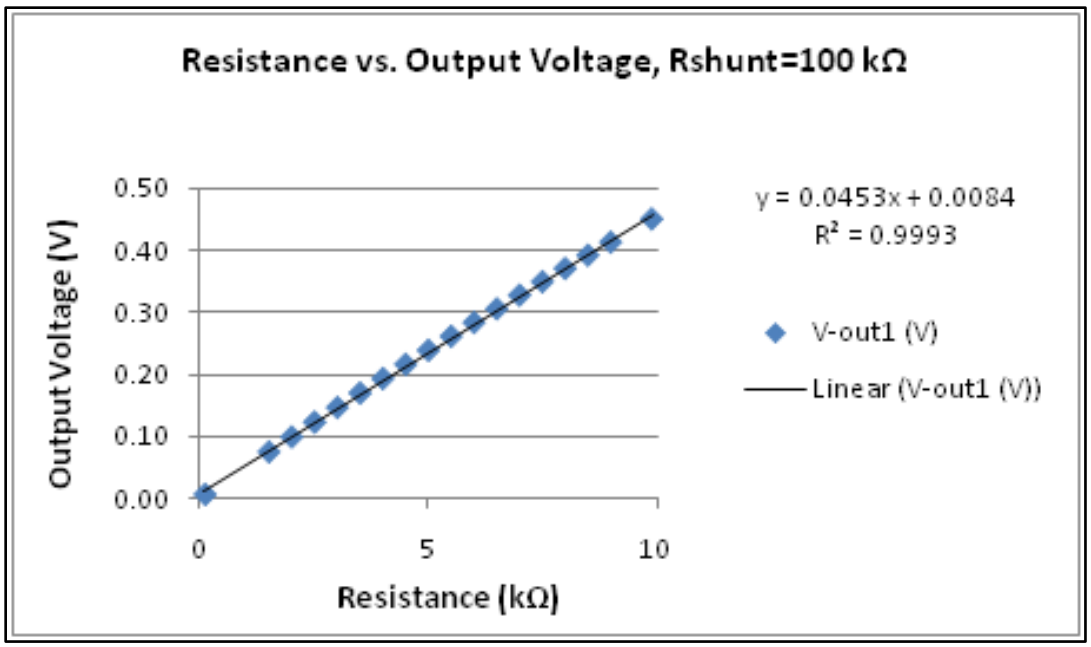

Figure 5.5: Resistance vs. Output Voltage (100 kΩ Shunt Resistance)

Both visually and mathematically, the 100 kΩ shunt resistor allows the linear model to fit the predicted voltage values significantly more closely than the 10 kΩ shunt resistor. There is inherent variability in R_{var} (the sensor) and the effect of this variability is decreased as the value of the shunt resistor is increased. These results led to the decision to use 100 kΩ shunt resistors in the circuit so that the pressure location along the length of the sensors could be more accurately detected and presented on the computer program.

5.2 DAQ Hardware

The input voltage was set at five volts, which is the value of voltage available on many commercially available DAQ boards as the set voltage source value. Due to the number of sensors used in this prototype being 35, a single DAQ board must be able to accommodate 70 analog inputs for the entire prototype to be operational simultaneously (i.e. two values per

sensor). One of the DAQ boards offered by National Instruments™, the NI PCI/PXI-6225, has 80 analog inputs as well as two pin connections dedicated to +5 volts of source voltage [41]. The pinout diagram for the PCI/PXI-6225 is shown in Figure 5.6.

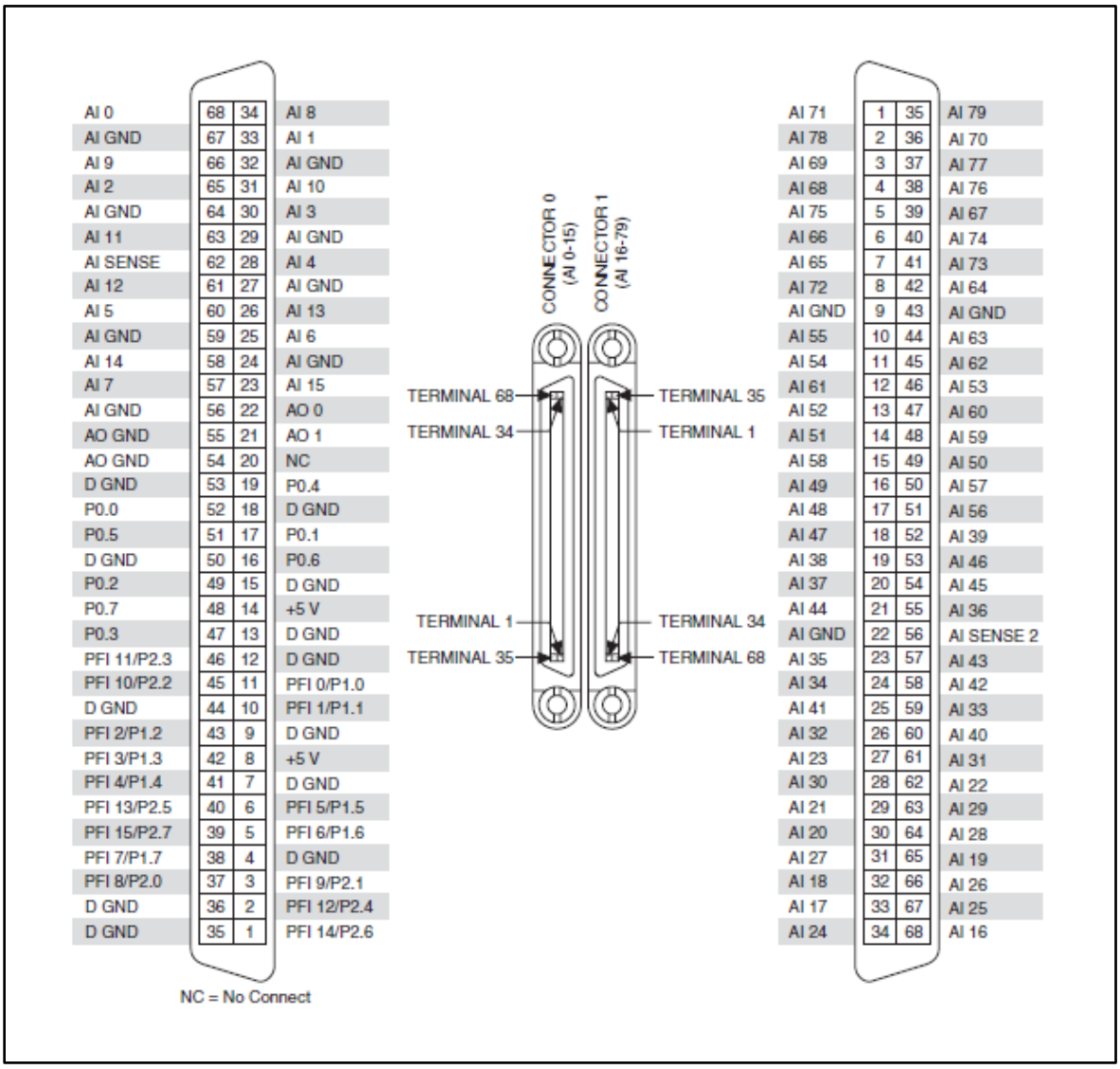

(Taken from [41])

Figure 5.6: National Instruments™ PCI/PXI-6225 DAQ Pinout

DAQ boards also have an analog output connection that allows the voltage source to be specified, which is the method that was used to supply five volts to the sensors' circuits in

this research. The DAQ board that was used for testing and development of the prototype was a NI PCI-6221 from National Instruments™, which had been used within the college on a previous research project and was available. The PCI-6221 has 16 analog inputs, which can be reflected in Figure 5.7.

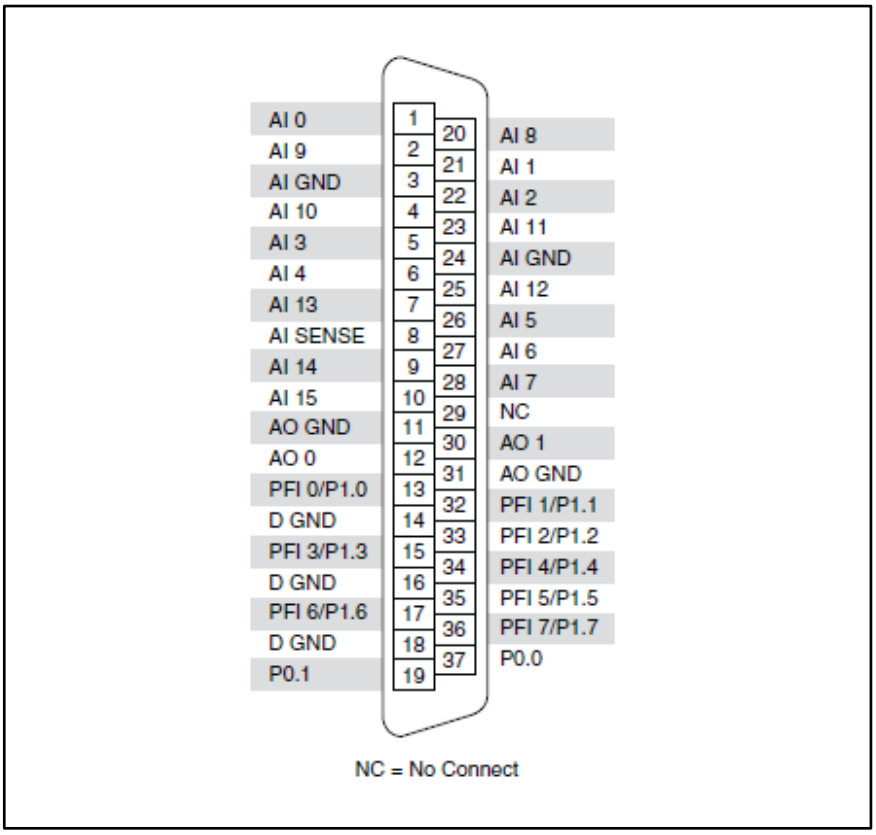

(Taken from [41])

Figure 5.7: National Instruments™ PCI-6221 DAQ Pinout

Considering that each sensor utilizes two analog inputs, this DAQ board allows for up to eight sensors to be connected and tested simultaneously. Note that in the PCI-6221 there is no dedicated connection for a voltage source fixed as five volts. Pin 12, identified as "AO 0" is used to supply a voltage that can be user-specified via a computer program. In order to connect the sensor system to this DAQ board, custom wiring needed to be prepared from

several commercially available components. This process will be described in the next section.

5.3 Construction of Custom Wiring

The first step in developing the custom wiring for the sensor system was to determine the lengths of the wires to be fabricated. Length measurements were taken that led from the sensors' terminal ends to the edge of the test area. These lengths were added to the length from the end of the sensors' respective tubes to the DAQ board. A value of 30 cm (12 in) was added to each of the measurements to ensure that the wiring would be relaxed, as opposed to under unwanted tension. Some sensors' terminal ends were closer to the left side of the test area and others' were closer to the right side of the test area. The reasoning for this will be described in further detail in Section 5.4. For those sensors with left-end terminals, a length of 107 cm (42 in) was added to account for the width of the table under which the wires were routed to reach the DAQ board. For each cluster, the same length was used for each sensor within that cluster. The clusters and their respective wiring lengths for each sensor are seen in Figure 5.8. The red arrows on the left side of the figure indicate that the wires led back under the table to reach the DAQ board and the red arrows on the right side of the figure indicate that the wires led down the right edge of the test area toward the DAQ board.

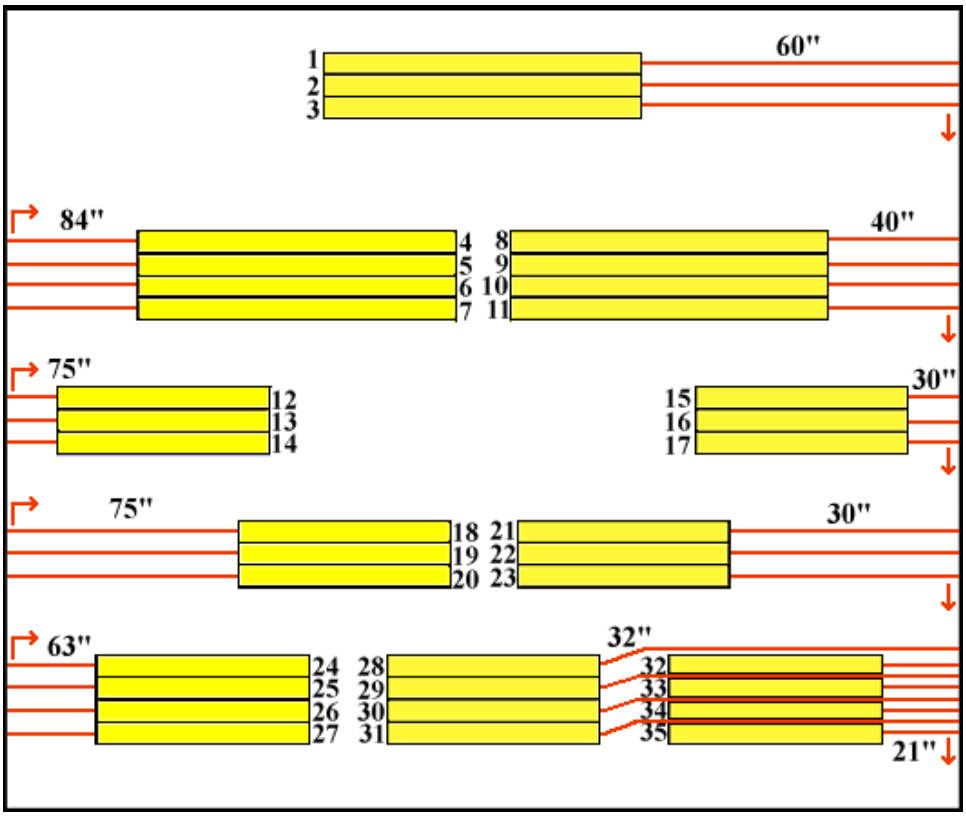

Figure 5.8: Wiring Lengths for Sensor Clusters

The next step involved choosing commercially available materials to fabricate the wires. Each of the sensors required three separate wire connections. With a total of 35 sensors in the layout, multiplying 35 by 3 resulted in 105 separate conductors of wire required to connect all of the sensors to their respective circuits. To avoid such a large number of standalone wires, flat ribbon cable was chosen to reduce the number of components connected to each sensor from three to one. While there were still three connections to the sensors, the 3-conductor ribbon cable reduced clutter and ensured that each of the wires within the ribbon would stay bundled together and avoid potential confusion related to the origin of the wires when the procedure called for the opposite ends to be connected to their

appropriate circuits. The flat cable purchased from distributor Digi-Key® Corporation was manufactured by 3M™ Electronics and contained six conductors. The cable was separated down the middle to obtain the desired 3-conductor wire. Another component needed to fabricate the wires was heat-shrink tubing. There were three colors (red, black and yellow) chosen to differentiate between the different wires within each ribbon cable. The tubing was manufactured by 3M™ and is described as a flexible polyolefin. The tubing would also serve the purpose of keeping an intimate contact between the conducting strands of the ribbon cable and the solid copper wire. The solid copper wire was needed to improve the connection of the wiring to an electrical breadboard and to the sensors' terminals as well. The solid copper wire was manufactured by Consolidated Electronic Wire & Cable.

The next step was to cut the cable to the lengths shown in Figure 5.8 and begin the soldering process. The three wires in the cable were pulled apart from one another to about 2.5 cm (1 in) each, just enough to be able to interact with each wire individually. About 7 mm (0.25 in) of the insulating jacket of each wire was stripped from the tip, as shown in Figure 5.9.

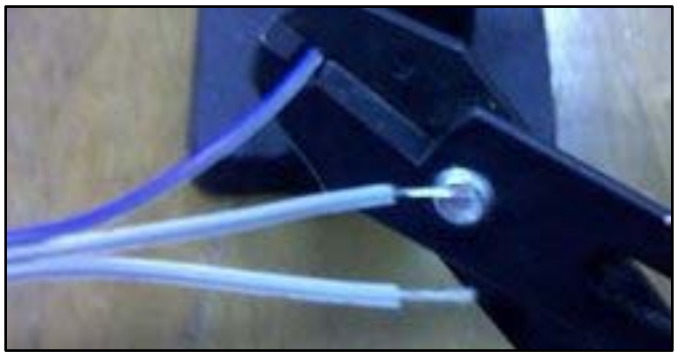

Figure 5.9: Stripping Insulation Off of Wires

Then, each of the exposed conductive wire strands were soldered to about 2 cm (0.75 in) of the solid copper wire, as seen in Figure 5.10. The cutting of the wire after soldering had cooled to room temperature and solidified is seen in Figure 5.11.

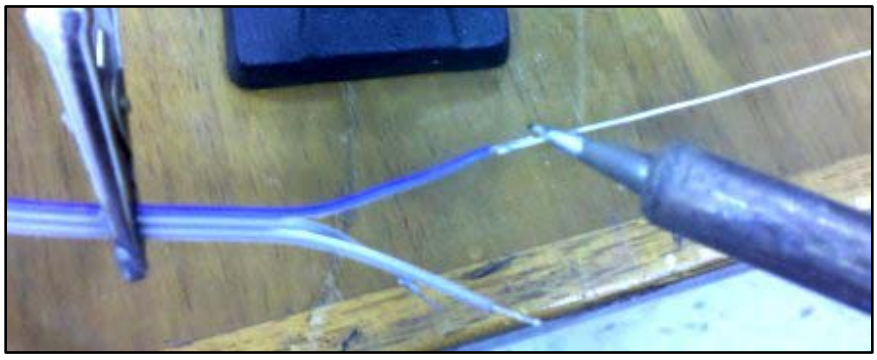

Figure 5.10: Soldering Solid Copper Wire to Conductor Strand of Ribbon Cable

Figure 5.11: Cutting Soldered Solid Copper Wire to Length

Once each of the three conductor strands had been soldered to the pin of solid copper wire, heat-shrink tubing was applied. Each of the soldered wires was threaded through a tube of their respective color. The tubing was cut to lengths of about 2 cm (0.75 in) and carefully placed so that it covered the entire soldered area of the wire. One end of the tubing covered

part of the insulating jacket of the ribbon cable and the other end covered part of the solid copper wire, as seen in Figure 5.12.

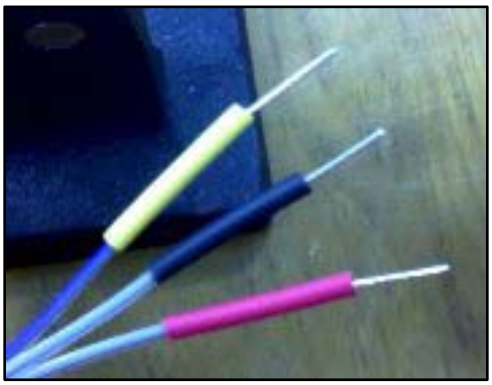

Figure 5.12: Heat-Shrink Tubing Before Heat Gun

At this point, a heat gun was used to direct heat at the tubing so that the tubing would collapse inward to hold the soldered components together and also provide insulation for the soldered area, as seen in Figure 5.13.

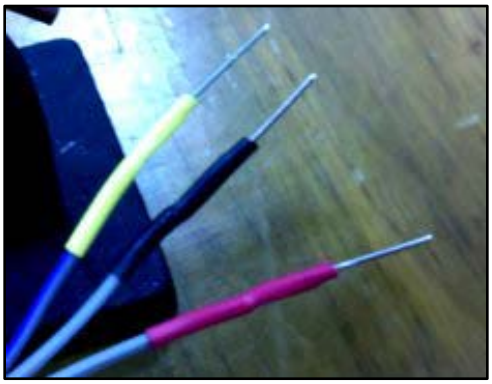

Figure 5.13: Heat-Shrink Tubing After Heat Gun

The same procedure just described was performed to create all 35 desired ribbon cables. Considering that each ribbon cable had two ends, and consequently six total wire ends, a total of 210 soldered wires were completed. The next step involved connecting these wires to the

system of circuits housed on a breadboard that would bridge the connection into the DAQ hardware.

5.4 Connecting Sensor System to DAQ Hardware

In order to understand the circuit wiring diagram, it is important to understand the layout of a breadboard. The breadboard used in this research contains hundreds of pinholes that can have various electrical components connected to them. A blank breadboard is seen in Figure 5.14.

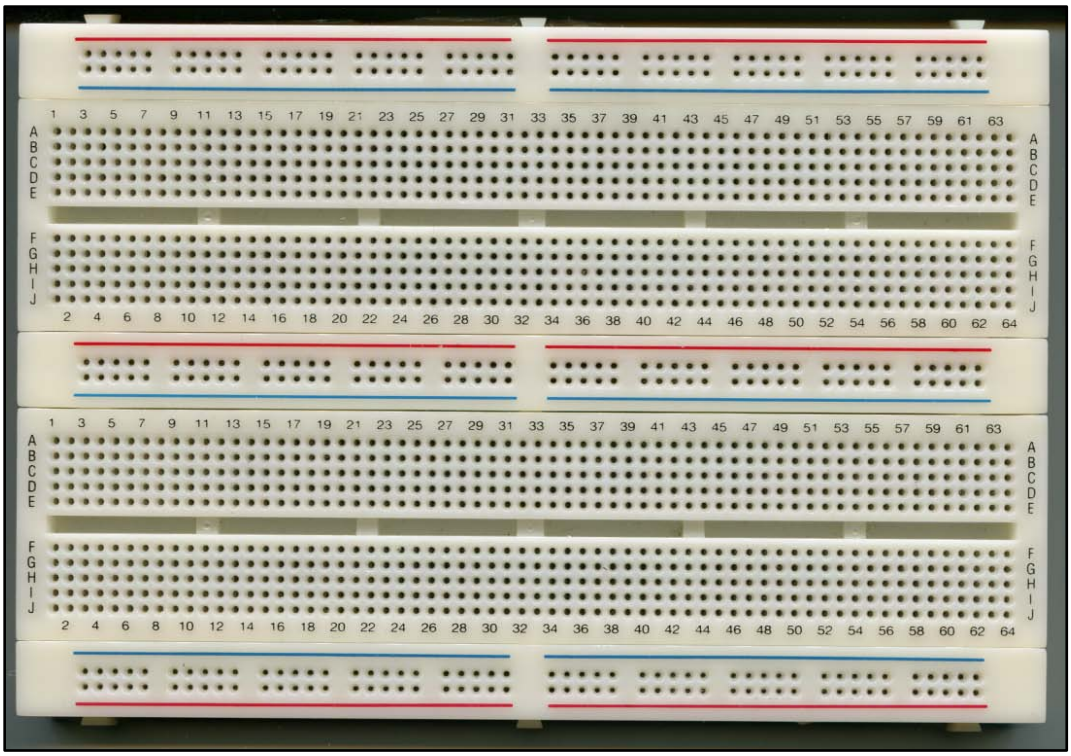

Figure 5.14: Blank Electrical Breadboard

This particular breadboard contains 140 nodes, which represent groups of pinholes that share an electrical connection. There are 128 vertical nodes and 12 horizontal nodes, with

examples highlighted by red rectangles in Figure 5.15 and Figure 5.16, respectively. If multiple nodes are connected to one another with a wire, then they have combined to become a single node.

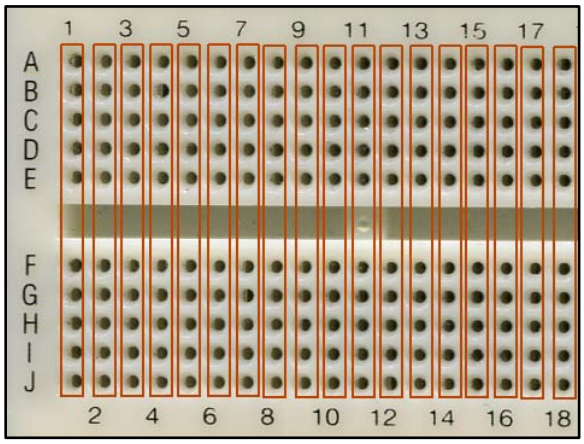

Figure 5.15: Highlighting 18 Vertical Nodes on a Breadboard

Figure 5.16: Highlighting 4 Horizontal Nodes on a Breadboard

The wiring diagram for the sensor system is depicted in Figure 5.17. While the diagram appears to contain one complex circuit, there are actually 16 separate circuits housed by the same breadboard and connector block. The columns of dots represent separate nodes and are uniquely numbered on the diagram. The sensors' corresponding connections to the connector block are indicated by alternating pairs of yellow and red wires, with identifiers for the sensors underneath. The color difference is meant to assist the reader in tracking connections between the breadboard and the connector block terminals. The green wires represent the voltage source connection to each of the 16 circuits. The small blue wire connecting the two horizontal nodes at the top of the breadboard allows the voltage source

connection to be shared among those two nodes to which the top end of the green wires are connected. The two horizontal nodes at the very bottom of the breadboard are also connected by a small blue wire, resulting in a single node. This node represents the ground of the circuits to which the sensors' ground wires are connected during testing. Longer blue wires on the diagram show how this node is connected to the analog input ground terminal of the connector block. The peanut-shaped components that arch over the middle row of horizontal nodes each represent the single 100-kΩ shunt resistor for each circuit.

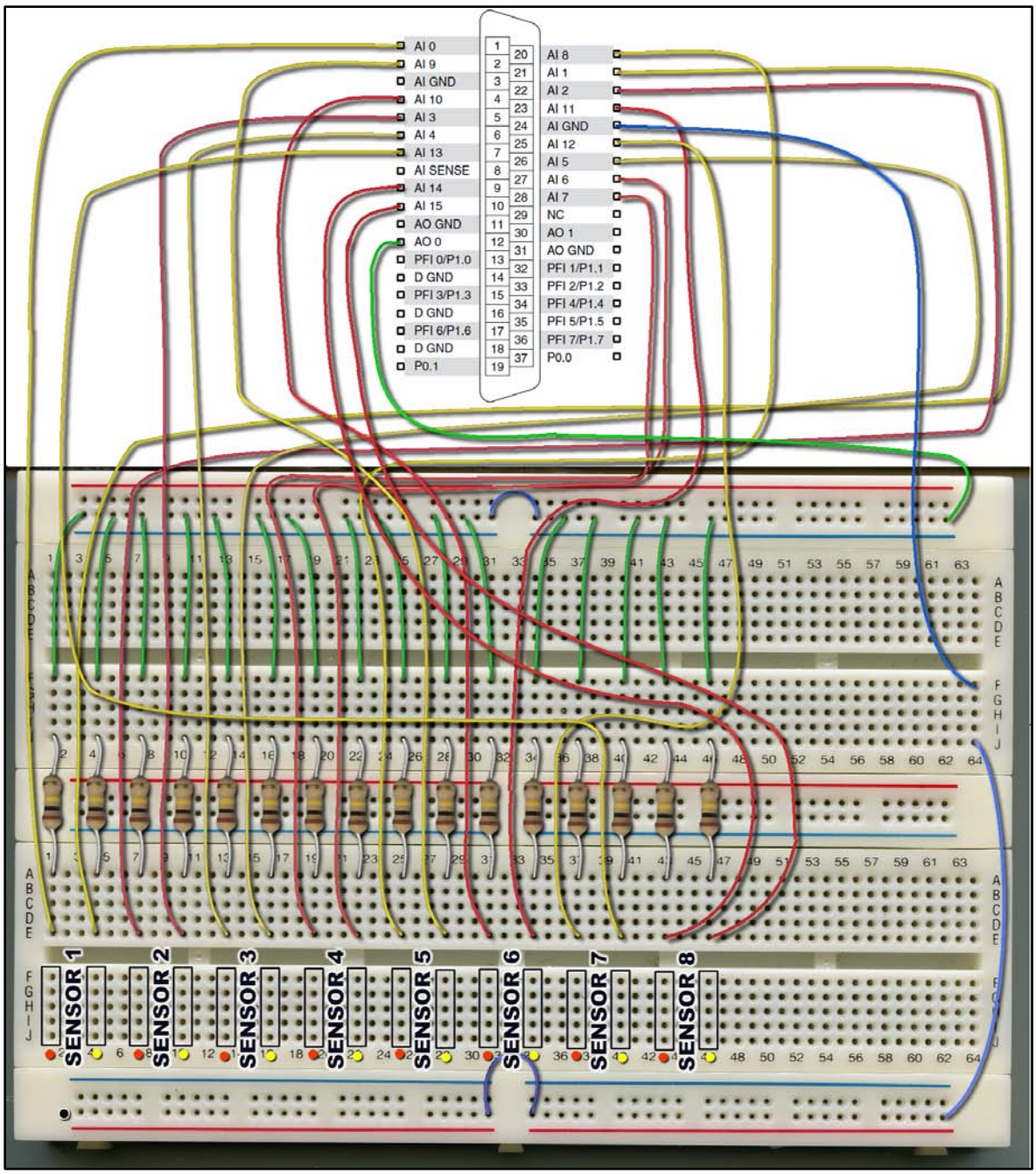

Figure 5.17: Wiring Diagram for Sensor System

Each of the ribbon cables connecting the sensors to the breadboard contains three wires. Of these three wires, two are used to transfer the two voltage readings from the sensors and

one is the ground wire. The ground wire is connected to the ground node on the breadboard, identified by a black circle on the bottom left corner of Figure 5.17. Of the other two wires, one is colored red and the other yellow, as seen surrounding each of the eight sensor identifiers. These red and yellow wires are connected to their respective nodes, highlighted by black rectangles and either red or yellow circles in Figure 5.17. The opposite end of the 3-conductor ribbon cable is attached to an individual sensor. In some cases, the wire connection involves a left-end terminal as seen in Figure 5.18, and in the remaining cases the connection is reversed, as seen in Figure 5.19. The difference between the two connections is that the red wire is switched with the yellow wire.

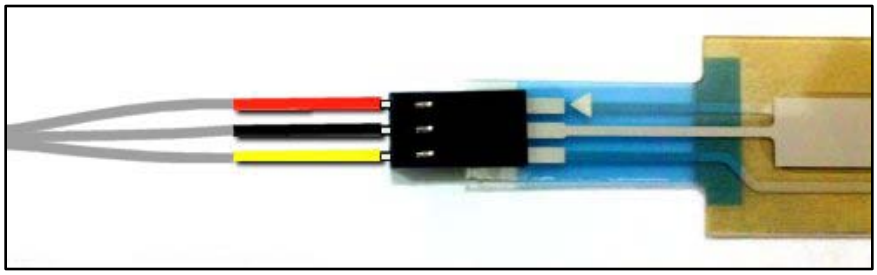

Figure 5.18: Wire Connection to Sensor (Left-end terminal)

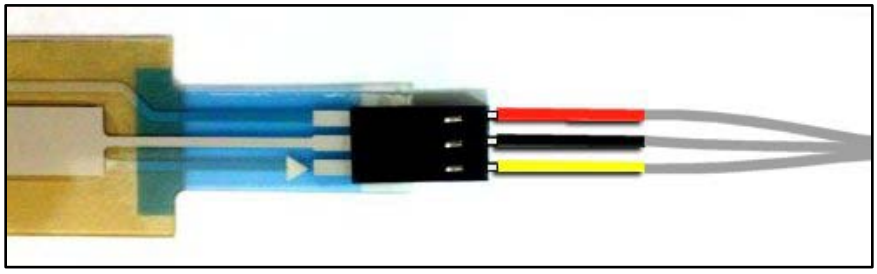

Figure 5.19: Wire Connection to Sensor (Right-end terminal)

The wire connections made with the sensors needed extra support to prevent slipped while inside the bed sheet. Therefore, heavy duty tape was wrapped around the junction of the wires and the connection housing on their respective sensors. The number identifier for

each sensor was marked on the tape, as seen in Figure 5.20 for sensors *26* and *27*, for example.

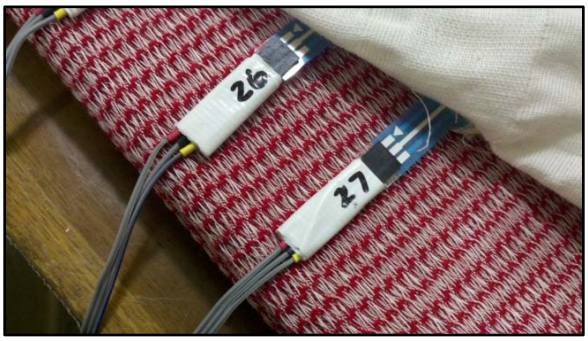

Figure 5.20: Taping of Wire Connection with Sensor

The sensors corresponding to each wiring order is seen in Figure 5.21. The blue sensors have left-end terminals and the red sensors have right-end terminals. This reversal of red and yellow wiring at the sensor end of the ribbon cable allows for the connection color sequence on the breadboard to stay constant, with the red wire always connected to the first node and the yellow wire connected to the second node for each sensor.

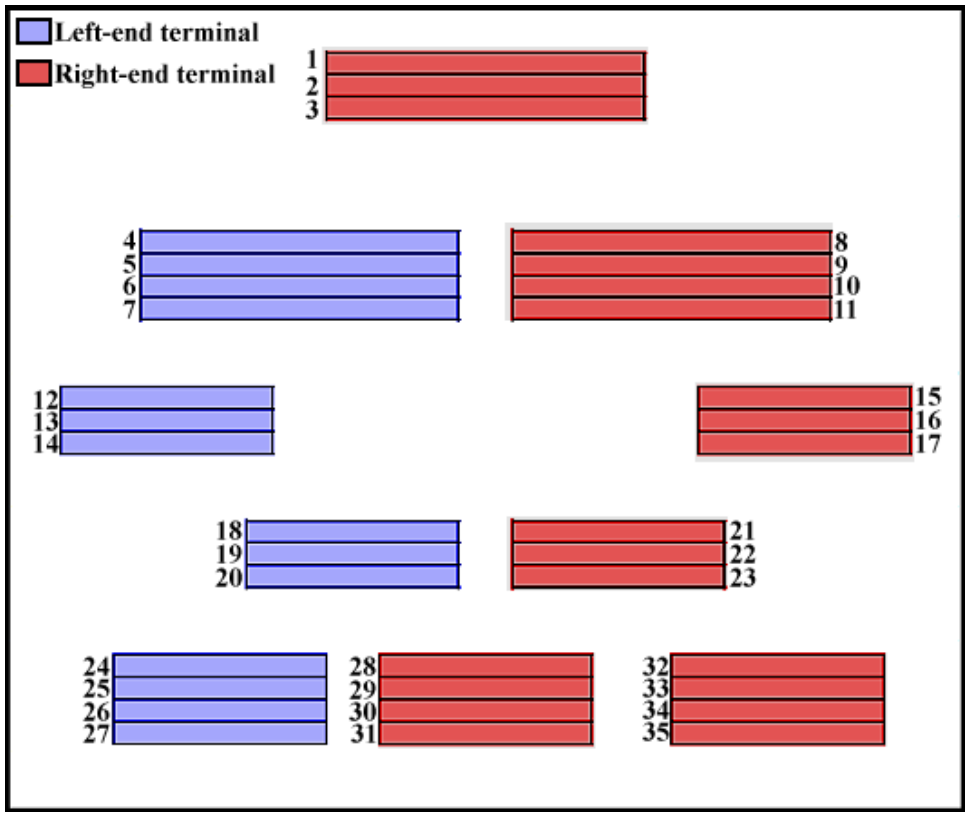

Figure 5.21: Identification of Left- and Right-End Terminal Sensors

These electrical connections between the sensors and the DAQ connector block were essential for a computer detection system's capability to read, manipulate and convert the voltages into information that could be understood by the end user.

5.5 LabVIEW Programming

In order for the sensors' voltage readings to be sampled and converted into usable and readable data, a computer detection system was developed, using the LabVIEW software, that could be used see pressure points exerted on the prototype sheet in real-time. The code pictured in Figure 5.22 shows the portion of the LABVIEW code that controls the GUI that

can be seen on the computer screen. The components seen in Figure 5.22 are described in Table 5.2 along with the parameters associated with each component.

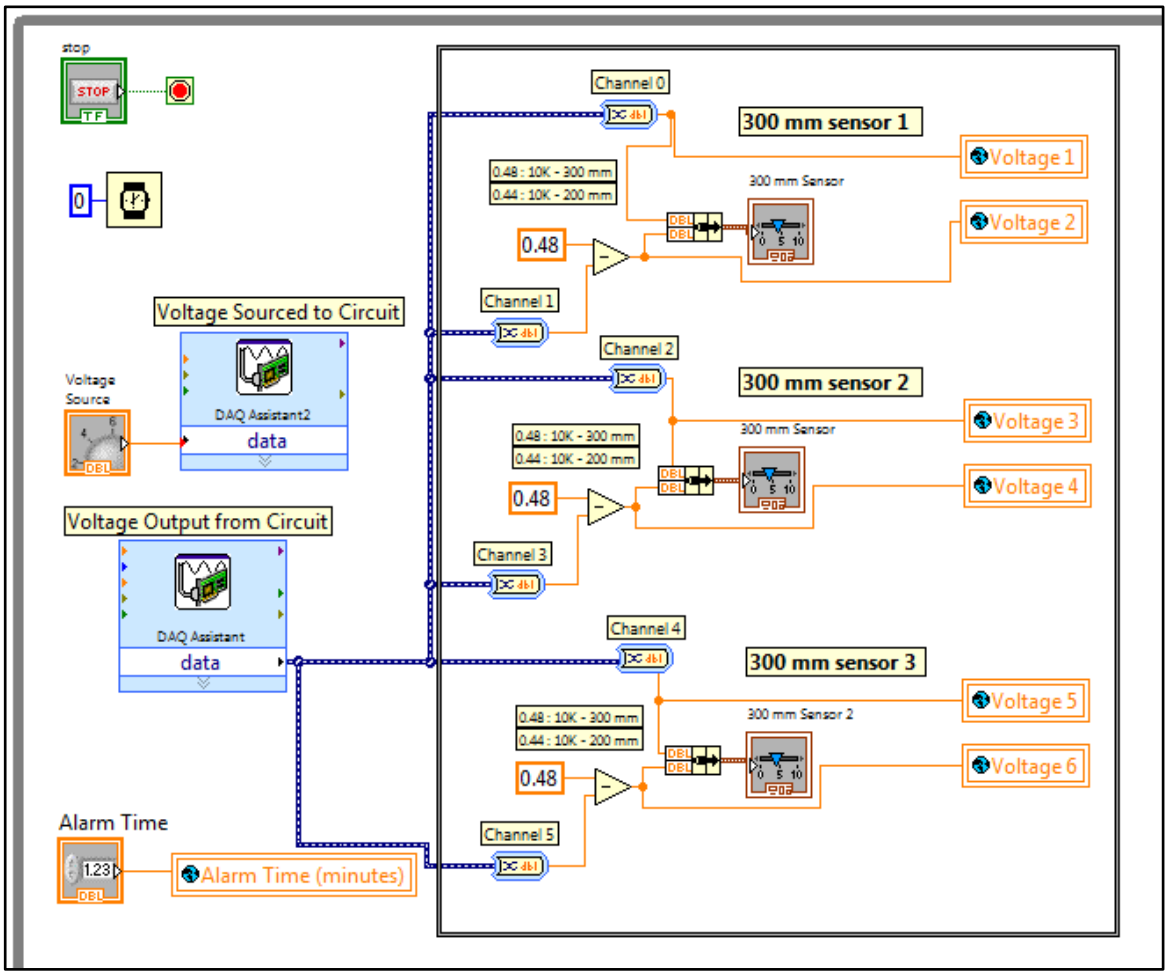

Figure 5.22: Portion of Code for "Test 1.vi" for Displaying Sensor Readings

Table 5.2: Definitions & Parameters of Components of GUI Display Code

Code Component	Definition & Parameters
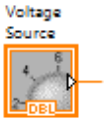	**<u>Voltage Source Control</u>** User inputs amount of voltage to be supplied to the circuit. This control is wired to the DAQ Assistant icon as input data

Table 5.2 Continued

Code Component	Definition & Parameters
	**DAQ Assistant for Voltage Source** This transmits information via analog output on DAQ hardware. The circuit is wired to the analog output terminal on the hardware and this tool converts the numerical value supplied by the user on the Voltage Source Control object to a voltage that powers the circuit. ***Parameters*** • Terminal Configuration: RSE (Referenced Single End) – The measurement is made with respect to the ground. • Timing Generation Mode: 1 Sample (On Demand) – This specifies that the task will generate one sample. • Signal Output Range: Max = 5, Min = 0 • Scaled Units: Volts • Channel: Analog Output 0 – Labeled as "AO 0" by DAQ hardware manufacturer
	**DAQ Assistant for Voltage Output** This retrieves information via analog input on DAQ hardware. The circuit is wired to the analog input terminals on the hardware and this tool converts the voltage to a dynamic data value that feeds into the Convert from Dynamic Data tool. ***Parameters*** • Terminal Configuration: RSE (Referenced Single End) – The measurement is made with respect to the ground. • Timing Acquisition Mode: Continuous Samples – This specifies that the task will acquire data until stopped. • Samples to Read: 1 • Rate (Hertz): 100 • Signal Input Range: Max = 5, Min = 0 • Scaled Units: Volts • Channel: Analog Input 0-15 – Labeled as "AI 0" through "AI 15" by DAQ hardware manufacturer o 16 total inputs retrieving voltage data from circuit
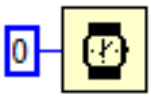	**Wait (milliseconds) Function** The value of "0" tells the program to wait 0 milliseconds (ms) and forces the current thread to yield control of the CPU.

Table 5.2 Continued

Code Component	Definition & Parameters
	**Convert from Dynamic Data** This takes the data from the DAQ Assistant for Voltage Output and converts a dynamic value from one analog input channel to a floating point number (double). For each sensor, there are 2 of these converters because two readings are obtained per sensor. This tool can only convert one channel, so several of these are connected to the DAQ Assistant for Voltage Output. ***Parameters*** • Resulting data type: Single Scalar – One scalar value is the result of the conversion. • Scalar Data Type: Floating point numbers (double) • Channel: 0-15 o Dependent on sensor
	**Minus Function** The sensors read voltages inward from both ends. In order to create a visible pressure point on the GUI indicator that is representative of the true pressure location, the measured voltage is subtracted from the maximum voltage, which is set for 0.48 V for 300-mm sensors and 0.40 V for 200-mm sensors, based on empirical measurements.
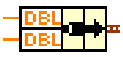	**Bundle Function** This assembles a cluster of floating point data from multiple individual elements. The bundled data is a type of array. For each sensor, one bundle function is used to pair both voltage readings together. The output of this leads to both the Global Variable and the Horizontal Bar Indicator
	**Voltage to Global Variable** By sending the voltage readings to a global variable, the readings can be retrieved by multiple VIs.
	**Horizontal Bar Indicator** The indicator is capable of displaying multiple floating point values along its length. This research applies one indicator per sensor, so two voltage readings are displayed on the GUI indicator. These voltages represent the pressure points on the sensor.
	**Alarm Time Control** The user inputs a time value, in minutes, which will result in an alarm event based on specific criteria once that time has passed.
	**Alarm Time to Global Variable** By avoiding hard-coding to the alarm section of programming and sending the time value to a global variable, the alarm time setting can easily be changed and applied to all sensors in one step.
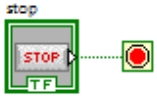	**Stop Button** The stop button on the GUI is connected to the "stop" code to exit the running program code.

The code pictured in Figure 5.23 shows the portion of the LABVIEW code that controls the clock counter that can be seen on the computer screen beside the horizontal indicators as well as the code that controls whether the alarm indicator is active. The components seen in the figure are defined in Table 5.3 and the context in which each is used is described. The code shown in Figure 5.23 only depicts the code for one voltage reading from one sensor. This code, with exception to the "Voltage 1", the "Time (sec)" and "True/False" components, is exactly the same for every voltage reading in each test's visual instrument and can be copied. These three components are unique for each of the sensing elements.

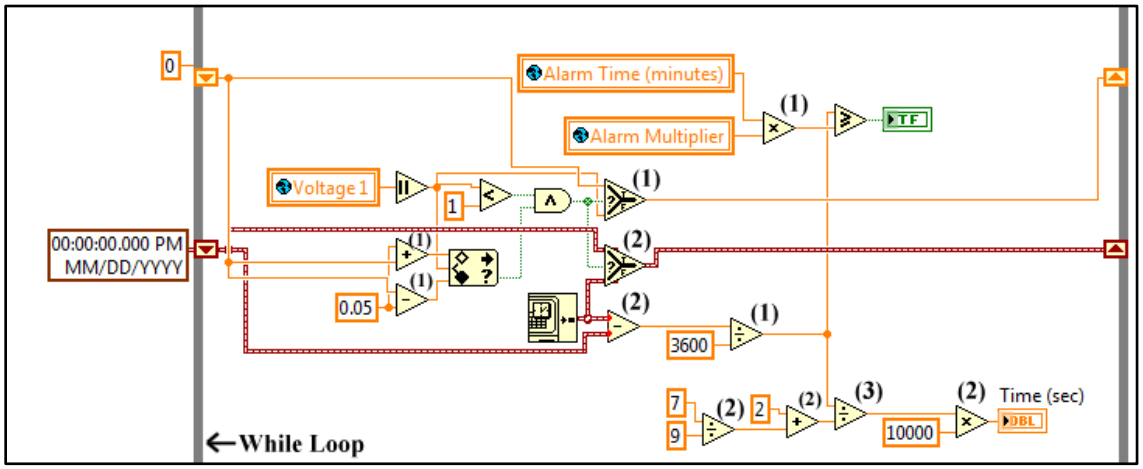

Figure 5.23: Example Code from "Test 1.vi" for Clock Counter and Alarm Status

Table 5.3: Definitions & Parameters of Components of Clock and Alarm Status Code

Code Component	Definition & Parameters
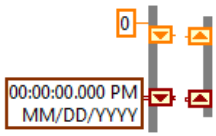	**Shift Registers** These are used to pass values from a previous iteration through the while loop to the next iteration. The left terminals of the two shift registers (one shift register is orange and the other is burgundy) shown here are connected to the initial values "0" and the "absolute time stamp," which are used for the first iteration. The right terminals store data on the completion of an iteration and passes that data to the left terminals for the next iteration, and so on. The significance of the initial values will be explained in context of the code components for which they are used.
	**Global Variable to Voltage** The VI retrieves the voltage value from the global variable.
	**Global Variable to Alarm Time Setting** The VI retrieves the alarm time setting from the global variable.
	**Global Variable to Alarm Time Multiplier** The VI retrieves the alarm time multiplier value from the global variable.
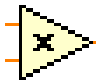	**Multiply Function** This function multiples the two input values and yields the resulting value. There are 2 instances of the Multiply function: (1)With the current sample rate settings, a value was required to ensure that the alarm time and the clock counter were synchronized to avoid false alarms. The time synchronization ensured that the alarm would be activated at the correct time. The alarm time multiplier value was set in the global variable as 0.0166. (2) The result of the third instance of the Divide function is multiplied by the value 10,000. The resulting value represents the number of seconds that have elapsed since the current pressure point detected by the sensor has been within the range defined by the "In Range and Coerce" function described below.
	**Absolute Value Function** The absolute value of the input value is returned by the function. The input value is the voltage value read from the sensor defined by "Global Variable to Voltage," above.
	**Less Than? Function** This returns "TRUE" if the first input is less than the second input. Any other case yields a "FALSE" value. While a pressure is being exerted on the sensors, the circuit design does not allow a voltage value of greater than 1 to be returned. This function will return a "FALSE" value if no pressure is detected by the sensor.

Table 5.3 Continued

Code Component	Definition & Parameters
	**Subtract Function** This function subtracts the value of the second input from the value of the first input. The result of the subtraction is yielded. There are 2 instances of the Subtract function: (1) The value 0.05 is subtracted from the value inherited from the left terminal of the orange shift register. (2) The value inherited from the left terminal of the burgundy shift register is subtracted from the timestamp produced by the "Get Date/Time in Seconds" function described below.
	**Addition Function** This function adds the two inputs together, yielding the result of the addition. There are 2 instances of the Addition function: (1) The value inherited from the left terminal of the orange shift register is added to the value 0.05. (2) The value 2 is added to the result of the second instance of the Divide function.
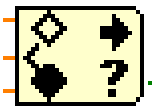	**In Range and Coerce Function** This function has 3 inputs. It determines whether the value of the second input falls within the range specified by the upper limit (first input value) and the lower limit (third input value). If the second input value falls within the range, then a Boolean value of "TRUE" is yielded, otherwise a "FALSE" value is yielded. ***Significance*** This function allows for a ±0.05 volt range to exist. When the voltage reading exists within this range, the voltage can change without the clock counter being reset. This prevents the clock counter from resetting when the patient slightly moves on the pressure sensor without actually relieving the pressure. If the voltage changes to a value outside of the ±0.05 volt range from the previous voltage measurement, then the value will yield a "FALSE" Boolean value.
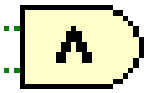	**And Function** Two inputs are of Boolean type. If both input values are "TRUE" then the function yields a "TRUE" value. Any other case will yield a "FALSE" value. The inputs analyzed here are the outputs yielded from the "Less Than?" and the "In Range and Coerce" functions above. If both inputs are "TRUE," then it means that the voltage value has not changed by more than 0.05 volt and the voltage value is less than 1 volt, indicating that there is a pressure being exerted on a localized position on the sensor.

Table 5.3 Continued

Code Component	Definition & Parameters
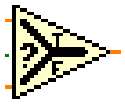	**Select Function** This function takes 3 inputs, 2 of which are numerical values and the third being a Boolean value. The code uses two of these functions: (1) The first numerical input is the value given by the left terminal of the orange shift register. The second numerical input is the output of the absolute value function applied to the voltage reading. The Boolean input is the output of the And function described above. The output of this function feeds to the right terminal of the orange shift register. (2) The first numerical input is the value inherited by the left terminal of the burgundy shift register. The second numerical input is the value output by the "Get Date/Time in Seconds" function described below. The Boolean input value is the output of the "And" function described above. The output of this function feeds to the right terminal of the burgundy shift register.
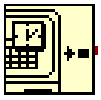	**Get Date/Time in Seconds Function** This returns a timestamp of the current time. It is given in the number of seconds that have elapsed since 12:00 AM, January 1, 1904.
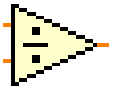	**Divide Function** This function divides the second input value by the first input value and yields the resulting value. There are 3 instances of the divide function: (1) The value 3600 (seconds in an hour) is divided into the result of the second instance of the Subtract function. This converts the seconds into hours. (2) The value 7 is divided by the value 9. (3) The result of the first Divide function is divided by the result of the second instance of the Addition function.
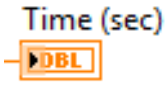	**Text Box (Time in seconds) Indicator** The input for this indicator is the output of the second instance of the Multiply function. This represents the number of seconds that have elapsed since the current pressure point detected by the sensor has been within the range defined by the "In Range and Coerce" function.

Table 5.3 Continued

Code Component	Definition & Parameters
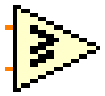	**Greater Than or Equal? Function** This function accepts 2 numerical input values. The first input value is analyzed as to whether it is greater than or equal to the second input value. A "TRUE" value indicates that the first input value is greater than or equal to the second input value. If the second input value is greater than the first input value, then a "FALSE" Boolean output value is generated. The first input value is the output of the first Divide function and the second input value is the output of the first instance of the Multiply function. ***Significance*** This function determines whether the time elapsed (in seconds) since a pressure point has not been relieved is greater than or equal to the alarm time setting. The output Boolean value is passed to the "True/False Boolean Indicator" described below.
	**True/False Boolean Indicator** The Boolean indicator is a mock LED light on the GUI that shines bright red if "TRUE" and dim burgundy if "FALSE." The input for this indicator is the output from the "Greater Than or Equal?" function described above. A value of "TRUE" indicates that the alarm has been activated and that the patient has been exerting the pressure point on the sensor for a time period greater than or equal to the alarm time setting and needs to be turned by a caregiver to relieve the pressure.

The global variable that has been referenced in the previous tables allows for data to be passed between multiple sub-visual instruments in LabVIEW. An advantage of using a global variable is the ability to make a change to a single numerical value and have that value retrieved by several code components without having to make the change at every instance where the numerical value may be needed. The latter activity may be described as hard coding, which can solve a problem, but offer little flexibility for future modifications to be made without changing the code [42]. The front panel of the global variable is seen in Figure 5.24.

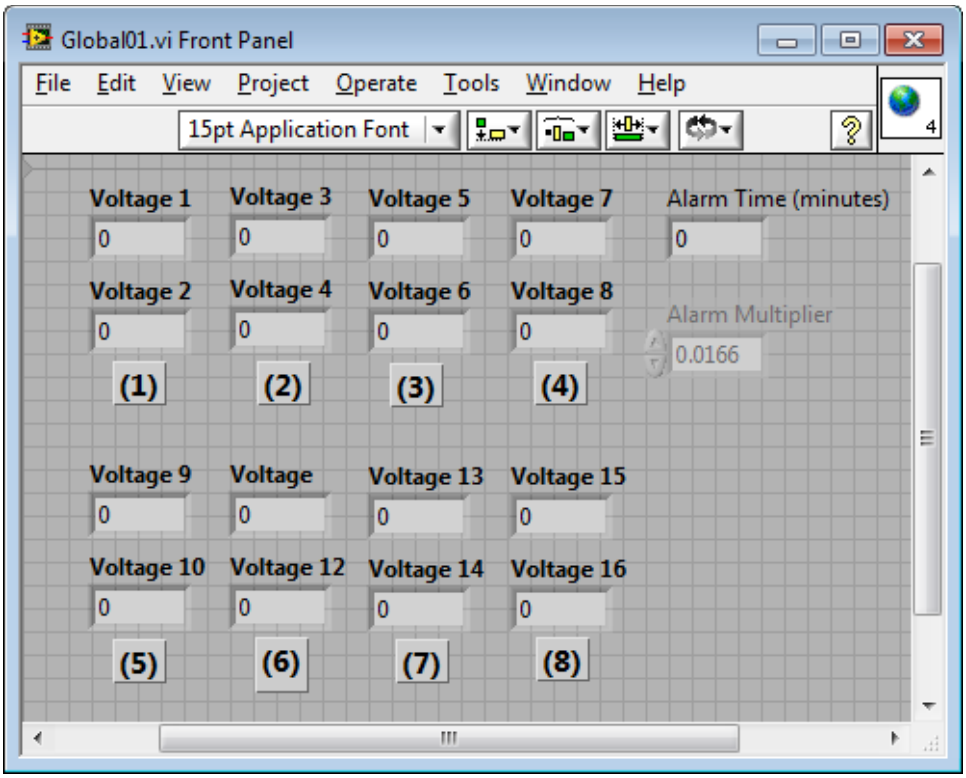

Figure 5.24: Front Panel of Global Variable

The 16 voltage placeholders obtain voltage readings from up to eight sensors (i.e. two voltages per sensor) because of the limitation of having only 16 analog inputs on the DAQ hardware. While the program is running, the global variable retrieves the voltage readings and places them in the respective placeholders for each sensor. In Figure 5.24, the numbers in parentheses correspond to the pair of voltage values directly above them. For example, "(1)" identifies "Sensor 1" and the two voltages associated with "Sensor 1" are "Voltage 1" and "Voltage 2." The "Alarm Time (minutes)" text box also transfers data from the GUI to multiple destinations. The "Alarm Multiplier," as described in the "Multiply Function" part of Table 5.3 is used to synchronize the alarm time setting with the clock counter. The image of the computer detection system GUI with no pressure present is shown in Figure 5.25.

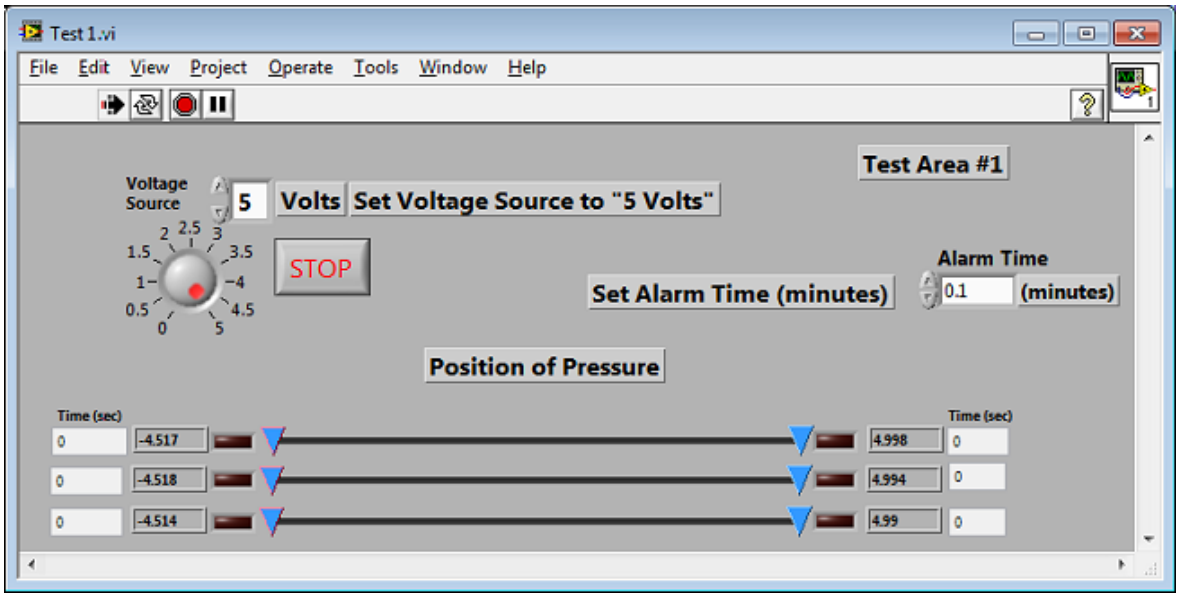

Figure 5.25: Screen of "Test1.vi" GUI with No Pressure Present

The two settings that can be made on the screen by the user are the "Voltage Source" and "Alarm Time" settings. In order for the horizontal pressure indicators to accurately reflect the points of pressure, the voltage should always be set at five volts. The alarm time setting can be set to any desired value in units of minutes. For example, the observed value for "Alarm Time" in Figure 5.25 of 0.1 minute translates to six seconds. There are three horizontal pressure indicators shown in this particular figure. For each of the six tests, the number of horizontal indicators reflects number of sensors being tested and their placement on the GUI is similar to their placement in the prototype sheet with respect to one another. The scale of the indicators is set so the minimum (left end) of the bar is zero. The maximum (right end) of the bar is 0.48 for 300-mm sensors and 0.4 for 200-mm sensors. This difference in maximum value is due to inherent resistance variability between the two different sensor lengths. The two blue triangles indicate the two outer pressure points along

the sensors' lengths. The "Time (sec)" textboxes show the values for each sensor described in the "Text Box (Time in seconds) Indicator" section of Table 5.3. The grayed-out boxes beside those time textboxes indicate the actual voltage values being detected by the sensors in real time. The next section outlines the testing method performed on the sensing system, lists the results from the tests and provides a discussion of those results.

5.6 Prototype Testing

Once the prototype construction was completed, a test method was devised to assess the viability of the system to perform the tasks for which it was designed. The test required the simulation of a patient's weight distributed at points of pressure close to those described in Sections 2.1.2 and 4.1.1.

A mannequin was borrowed from the Textile Protection and Comfort Center at North Carolina State University's College of Textiles. The mannequin had rotatable limbs with joints at the elbows, shoulders, waist and knees. At 165 lb, the weight of the mannequin was comparable to that of a human male. Important to note is that the shell of the mannequin was hard and rigid as opposed to moldable and fleshy, which would describe that of a human patient. The rigid shell, at points of pressure, was unable to flatten out like human skin is capable of doing while resting on a surface. This characteristic required the pressure points to be placed directly onto the sensors in order for a pressure reading to be obtained. The mannequin is shown lying down on the prototype sheet in Figure 5.26.

Figure 5.26: Mannequin Lying on Prototype Sheet

Another feature of the mannequin that caused concern was that its head and neck were fixed to its torso. The head was incapable of relaxing onto the prototype sheet's surface, and therefore an alternative method was needed to test the head area of the prototype. An object that was available, with a spherical shape similar to that of the back of a human head, was a 13.6-pound bowling ball. With the ball sitting stationary on top of one of the head sensors, its weight was detectable by the system. The ball is shown sitting on the head area of the prototype sheet in Figure 5.27.

Figure 5.27: Bowling Ball Sitting on Head Area during Testing

There were several criteria analyzed during testing. The first condition tested was the ability of the sensors within the test area to detect pressure. The second condition, which built upon the first condition, investigated whether the unrelieved pressure was able to be timed. For example, once a pressure was exerted, a clock in the program counts how long that pressure has been present on the sensor without being removed or shifted past the prescribed threshold. A third condition explored whether the alarm system for unrelieved pressure effectively activated at user-defined time periods. For instance, with an alarm time set at one minute, an unrelieved pressure would result in an activated alarm event when 60 seconds was reached on the counting clock. Testing was performed both with the prototype sheet laying directly on a wooden table top surface and with a cushioned layer placed between the sheet and the table.

The prototype's sensors were divided into six testing areas. The limitation of the DAQ hardware only allowed for 16 analog inputs, which was the equivalent of eight sensors

maximum for simultaneous testing. Table 5.4 provides a list of the sensors corresponding to their respective test areas.

Table 5.4: List of Sensors Corresponding to Test Areas

Testing Area	Sensors Involved	Quantity
1	1, 2, 3	3
2	4, 5, 6, 7, 8, 9, 10, 11	8
3	12, 13, 14, 18, 19, 20	6
4	15, 16, 17, 21, 22, 23	6
5	24, 25, 28, 29, 32, 33	6
6	26, 27, 30, 31, 34, 35	6

In each test, the sensors' detection capability was reported both as result of the mannequin's resting weight and of simple "touch testing" each individual sensor. Touch testing involved monitoring the computer detection system's screen and confirming the response of the on-screen indicator while pressing down on each sensor with a finger. All sensors were successful in the touch test for each test area, meaning that the location of the known pressure applied by the finger was reflected on the on-screen indicator during the time that the pressure was applied. Also important to note is that no false positives were encountered. This means that when no pressure was being applied, no pressure readings were detected by the system, which was the expected case. The mannequin was used in tests two through six. Screen captures from every test are included in Appendices G through L, although an example screen image will be included in the subsequent sections for each test. As previously discussed, for test one, a bowling ball was used due to the mannequin head's incapability to rest on the prototype sheet surface.

5.6.1 Test Area #1 Results

The first test area was concentrated on the part of the prototype sheet in the vicinity of the head, as highlighted in Figure 5.28.

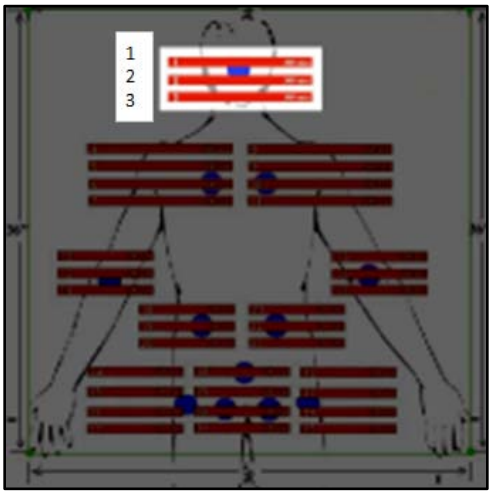

Figure 5.28: Prototype Test Area #1

5.6.1.1 Hard Surface

The prototype sheet laid directly on top of a hard table-top surface for this part of testing. For test one, the bowling ball was placed directly onto the center of the group of three sensors. The spherical contour of the ball, similar to the back of a human head, resulted in the weight only being detected by sensor #2. At time intervals of one minute and ten minutes with the ball resting on the sensor, the pressure detection had accumulated, proven by the clock counter on the computer detection system GUI. An alarm indicator light was activated at both time intervals of one minute and ten minutes. Once the alarm indicator for one minute was activated and the result was recorded, the alarm setting was changed to ten minutes, which de-activated the alarm until the clock counter reached ten minutes. The

system allowed for the alarm time to be set without interrupting the pressure sensors' clock counters. The results of the detection and alarm capability are listed in Table 5.5.

Table 5.5: Test 1 Hard Surface Results

		Alarm Activation	
Sensor #	**Detection**	**1 min. (60 sec.)**	**10 min. (600 sec.)**
1	No	--	--
2	Yes	Yes	Yes
3	No	--	--

A screen capture of the computer detection system GUI after 604 seconds is shown in Figure 5.29. The activated alarm is indicated by the brighter red LED rectangles on each side of the second sensor horizontal indicator and the triangle position point detects pressure close to the middle of the sensor. The dim LED rectangles show deactivated alarm indicators.

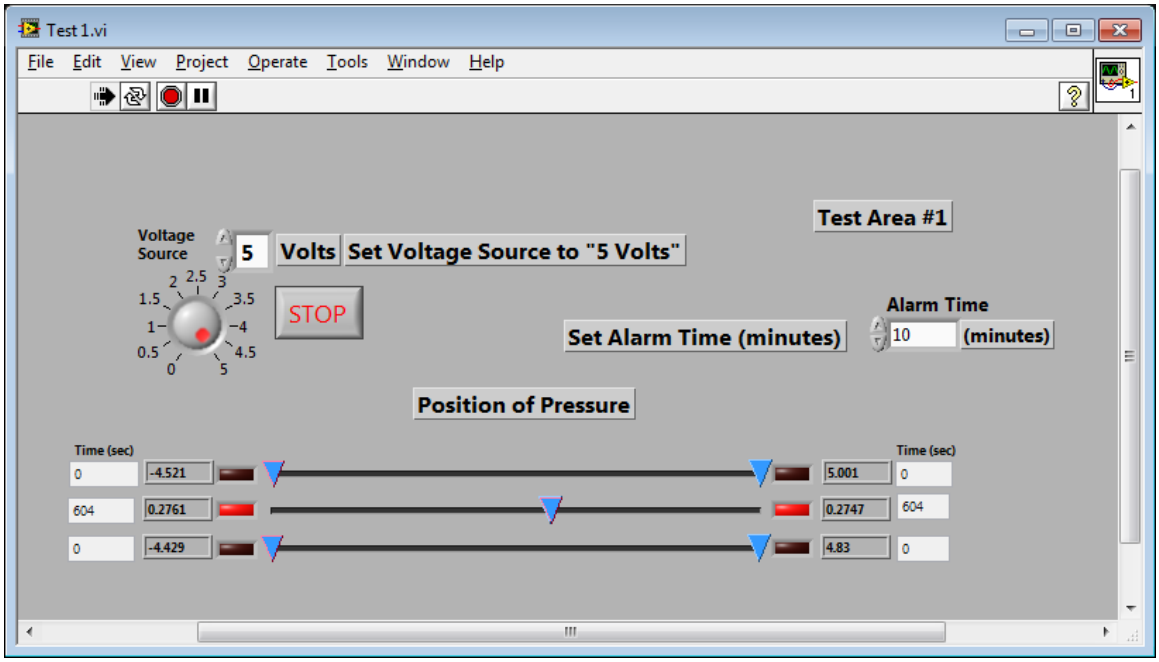

Figure 5.29: GUI, Test 1, Hard Surface, @ 604 Seconds with Alarm

5.6.1.2 Cushioned Surface

The prototype sheet was placed on top of a hard table-top surface with a cushion placed in between the sheet and table. The cushion consisted of the same woven fabric described in Section 3.1 that was used as a cushion for sensor viability testing. The bowling ball was placed onto the middle of the second sensor, making it lay in the center of the three sensors. The testing on the cushioned surface allowed for detection by all three sensors. This was due to the ability of the bowling ball's spherical contour to sink into the cushion where it made contact with each sensor.

Another difference noticed between the cushion test and the hard surface test was that two pressure points on each horizontal indicator were visible. The cushioned surface created a wider contour of force from the weight of the bowling ball compared to the hard surface test. This force detection length was essentially an arc length between the outer force locations exerted on the sensor by the ball. These wider force detection contours on each of the three sensors were reflected in the image on the computer screen. While the hard surface test appears to only have one location of force in Figure 5.29, there were actually two force locations very close to one another that were present at the ends of the narrow force contour of the bowling ball. The contact area increased with the presence of the cushion. The results of the detection and alarm capability of the cushion test are listed in Table 5.6 and a screen capture of the computer detection system GUI after 604 seconds is shown in Figure 5.30 with pressure positions indicated by the triangles.

Table 5.6: Test 1 Cushioned Surface Results

		Alarm Activation	
Sensor #	**Detection**	**1 min. (60 sec.)**	**10 min. (600 sec.)**
1	Yes	Yes	Yes
2	Yes	Yes	Yes
3	Yes	Yes	Yes

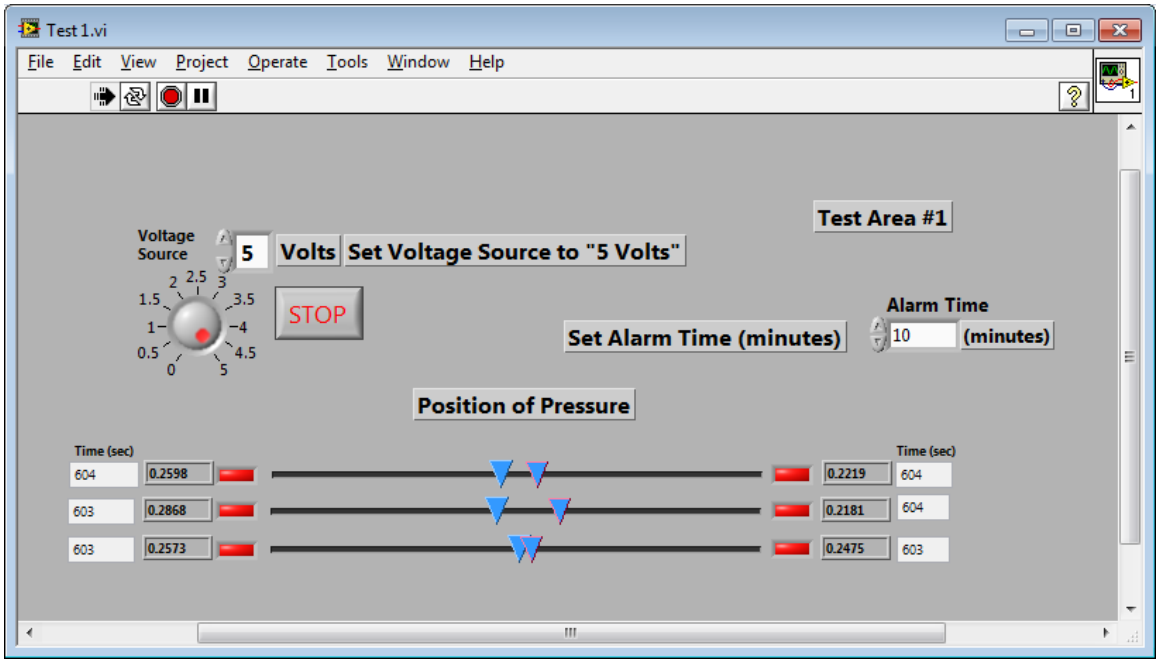

Figure 5.30: GUI, Test 1, Cushioned Surface, @ 604 Seconds with Alarm

5.6.2 Test Area #2 Results

The second test area was concentrated on the part of the prototype sheet encompassing the area of the shoulders and shoulder blades, leading down to the upper back, as highlighted in Figure 5.31.

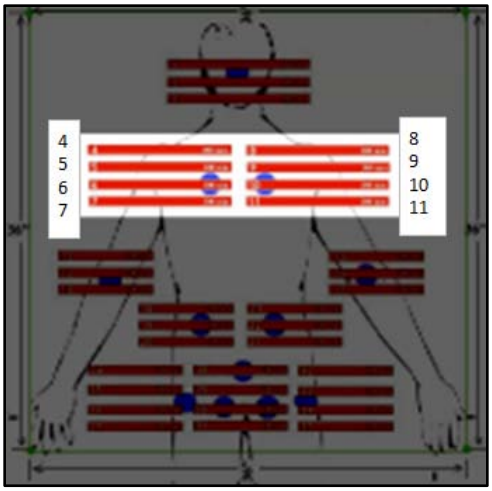

Figure 5.31: Prototype Test Area #2

5.6.2.1 Hard Surface

The mannequin was placed onto the prototype sheet directly on top of the table-top surface. Although sensors 13 and 16 were part of tests three and four, respectively, they were used as target points for the mannequin's elbows to be placed for alignment purposes for each of the remaining tests. Only three of the eight sensors detected pressure during this test. Part of this is due to the hard shell of the mannequin's body. This may have limited the area of applied pressure on the test area. The contour of the mannequin's shoulder blade and upper back caused pressure to be detected on sensors five, eight and nine. Another factor that may have influenced this result was the placement of the elbows on the centers of sensors 13 and 16. Had the mannequin been shifted in either direction, different sensors may have been able to detect the pressure, although the pressure detection seen in sensors five, eight and nine may have been sacrificed. The results of the detection and alarm capability are listed in

Table 5.7 and a screen capture of the computer detection system GUI after 600 seconds is shown in Figure 5.32.

Table 5.7: Test 2 Hard Surface Results

		Alarm Activation	
Sensor #	**Detection**	**1 min. (60 sec.)**	**10 min. (600 sec.)**
4	No	--	--
5	Yes	Yes	Yes
6	No	--	--
7	No	--	--
8	Yes	Yes	Yes
9	Yes	Yes	Yes
10	No	--	--
11	No	--	--

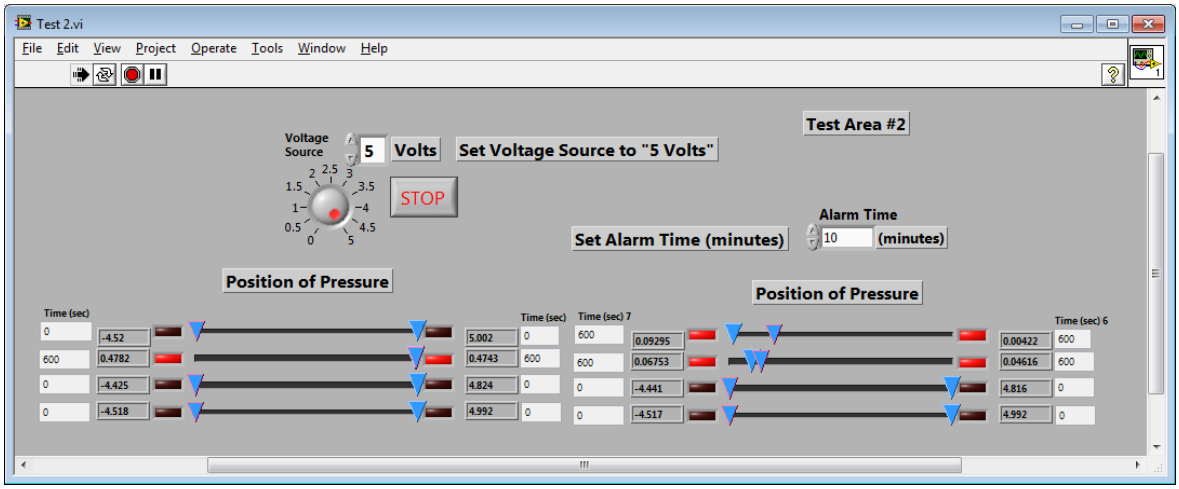

Figure 5.32: GUI, Test 2, Hard Surface, @ 600 Seconds with Alarm

5.6.2.2 Cushioned Surface

The cushion was placed between the prototype sheet and the table surface. With the mannequin in position, the same sensors that detected pressure during the hard surface testing were able to detect pressure again, but with the addition of sensor 4 showing pressure detection. The cushioning likely allowed the contour of the mannequin's upper back to sink

in and come in contact with the additional sensor. The results of this test are listed in Table 5.8 and a screen capture of the computer detection system GUI is seen in Figure 5.33.

Table 5.8: Test 2 Cushioned Surface Results

		Alarm Activation	
Sensor #	**Detection**	**1 min. (60 sec.)**	**10 min. (600 sec.)**
4	Yes	Yes	Yes
5	Yes	Yes	Yes
6	No	--	--
7	No	--	--
8	Yes	Yes	Yes
9	Yes	Yes	Yes
10	No	--	--
11	No	--	--

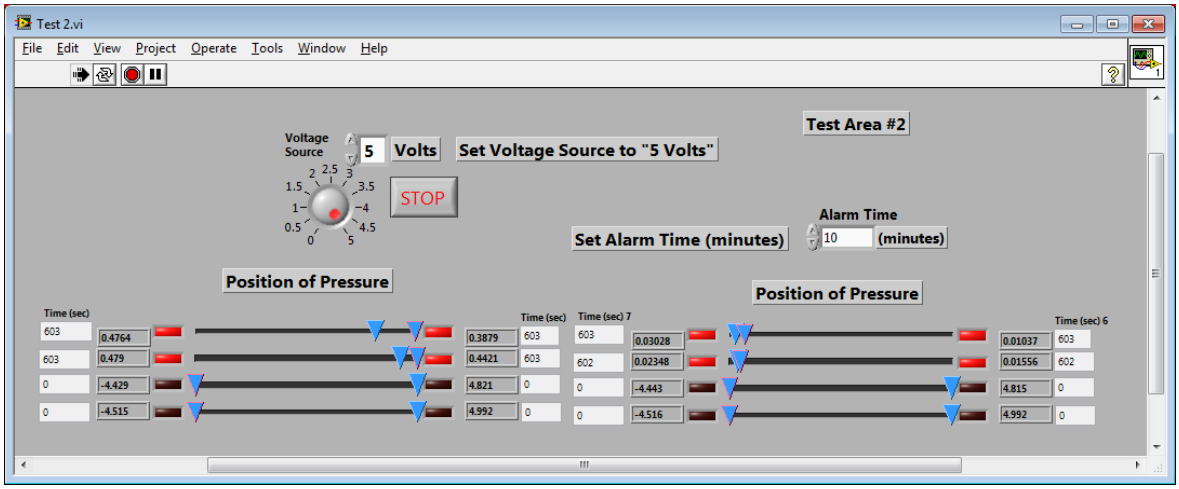

Figure 5.33: GUI, Test 2, Cushioned Surface, @ 603 Seconds with Alarm

5.6.3 Test Area #3 Results

The third test area was concentrated on the part of the prototype sheet encompassing the area of the mannequin's right elbow and right-lower back, as highlighted in Figure 5.34.

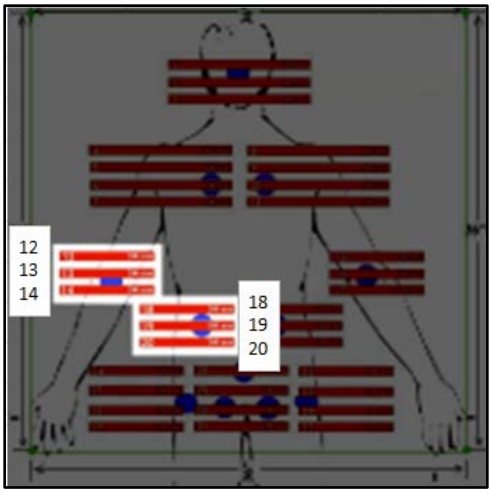

Figure 5.34: Prototype Test Area #3

5.6.3.1 Hard Surface

With the mannequin in position and the prototype sheet laying directly on the table-top surface, only three sensors were able to detect pressure. Of the sensors in the elbow area, two detected pressure and of the three lower back area sensors, one was able to detect pressure. Compared to other tests with the hard surface, the hard shell of the mannequin limited the ability of the body to have a flat contact interface with the prototype sheet, thus reducing the number of pressure points that could be detected. The results of this test are listed in Table 5.9 and a screen capture of the computer detection system GUI is seen in Figure 5.35.

Table 5.9: Test 3 Hard Surface Results

		Alarm Activation	
Sensor #	**Detection**	**1 min. (60 sec.)**	**10 min. (600 sec.)**
12	No	--	--
13	Yes	Yes	Yes
14	Yes	Yes	Yes
18	No	--	--
19	No	--	--
20	Yes	Yes	Yes

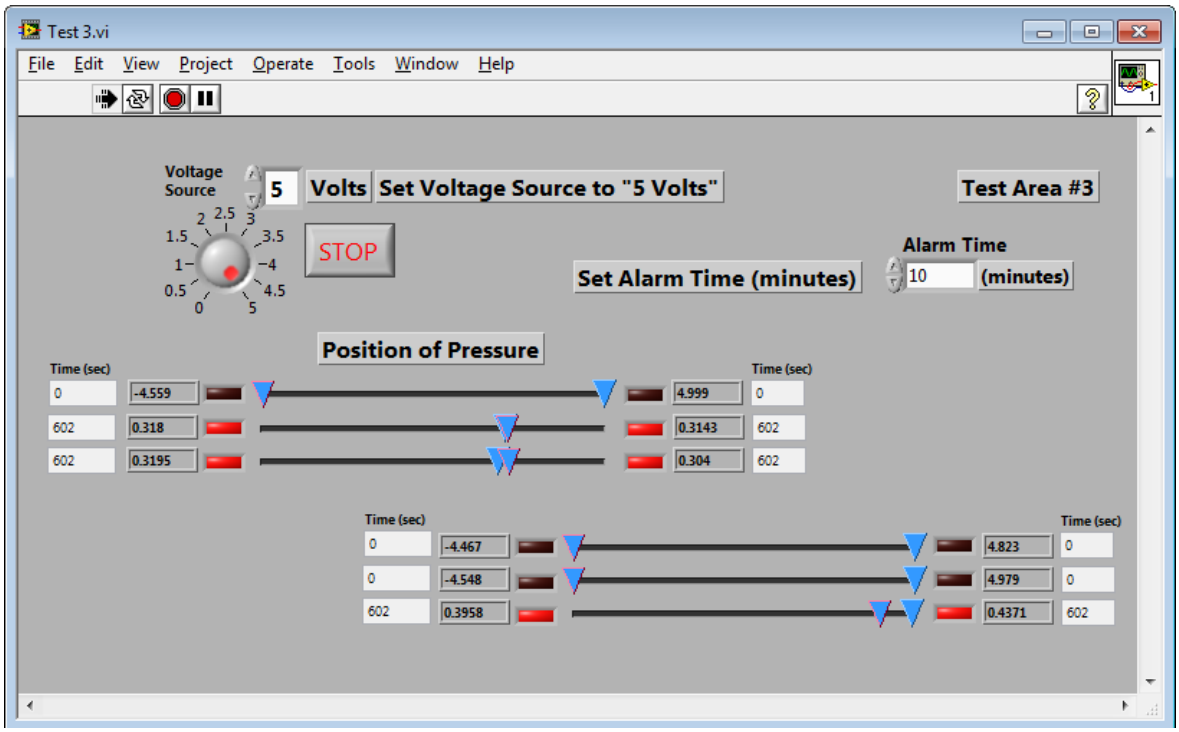

Figure 5.35: GUI, Test 3, Hard Surface, @ 602 Seconds with Alarm

5.6.3.2 Cushioned Surface

The cushioning was placed between the prototype sheet and the table surface with the mannequin in the same position as placed during hard surface testing. An interesting result was that one of the sensors in the area of the elbow (sensor 13) did not detect the

mannequin's elbow during the cushion testing while it did detect the pressure during hard surface testing. A potential issue was noticed with the sensors as a result of this observation. Recall from Section 2.3.1.3 that the SoftPot sensor uses the technology shown in Figure 5.36 to detect pressure.

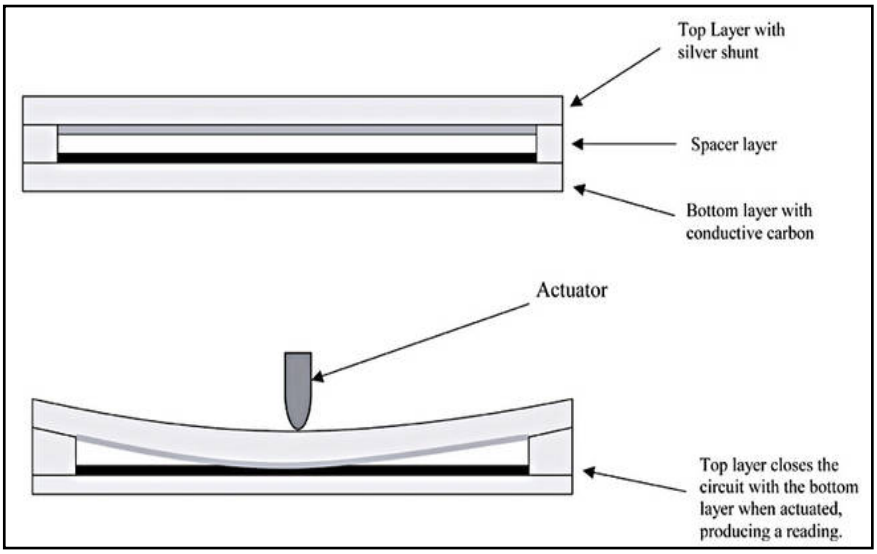

(Taken from [31])

Figure 5.36: Schematic of SoftPot Potentiometer

There is a gap into which a pressure point must be able to penetrate in order to close the circuit. If a pressure point is broad and flat enough, it will bridge the gap and prevent the circuit from being closed. Considering the mannequin's hard shell and its lack of capability to conform to a surface like human skin, this issue may not be significant enough to threaten the actual end use of the prototype. Regardless, not all humans' flesh and anatomies react the same way to pressure and the removal of any inherent limitations in the system's performance is important. Therefore, improvement ideas on this characteristic of the SoftPot sensor will be described in detail later in Chapter 6. The results of this test are listed in Table 5.10 and a screen capture of the computer detection system GUI is seen in Figure 5.37.

Table 5.10: Test 3 Cushioned Surface Results

		Alarm Activation	
Sensor #	**Detection**	**1 min. (60 sec.)**	**10 min. (600 sec.)**
12	No	--	--
13	No	--	--
14	Yes	Yes	Yes
18	Yes	Yes	Yes
19	Yes	Yes	Yes
20	Yes	Yes	Yes

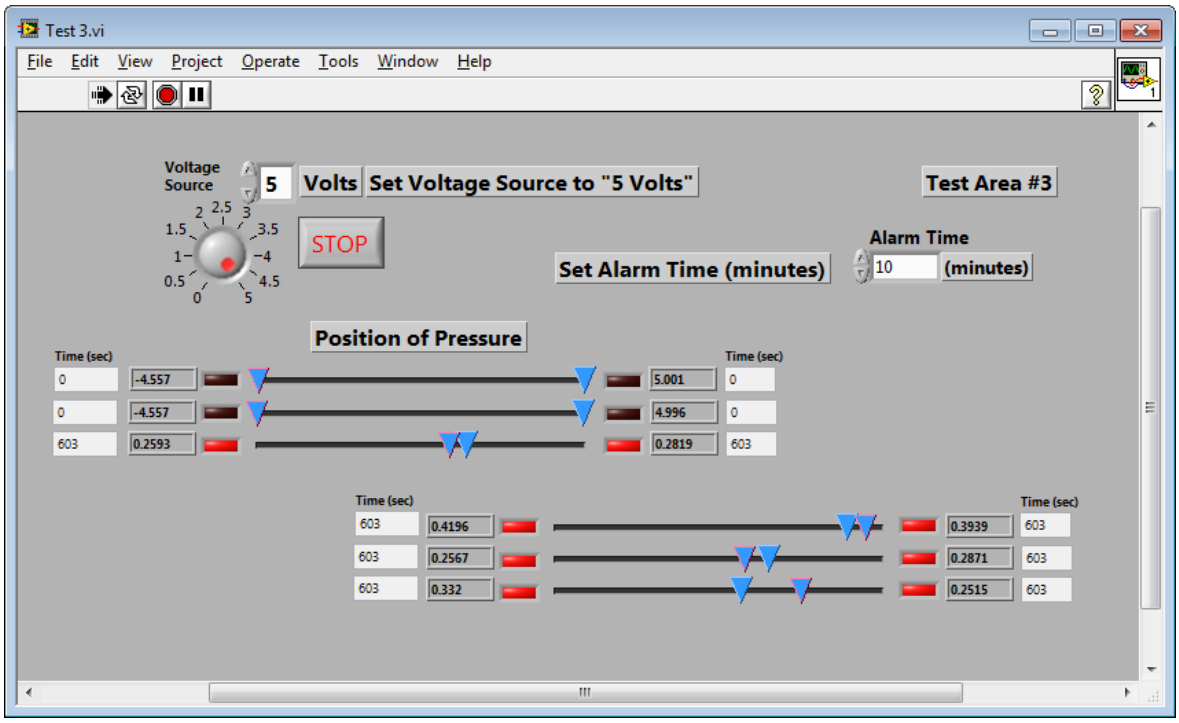

Figure 5.37: GUI, Test 3, Cushioned Surface, @ 603 Seconds with Alarm

5.6.4 Test Area #4 Results

The fourth test area was concentrated on the part of the prototype sheet encompassing the area of the mannequin's left elbow and left-lower back, as highlighted in Figure 5.38. This area simply mirrored the area tested in the third test area across the spinal axis.

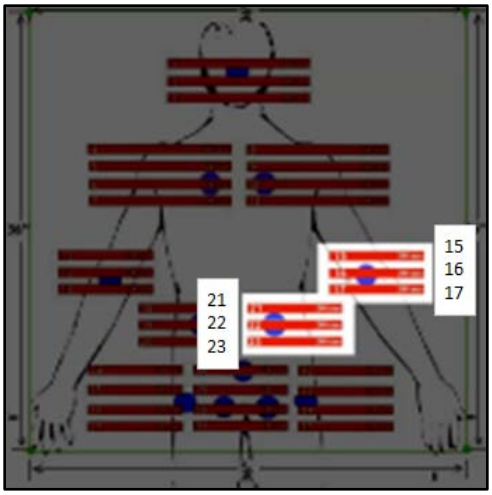

Figure 5.38: Prototype Test Area #4

5.6.4.1 Hard Surface

With the mannequin in position and the prototype sheet laying directly on the table-top surface, only two sensors were able to detect pressure. Of the sensors in the elbow area, one detected pressure and of the three lower back area sensors, one detected pressure. The test results are listed in Table 5.11 and a screen capture of the computer detection system GUI is seen in Figure 5.39.

Table 5.11: Test 4 Hard Surface Results

		Alarm Activation	
Sensor #	**Detection**	**1 min. (60 sec.)**	**10 min. (600 sec.)**
15	Yes	Yes	Yes
16	No	--	--
17	No	--	--
21	Yes	Yes	Yes
22	No	--	--
23	No	--	--

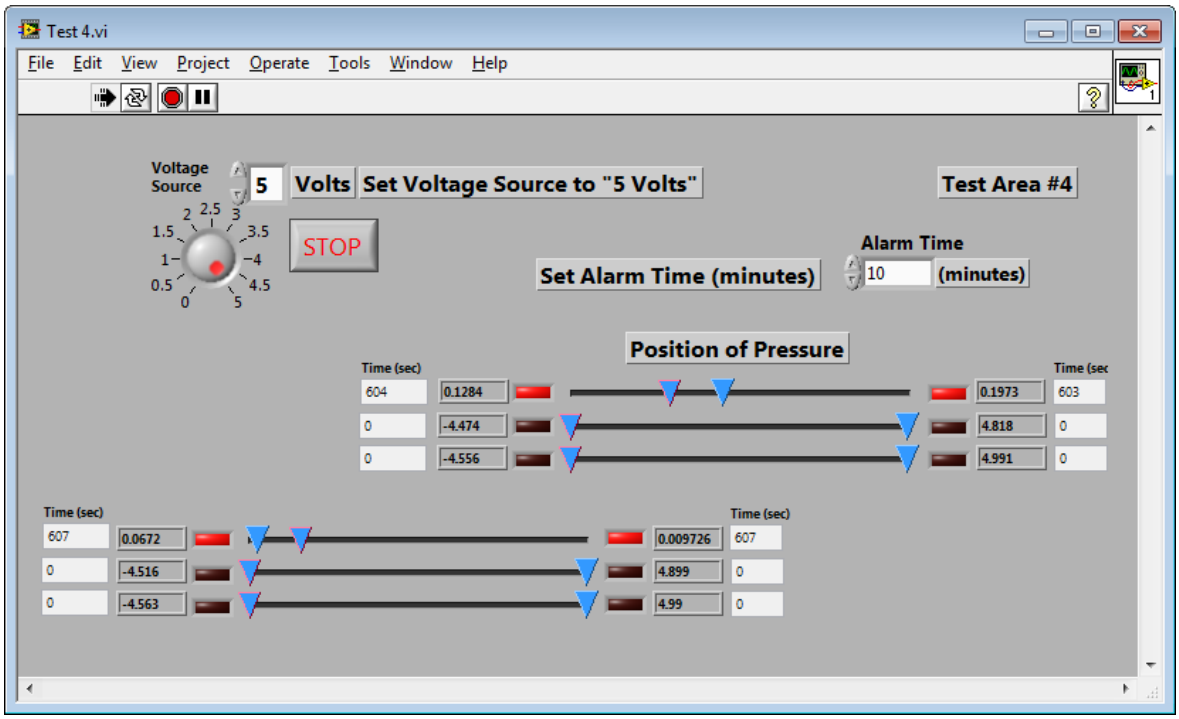

Figure 5.39: GUI, Test 4, Hard Surface, @ 607 Seconds with Alarm

5.6.4.2 Cushioned Surface

With the cushion in place under the prototype sheet, there were three sensors that detected pressure from the mannequin. In the elbow area, one sensor detected pressure and in the lower back area, two sensors detected pressure. Sensor 22 reset at around 230 seconds, possibly due to weak pressure exertion by the mannequin. The results are listed in Table 5.12 and a screen capture of the computer detection system GUI at 814 seconds is seen in Figure 5.40.

Table 5.12: Test 4 Cushioned Surface Results

		Alarm Activation	
Sensor #	**Detection**	**1 min. (60 sec.)**	**10 min. (600 sec.)**
15	No	--	--
16	Yes	Yes	Yes
17	No	--	--
21	No	--	--
22	Yes	Yes	Yes
23	Yes	Yes	Yes

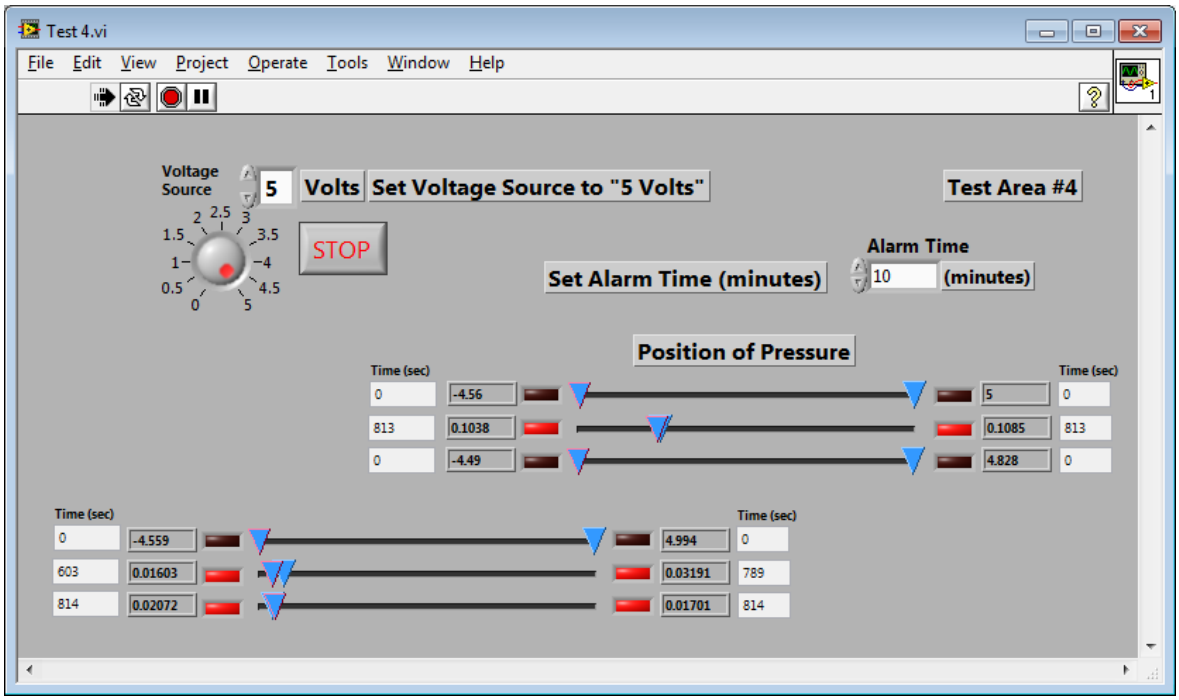

Figure 5.40: GUI, Test 4, Cushioned Surface, @ 814 Seconds with Alarm

5.6.5 Test Area #5 Results

The fifth test area was concentrated on the part of the prototype sheet encompassing the area of the mannequin's lower back and upper hips, as highlighted in Figure 5.41.

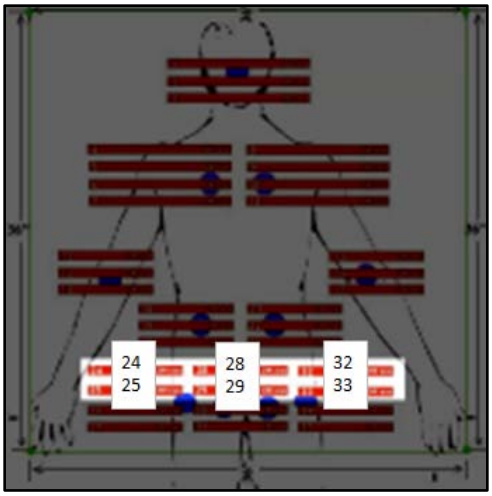

Figure 5.41: Prototype Test Area #5

5.6.5.1 Hard Surface

The prototype sheet was placed directly on the table-top surface while the mannequin was laying on it in the same position described in Section 5.6.2.1 and used for the previous test areas. There were actually no pressure points detected by the sensors in this test, as reflected by Table 5.13. The contour of the mannequin's lower back arched over the test area and the rigid shell prevented any contact with the sensors. It should be noted that the sensors were still responsive to touch pressure from pressing down with a finger.

Table 5.13: Test 5 Hard Surface Results

		Alarm Activation	
Sensor #	**Detection**	**1 min. (60 sec.)**	**10 min. (600 sec.)**
24	No	--	--
25	No	--	--
28	No	--	--
29	No	--	--
32	No	--	--
33	No	--	--

5.6.5.2 Cushioned Surface

With the cushion in place between the prototype sheet and the table-top surface, the mannequin was able to be detected by one of the sensors in the test area, as reflected by the results in Table 5.14. The detection lasted for the entire test time of ten minutes and an alarm was activated at the expected time of 600 seconds for both sides of the sensor. At about the one-minute mark of the test, the left side of the sensor's pressure detection reset, possibly due to a weak contact between the rigid shell of the mannequin and likely the contour of the mannequin's lower back arching over the test area, as described in Section 5.6.5.1. A screen capture of the computer detection system GUI at 662 seconds is seen in Figure 5.42.

Table 5.14: Test 5 Cushioned Surface Results

		Alarm Activation	
Sensor #	**Detection**	**1 min. (60 sec.)**	**10 min. (600 sec.)**
24	No	--	--
25	No	--	--
28	Yes	Yes	Yes
29	No	--	--
32	No	--	--
33	No	--	--

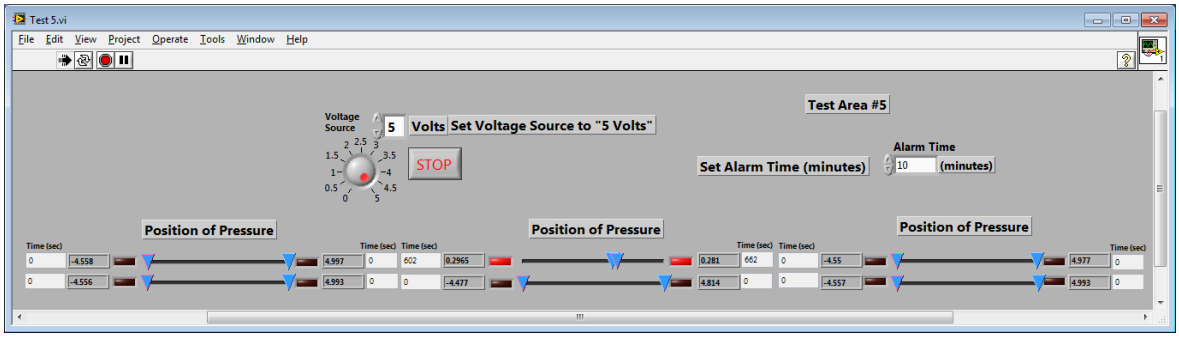

Figure 5.42: GUI, Test 5, Cushioned Surface, @ 662 Seconds with Alarm

5.6.6 Test Area #6 Results

The sixth, and final, test area was concentrated on the part of the prototype sheet encompassing the area of the mannequin's lower hips, as highlighted in Figure 5.43, just below the area tested in the fifth test area.

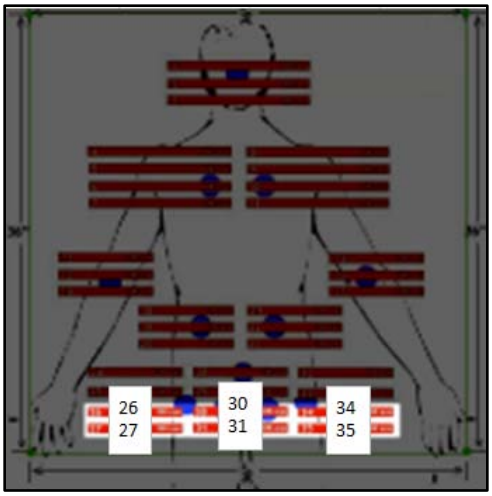

Figure 5.43: Prototype Test Area #6

5.6.6.1 Hard Surface

With the prototype sheet placed directly on the table-top surface, no pressure points were detected by the six sensors in the test area, as indicated by the results in Table 5.15. The contour of the mannequin arched over the sensors in this test area, which is likely the cause for this result.

Table 5.15: Test 6 Hard Surface Results

		Alarm Activation	
Sensor #	**Detection**	**1 min. (60 sec.)**	**10 min. (600 sec.)**
26	No	--	--
27	No	--	--
30	No	--	--
31	No	--	--
34	No	--	--
35	No	--	--

5.6.6.2 Cushioned Surface

The cushion was placed between the prototype sheet and the table-top surface and the mannequin was placed into position. Only one of the sensors was able to detect pressure, as suggested by the results in Table 5.16. The cushion likely allowed the rigid contour of the mannequin to come into contact with Sensor 31. A screen capture of the computer detection system GUI at the 603-second mark is seen in Figure 5.44.

Table 5.16: Test 6 Cushioned Surface Results

		Alarm Activation	
Sensor #	**Detection**	**1 min. (60 sec.)**	**10 min. (600 sec.)**
26	No	--	--
27	No	--	--
30	No	--	--
31	Yes	Yes	Yes
34	No	--	--
35	No	--	--

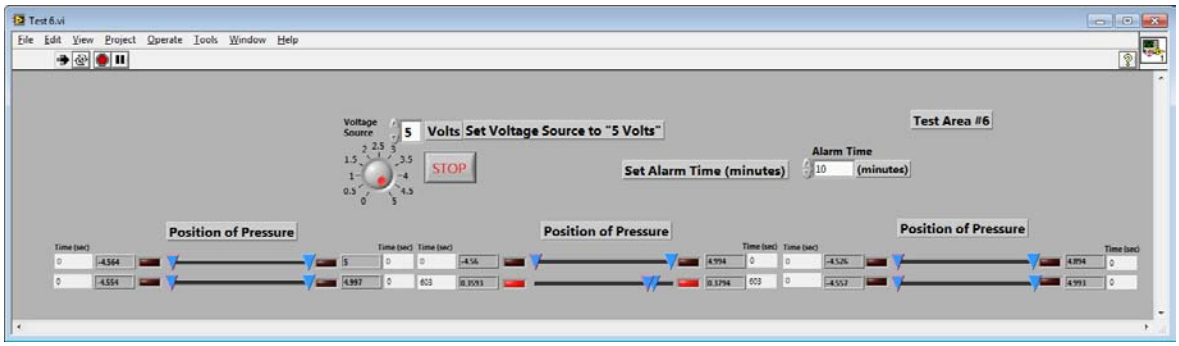

Figure 5.44: GUI, Test 6, Cushioned Surface, @ 603 Seconds with Alarm

5.6.7 Summary of Testing Results

To review, there were three criteria analyzed during the testing. The sensors were tested as to whether they could detect pressure and report the reading to the computer detection system. The unrelieved pressure points were observed to see whether the time of the pressure presence was accumulated and recorded. Lastly, the computer detection system was tested to see whether the set alarm time would yield an activated alarm event at the time the unrelieved pressure reached the alarm time.

The results of the test areas one through six were successful in terms of whether the alarm was able to be activated at certain times of unrelieved pressure. This success would not have been possible without success from the first two criteria mentioned in the last paragraph. The alarm required the timing to be operational and the timing required the pressure detection to work properly. Therefore, the test results indicate that the sensing system is capable of performing the tasks for which it was designed. There are, however, several design modifications that may enhance the overall functionality of the system. These improvements are described in the next chapter.

6 Conclusions and Path Forward

Details outlining the development of the pressure-sensing bed sheet and computer detection system have been described in Chapters 3, 4 and 5. The next section will provide the conclusions that have been made based on prototype development and testing, followed by a section describing several design enhancement ideas that will help to provoke further development.

6.1 Conclusions

In order to reduce the number of occurrences of bedsores in hospital patients, the avoidable risks associated with bedsore formation, such as caregiver negligence, must first be mitigated. The purpose of this research has been to provide an improved method for alarming medical caregivers when to physically turn their patients, thus relieving built-up pressure and allowing blood circulation. This research was performed with the goal of developing a design of a smart textile device used to assist in the prevention of bedsores in bedridden, or otherwise immobile, patients.

Recall, from Section 1.2, the specific research objectives:

- RO1: To develop an understanding of the state of the art of commercially available pressure sensors and determine which of the potential candidates will best fit this project's needs
- RO2: To determine a method for integrating electrical pressure sensors into a textile substrate
- RO3: To develop a sensing bed sheet that detects an array of pressure over a period of time and alerts medical personnel at specified time limits

The specific research objectives described in Section 1.2 were met successfully. An understanding of the state of the art of commercially available pressure sensors was developed in response to "RO1." The research provided in the literature review in Chapter 2 outlined details on various commercially-available pressure sensors. This included detail on how the different types of pressure sensors function as well as an analysis of how well the sensor type would serve the application of reducing the risk of bedsore formation. This sensor applicability within the bed sheet system was further tested in Chapter 3 when a determination was made to use the SoftPot potentiometer pressure sensor due to its superior consistency in detecting position of pressure points. The other commercially-available sensors tested—the piezoresistance-based pressure sensors—were observed to provide erratic and inconsistent resistance readings relative to the consistency exhibited by the SoftPot potentiometer. In response to "RO2," A method for integrating those sensors into a textile substrate was designed. The details of completing this research objective were given in Chapter 4 when the layout of the sensors was described as well as the fabric design to accompany the sensor layout. The end result of this research was the fabrication of a prototype of a sensing bed sheet that successfully detects pressure over a period of time and has the capability of alerting a caregiver at desired time limits, which supports the objective described in "RO3." Chapters 4 and 5 both provided all detail involved with the fabrication process, which included the weaving of the textile substrate, the embedment of the sensors, the creation of the custom-length electrical wires connecting the sensors and the circuit and the development of the computer programming code using LabVIEW software. The combination of these components resulted in a working prototype of a computer detection

system. The test results given in Section 5.6 show that the system successfully detects and displays pressure points on a screen while keeping track of accumulated time elapsed since the pressure was introduced. The program's screen demands a user-specified time setting that dictates when an alarm is to be activated due to unrelieved pressure. The programming automatically resets the time elapsed when the applied pressure is removed, thus reducing the chance of false alarms and helping maintain caregiver efficiency when patient-turning is not necessary.

While this research has been heavily focused on the application of bedsore risk mitigation, it must be restated how other applications could benefit from embedding sensors into textile substrates. Examples include rooms that can respond to the presence of people, which could be useful in security systems in buildings and, perhaps, for aesthetic purposes in interactive art galleries. In each case, the rooms would have sensors embedded into their carpeting. The electronic industry could benefit by using the pressure sensors in a knob control mechanism in an application like audio volume control. These only represent a few examples, although there are vast possibilities for other potential applications for inserting sensors into textile substrates.

6.2 Recommendations for Future Work

There exist areas for improvement in the prototype design described in the Chapters 4 and 5. These potential improvements can be categorized as relating to the hardware of the design or the software of the design and will be described in the next sections where the proposed modifications will be compared with the current design.

6.2.1 Potential Physical Design Improvement

The components of the design that may benefit from physical modifications may include the fabric design, the pressure sensors, or both in conjunction with one another.

6.2.1.1 Consideration of Fabric Contraction

The current design's fabric construction plan, as described in Section 4.2, results in a fabric that is very close to its planned 91.4-cm (36-in) greige length. However, there is a contraction of the length due to several factors. One of these factors is the relaxation of the yarns after being removed from high tension on the loom. Another factor, likely unique to the situation introduced by this research, may include the insertion of the sensors into the tubes of the fabric. Even though the sensors are very flat, and the tubes' widths allow for the sensors to have a small amount of freedom to move in the direction of the tube width, the sensors' slight thickness causes the 17 tubes' collective width to contract slightly, thus reducing the overall length of the fabric. Future planning for different human sizes should take into account the fabric contraction so that the sensors are aligned with the common areas of bedsore formation described in Sections 2.1.2 and 4.1.1. The adjustment that should be made with respect to fabric contraction would involve the spacing of the fabric tubes. This means that the number of repeats of the single layer 3x3 warp rib design (Section 4.2.1.3) would need to be increased in the appropriate areas, which are highlighted in Figure 6.1.

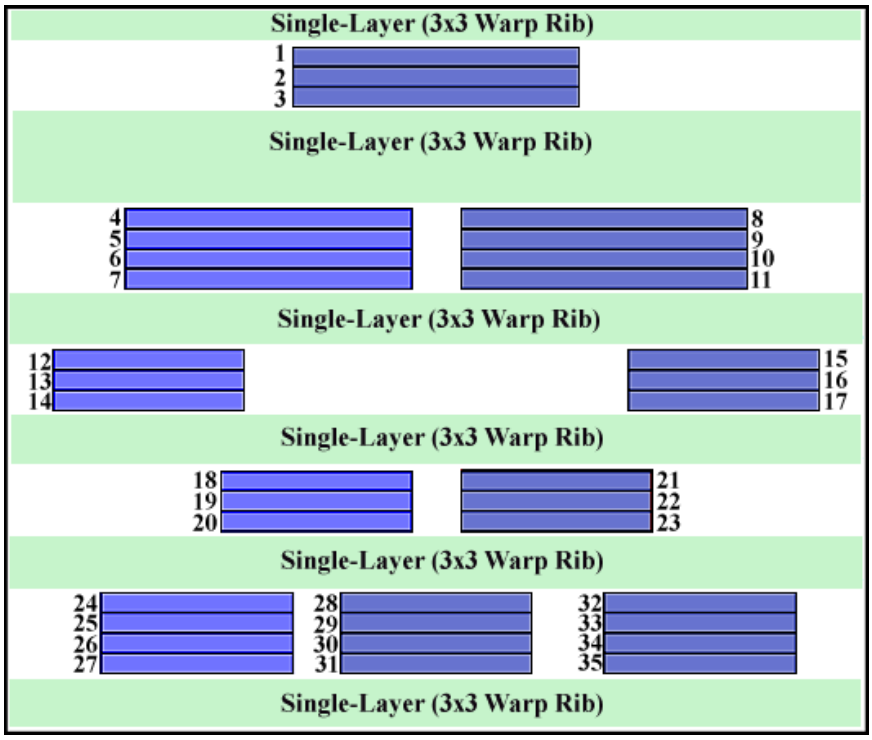

Figure 6.1: Adjustment Zones for Fabric Contraction Consideration

6.2.1.2 Sensor Layout for Full Body Length

The current prototype design is only suitable to detect pressure from the top of the head to the top of the thighs. An improved, and more complete, design would contain more sensors that could detect other pressure sensitive areas of the body, such as the feet. Although calves were not found to be a common site of bedsore formation in the research, they do make contact with the bed surface for long periods of time in immobilized patients. Therefore, sensors being placed in the calf area may provide an improvement in safety regarding the prevention of bedsores.

6.2.1.3 Horizontal Anchoring of Sensors

In the current design, the sensors are free to move horizontally along the tube's length if they are forced to do so. This may be seen as an advantageous capability for adjustment purposes for patients that may be wider or thinner than may be optimal for the layout in Figure 6.2, recalled from Section 4.1.3.

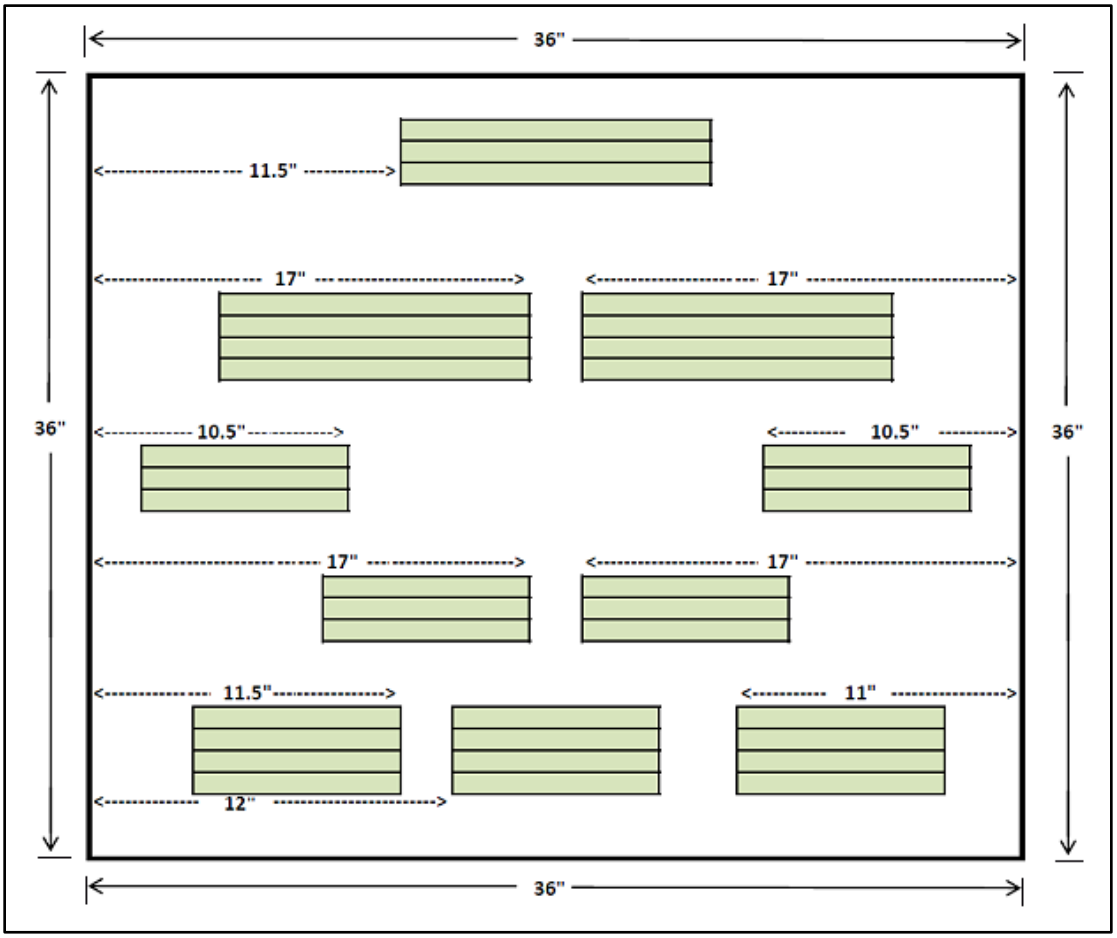

Figure 6.2: Diagram of Sensors' Horizontal Arrangement

There may be a desire, however, to anchor the sensors in place horizontally to ensure that they are in the prescribed area and will sense pressure points at spots at risk for bedsore formation. The SoftPot sensors are manufactured with an adhesive backing if the end user

chooses to remove the label. This may alleviate horizontal slippage to a degree, but there remains a risk that the adhesive could gather loose fibers and other dust components from the yarns and other sources, therefore reducing the effectiveness of the adhesive to anchor the sensor in place. Other solutions should be investigated to mechanically hold the sensors in place to ensure proper pressure detection.

6.2.1.4 Removal of Sensor Detection Gap Bridge

As described in Section 5.6.3.2, there exists a gap into which a pressure point must be able to penetrate in order to close the circuit and returning pressure detection. One suggested modification is to add a material to the sensors that is thinner than the detection gap and rigid enough to transfer the force so that the circuit can be closed. The schematics in Figure 6.3 show the force reactions in the current design and in a proposed design. The green material in part B of the figure is the material that allows the force to be transferred into the detection gap resulting in a closed circuit.

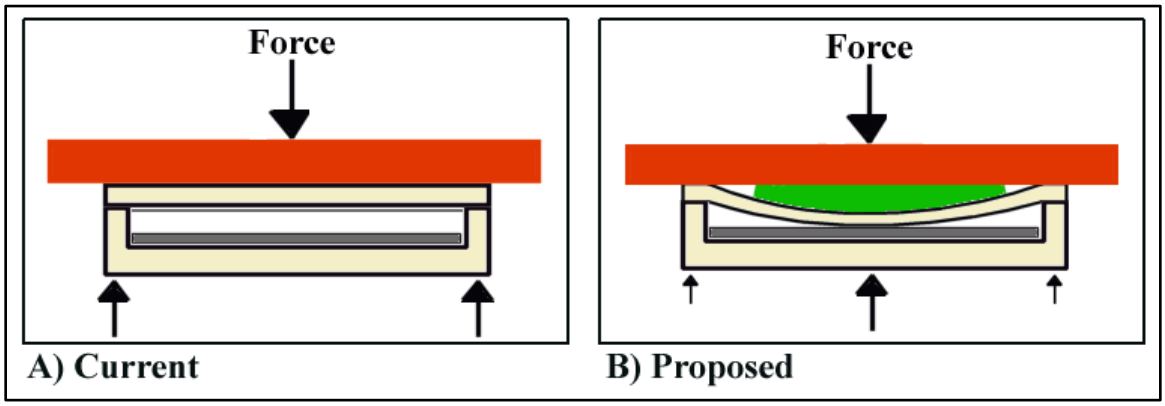

Figure 6.3: Schematic of A) Current and B) Proposed Designs for Filling Detection Gap

A small test was performed to analyze the effectiveness of mounting tape to serve as the "gap-filling" material. The tape used was Scotch® brand "Heavy Duty Mounting Tape" and Figure 6.4 shows the appearance of the Scotch® brand tape on the sensor.

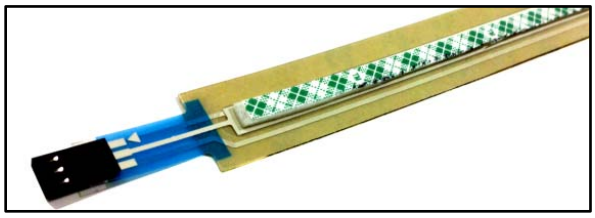

Figure 6.4: Sensor with Mounting Tape Attached

Another type of mounting tape was also briefly tested (Bulldog® Stic Mount® Adhesive Roll). Visual observations of the sensors' detection behavior were made comparing the effect of Scotch® brand tape, the Bulldog® brand tape and the absence of mounting tape. The Scotch® brand tape worked better than both the Bulldog® brand tape and the absence of tape in that the pressure was able to be detected with a simple flat weight being placed on top of the sensor for several minutes. Also, the clock counter was able to accumulate time for the entire time period that the pressure was being exerted. The Bulldog® taped sensor appeared to start to detect pressure constantly at first, but with time, the pressure detection disappeared. One characteristic different between the Scotch® and Bulldog® tapes was that the former was more rigid than the latter in that it had a higher resistance to elongation when stretched. The ability of the Bulldog® tape to stretch indicates that its microstructure allows for the applied force to be distributed to areas indirectly affected by the force, thus relaxing the force in the spot of the flat weight enough for the circuit to not remain closed. With these preliminary observations on the mounting tape's effect on the sensor's performance, it is

recommended that a similar material be attached to all sensors in future work to ensure that the detection gap is not bridged by broad pressure surfaces.

6.2.1.5 Sensor Connector Change for Flat Design

The current sensors that were purchased from Digi-Key® Corporation were all manufactured with "Crimpflex Female Receptacles with Plain Housings" [31]. There are six different available connector options provided by Spectra Symbol, including the one just mentioned. One problem that may exist as a result of the Crimpflex female receptacle is related to its bulkiness. The thickness of the plastic receptacle, compared to the sensing area's thickness measured as 0.57 mm (0.0225 in), was measured as 2.54 mm (0.1 in), which is more than four times as thick. The current design's connector and two proposed alternative connector types are seen in Figure 6.5. The two proposed types would reduce the thickness and potentially remove dangerous pressure points that could lead to bedsores in the patients lying on them.

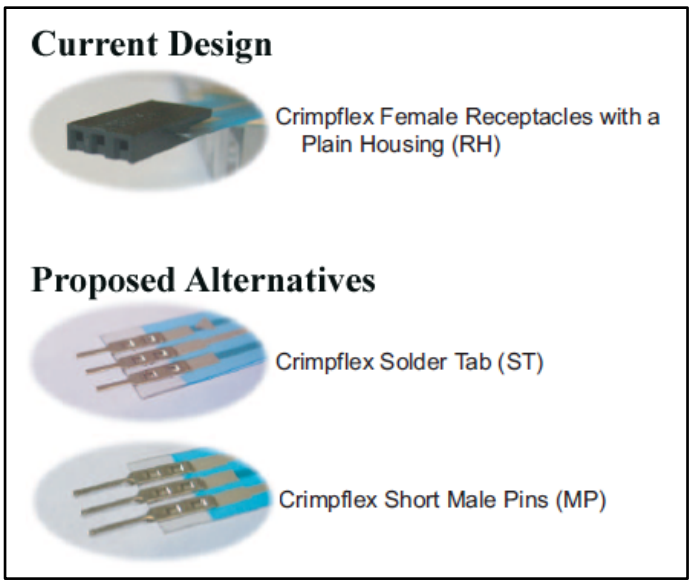

(Adapted from [31])

Figure 6.5: SoftPot Connector Types for Current Design and Proposed Alternatives

6.2.2 Potential Theoretical Design Improvement

In addition to the improvements proposed for several physical components of the sensing system, there also exist potential improvements to the theoretical components of the system. These include modifications to the LabVIEW code that may either improve the performance capability of the system directly or reduce the clutter by simplifying repetitive code where possible.

6.2.2.1 Alarm Time Setting Specific to Sensors

The current system applies the same alarm time setting to all sensors in the prototype. Human skin may react differently to pressure in different parts of the body. For example, the skin covering elbows and heels have different thickness compared to skin at the shoulder blades and lower back. The onset of bedsore formation may occur at varying times in

different parts of the body. A potential improvement to the current design would differentiate the alarm time setting among the different areas of the body, creating the capability to specify the alarm time for those different sensors in different areas on the prototype. This would not only improve the safety of the patient, but if certain body parts can sustain longer pressure than others, then an unnecessary alarm could be avoided allowing the caregiver to perform other needed tasks in the hospital or home.

6.2.2.2 Improved Pressure Deviation Tolerance

The current system is coded to allow a tolerance of ±0.05 volt deviation (or nearly 3 cm (1 in) of pressure point movement along the sensor length in either direction) to prevent the clock counter from resetting. An improved method would also take into consideration the time between when a pressure point was relieved from and when it re-introduced to a sensor. The skin does not recover at the pressure relief instantly, especially if the pressure that was being applied had been unrelieved for a long time. With a time delay introduced, which would prevent a clock reset at the instant of voltage deviation of more than ±0.05 volt, there would be an increase in the level of safety for the patient because their skin would be allowed to recover.

6.2.2.3 Sub-Visual Instrument for Code Simplification

The LabVIEW code that was developed in this research used a similar coding diagram for every pressure-sensing element, which includes two elements per physical sensor. This translates to 70 coding diagrams that all perform the same basic task for their respective pressure-sensing element. It is possible to develop a new sub-visual instrument (subVI) that

can be recalled by each element, vastly reducing the amount of code needed to perform the same task that is currently performed by the code described in Section 5.5. The simplified code would allow for modifications to be made once, rather than 70 times (once for each element). A subVI reduces the amount of hard coding in the design and improve the flexibility of the code to be amended in the future.

Several areas of improvement relating to the prototype design have been identified and the implications of each potential modification have been described. The research herein provides a framework for future researchers to perfect a design that may eventually reduce the occurrence of bedsores in hospital patients and, consequently, save lives.

7 References

[1] Health Council of the Netherlands. (1999), Pressure ulcers.)

[2] M. D. Gordon, M. M. Gottschlich, E. I. Helvig, J. A. Marvin and R. L. Richard. (2004, SEP-OCT). Review of evidenced-based practice for the prevention of pressure sores in burn patients. *J. Burn Care Rehabil. 25(5),* pp. 388-410.

[3] B. A. Kuhn and S. J. Coulter. (1992, 1992). Balancing the pressure ulcer cost and quality equation. *Nurs. Econ. 10(5),* pp. 353-359. Available: http://search.ebscohost.com/login.aspx?direct=true&db=c8h&AN=1993154343&site=ehost-live&scope=site.

[4] A. C. Voss, S. A. Bender, M. L. Ferguson, A. C. Sauer, R. G. Bennett and P. W. Hahn. (2005), Long-term care liability for pressure ulcers. *J. Am. Geriatr. Soc. 53(9),* pp. 1587-1592. Available: http://dx.doi.org/10.1111/j.1532-5415.2005.53462.x.

[5] R. H. Goebels and M. R. Goebels. (1999), Clinical practice guidelines for pressure ulcer prevention can prevent malpractice lawsuits in older patients. *J Wound Ostomy Continence Nurs 26(4),* pp. 175-184.

[6] M. Reddy, S. S. Gill and P. A. Rochon. (2006, AUG 23). Preventing pressure ulcers: A systematic review. *JAMA-J. Am. Med. Assoc. 296(8),* pp. 974-984.

[7] D. R. Berlowitz, G. H. Brandeis, J. Anderson, W. Du and H. Brand. (1997, March). Effect of pressure ulcers on the survival of long-term care residents. *The Journals of Gerontology Series A: Biological Sciences and Medical Sciences 52A(2),* pp. M106-M110.

[8] USC/Rancho pressure ulcer prevention: Stages of pressure ulcers. *2010(7/13/2010),* Available: http://www.usc.edu/programs/pups/articles-in-depth/stages-of-pressure-ulcers.html.

[9] D. Nayak, K. Srinivasan, S. Jagdish, R. Rattan and V. S. Chatram. (2008, AUG). Bedsores: "top to bottom" and "bottom to top". *Indian J. Surg. 70(4),* pp. 161-168.

[10] R. K. Daniel, D. L. Priest and D. C. Wheatley. (1981), Etiological factors in pressure sores: An experimental model. *Arch Phys Med Rehabil 62(10),* pp. 492-498.

[11] Reduction of Hospital-acquired Pressure Ulcers at Texas Health Arlington Memorial Hospital. Available: http://www.youtube.com/watch?v=1AwndgGnjag.

[12] D. Collison. Pressure sores: Skin disorders: Merck manual home edition. *2011(1/19/2011),* Available: http://www.merckmanuals.com/home/sec18/ch205/ch205a.html.

[13] J. Rosenfeld. Are there any federal regulations that apply to the prevention of bed sores? *2010(6/19/2010),* Available: http://www.bedsorefaq.com/are-there-any-federal-regulations-that-apply-to-the-prevention-of-bed-sores/.

[14] J. Rosenfeld. How does the use of the braden scale help in the prevention of bed sores? *2010(6/19/2010),* Available: http://www.bedsorefaq.com/how-does-the-use-of-the-braden-scale-help-in-the-prevention-of-bed-sores/.

[15] C. Gomez. What kind of mattress is on a hospital bed? | eHow.com. *2010(7/29/2010),* Available: http://www.ehow.com/about_6495494_kind-mattress-hospital-bed_.html.

[16] Hospital bed mattress | replacement mattress for hospital bed | hospital mattress | invacare | guardian | mattress systems. *2010(7/29/2010),* Available: http://www.phc-online.com/Hospital_Bed_Mattress_s/70.htm.

[17] Hospital bed mattress. *2011(1/18/2011),* Available: http://www.rehabmart.com/category/Hospital_Bed_Mattress.htm.

[18] Mattress overlay - volkner.com - sleep better and have a healthier life. *2010(7/29/2010),* Available: http://www.volkner.com/mattress-overlay.html.

[19] Stage IV 3000 alternating pressure relief mattress and low air loss $4979.00 FREE shipping from uCan health. *2011(1/18/2011),* Available: http://ucanhealth.com/goto.php?page=detail.php&graph1=SYS3000.

[20] How it works - strain gauge pressure transducer. *2010(7/20/2010),* Available: http://www.rdpe.com/ex/hiw-sgpt.htm.

[21] National high magnetic field laboratory - wheatstone bridge tutorial. *2010(7/20/2010),* Available: http://www.magnet.fsu.edu/education/tutorials/java/wheatstonebridge/index.html.

[22] Demystifying piezoresistive pressure sensors - maxim. *2010(7/20/2010),* Available: http://www.maxim-ic.com/app-notes/index.mvp/id/871.

[23] B. Kinney and M. Pinto. Pressure - BIOE 414 instrumentation projects - university of illinois - engineering wiki. *2011(1/14/2011),* .Available: https://wiki.engr.illinois.edu/display/BIOE414/Pressure

[24] Images Scientific Instruments: Flex sensors. *2010(2/8/2010),* Available: http://www.imagesco.com/sensors/flex-sensor.html.

[25] FlexiForce®: Single button force sensing resistor. *2010(8/5/2010),* Available: http://www.tekscan.com/flexiforce/flexiforce.html.

[26] Force sensors and pressure sensors. *2010(8/5/2010),* Available: http://www.imagesco.com/sensors/force-sensors.html.

[27] J. Pierson. (1992), *The Art of Practical and Precise Strain Based Measurement (7/21/2010)* Available: http://www.google.com/url?sa=t&source=web&cd=1&ved=0CBgQFjAA&url=http%3A%2F%2Fwww.webprofile.info%2Fjpierson%2FArt_of_Measurement.pdf&ei=t6ScTYH4FJT2gAe59_2aBw&usg=AFQjCNF0fUAsmaBM9t2efINmYUZXSd-gXA&sig2=-cABlWMiXDTLMOYZLz0gkg.

[28] C. D. H. Williams. Introduction to sensors. *2010(7/21/2010),* Available: http://newton.ex.ac.uk/teaching/CDHW/Sensors/.

[29] ConTacts discrete tactile sensors - overview. *2010(2/8/2010),* Available: http://www.pressureprofile.com/products-contacts.

[30] P. Woolf. PressureSensors - ControlsWiki. *2010(7/21/2010),* Available: http://controls.engin.umich.edu/wiki/index.php/PressureSensors.

[31] Membrane potentiometers SoftPot. *2010(2/7/2010),* Available: http://www.spectrasymbol.com/typo3/site/en/home.html.

[32] L. Shu, T. Hua, Y. Wang, Q. Li, D. D. Feng and X. Tao. (2010, MAY). In-shoe plantar pressure measurement and analysis system based on fabric pressure sensing array. *IEEE T. Inf. Technol. Biomed. 14(3),* pp. 767-775.

[33] A. A. P. Wai, V. F. S. Fook, M. Jayachandran, J. Biswas, C. Nugent, M. Mulvenna, J. Lee and P. Y. L. Kiat. (2008, 10/01). Smart wireless continence management system for persons with dementia. *Telemedicine and e-Health 14(8),* pp. 825-832. Available: http://dx.doi.org/10.1089/tmj.2008.0084.

[34] Loom reed, taken by "brassedoff.net". *2011(4/14/2011),* Available: http://www.flickr.com/photos/21165321@N04/4410662359/.

[35] Bedding buying guide - how to choose bedding - cuddledown. *2011(1/18/2011),* Available: http://www.cuddledown.com/product/articles/buying-guides/bedding+guide.do.

[36] 3M electronics manufacturing : 3M™ velostat™ electrically conductive film. *2011(3/30/2011),* Available: http://www3.3m.com/catalog/uk/en002/electronics_mfg/static_control_packaging/node_XC8BXSPKHPbe/root_K3BHNB8005gv/vroot_5KR9K2C2KZge/gvel_JQGPTT9723gl/theme_uk_staticcontrolpackaging_3_0/command_AbcPageHandler/output_html.

[37] V. Ahlstrom and K. Longo. (2003), *Human Factors Design Standard (HFDS) 2011(1/31/2011).* Available: http://hf.tc.faa.gov/hfds/default.htm.

[38] Angle, linear position measuring | digi-key. *2011(4/12/2011),* Available: http://search.digikey.com/scripts/DkSearch/dksus.dll?Cat=1967060&k=softpot.

[39] A. M. Seyam, "Structural Design of Woven Fabrics," *Textile Progress*, vol. 31, 2002.

[40] P. Horowitz and W. Hill. (1989), *The Art of Electronics* (2nd ed.) Available: http://books.google.com/books?id=bkOMDgwFA28C&pg=PA8&dq=what+is+a+voltage+divider&hl=en&ei=zSWjTYitFsLIgQfVwdHaBQ&sa=X&oi=book_result&ct=result&resnum=1&ved=0CEEQ6AEwAA#v=onepage&q=what%20is%20a%20voltage%20divider&f=false.

[41] DAQ M Series User Manual. National Instruments Corporation. 2008.

[42] Hard coded definition from PC magazine encyclopedia. *2011(5/9/2011),* Available: http://www.pcmag.com/encyclopedia_term/0,2542,t=hard+coded&i=44076,00.asp.

[43] European Pressure Ulcer Advisory Panel and National Pressure Ulcer Advisory Panel. (2009), Prevention and treatment of pressure ulcers: Quick reference guide. *2010(4/17/2010),* Available: http://www.npuap.org/resources.htm.

[44] Neoprene Pressure Sensor Matrix. HOW TO GET WHAT YOU WANT. *2010(10/8/2010),* Available: http://www.kobakant.at/DIY/?p=213.

8 Appendices

A Bedsore Classification and Grading

Table 8.1: International Pressure Ulcer Classification System

Category/Stage I **"Non-blanchable erythema"**	"Intact skin with non-blanchable redness of a localized area usually over a bony prominence. Darkly pigmented skin may not have visible blanching; its color may differ from the surrounding area. The area may be painful, firm, soft, warmer or cooler as compared to adjacent tissue. Category I may be difficult to detect in individuals with dark skin tones. May indicate "at risk" persons."
Category/Stage II **"Partial thickness"**	"Partial thickness loss of dermis presenting as a shallow open ulcer with a red pink wound bed, without slough. May also present as an intact or open/ruptured serum-filled or sero-sanginous filled blister. Presents as a shiny or dry shallow ulcer without slough of bruising. Bruising indicates a deep tissue injury. This category should not be used to describe skin tears, tape burns, incontinence associated dermatitis, maceration or excoriation."
Category/Stage III **"Full thickness skin loss"**	"Full thickness tissue loss. Subcutaneous fat may be visible but bone, tendon or muscle is not exposed. Slough may be present but does not oscure the depth of tissue loss. May include undermining and tunneling. The depth of a Stage III pressure ulcer varies by anatomical location. The bridge of the nose, ear, occiput and malleolus do not have (adipose) subcutaneous tissue and ulcers in this category can be shallow. In contrast, areas of significant adiposity can develop extremely deep Stage III pressure ulcers. Bone/tendon is not visible or directly palpable."
Category/Stage IV **"Full thickness tissue loss"**	"Full thickness tissue loss with exposed bone, tendon or muscle. Slough or eschar may be present. Often includes undermining and tunneling. The depth of a Stage IV pressure ulcer varies by anatomical location. The bridge of the nose, eat, occiput and malleolus do not have (adipose) subcutaneous tissue and these ulcers can be shallow. Stage IV ulcers can extend into muscle and/or supporting structures making osteomyelitis or osteitis likely to occur. Exposed bone/muscle is visible or directly palpable." (Taken from [43])

Table 8.2: The Braden Scale for Predicting Pressure Ulcer Risk

	1	2	3	4
Sensory Perception *Ability to respond meaningfully to pressure-related discomfort*	Completely Limited • Unresponsive to painful stimuli -OR- • Limited ability to feel pain over most of body surface	Very Limited • Responds only to painful stimuli • Cannot communicate discomfort -OR- • Has sensory impairment limiting ability to feel discomfort over ½ of body	Slightly Limited • Responds to verbal commands but cannot always communicate discomfort -OR- • Has sensory impairment limiting ability to feel discomfort in 1 or 2 extremities	No Impairment • Responds to verbal command. • No sensory deficit to limit ability to feel or express discomfort
Moisture *Degree to which skin is exposed to moisture*	Constantly Moist • Perspiration, urine, etc keep skin moist almost constantly • Dampness detected every time patient moved or turned	Moist • Skin often, but not always moist • Sheets must be changed at least once per shift	Occasionally Moist • Skin occasionally moist • Sheets must be changed about once per day	Rarely Moist • Skin usually dry • Sheets only require changing at routine intervals
Activity *Degree of physical activity*	Bedfast • Confined to bed	Chairfast • Walking ability severely limited or nonexistent • Cannot bear own weight and/or must be assisted into chair or wheelchair	Walks Occasionally • Walks during the day occasionally, but for very short distances with or without assistance • Spends majority of each shift in bed or chair	Walks Frequently • Walks outside room at least twice a day and inside room at least once every 2 hours during working hours
Mobility *Ability to change and control body position*	Completely Immobile • Does not make even slight changes in body or extremity position without assistance	Very Limited • Makes occasional slight changes in body or extremity position • Unable to make frequent or significant changes without assistance	Slightly Limited • Makes frequent, though slight, changes in body or extremity position without assistance	No Limitations • Makes major and frequent changes in position independently

Table 8.2 Continued

Nutrition *Usual food intake pattern*	Very Poor • Never eats a complete meal • Rarely eats more than a third of any food offered • Takes fluids poorly -OR- • Is NPO and/or maintained on clear liquids or IV for more than 5 days	Probably Inadequate • Rarely eats complete meal • Generally eats only about ½ of any food offered • Occasionally takes dietary supplement -OR- • Receives less than optimal amount of liquid diet or tube feeding	Adequate • Eats over ½ of most meals • Occasionally will refuse meal, but will take supplement if offered -OR- • Is on tube feeding or TPN regimen, which typically meets most of nutritional needs	Excellent • Eats most of every meal and never refuses a meal • Does not require supplementation
Friction and Shear	Problem • Requires moderate to maximum assistance in moving • Complete lifting without sliding is impossible • Frequently slides down in chair or bed, requiring frequent repositioning with maximum assistance • Spasticity, contractures, or agitation leads to almost certain friction	Potential Problem • Moves feebly or requires minimum assistance • Skin probably slides to some extent on sheets, chair, etc during a move • Maintains relatively good position in chair or bed most of time, but occasionally slides	No Apparent Problem • Moves in bed and in chair without assistance and has sufficient muscle strength to lift up completely during a move • Maintains good position in bed or chair at all times	
				TOTAL SCORE:
				(Adapted from [14])

B Technical Comparison of ConTact Sensors

Table 8.3: Technical Comparison between 3 ConTacts types

	Conformable	Industrial	Hybrid
Sensor Thickness	1.1 mm	0.3 mm	0.7 mm
Max Pressure Range	0-50 psi	0-2000 psi	0-50 psi
Min Pressure Range	0-2 psi	0-50 psi	0-2 psi
Standard Sizes	10x10mm 25x25mm 50x50mm	10x10mm 25x25mm 50x50mm	10x10mm 25x25mm
Temperature Range	-20 to +100 °C	-40 to +200 °C	-20 to +100 °C
Non-Repeatability	< 2%	< 2%	< 2%
Sensor Material	Conductive cloth	Kapton™	Kapton™ and Conductive Cloth
Conformable/Moldable	Yes	No	Somewhat
			(Adapted from [29])

C Neoprene Bend Sensor Fabrication Instructions

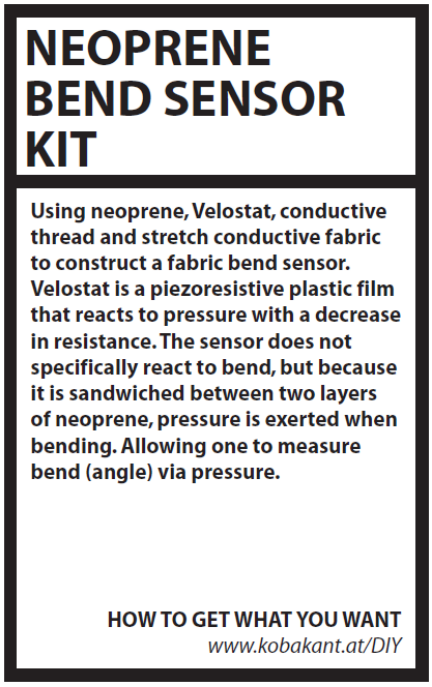

(Adapted from [44])

Figure 8.1: Introduction Neoprene Bend Sensor Kit

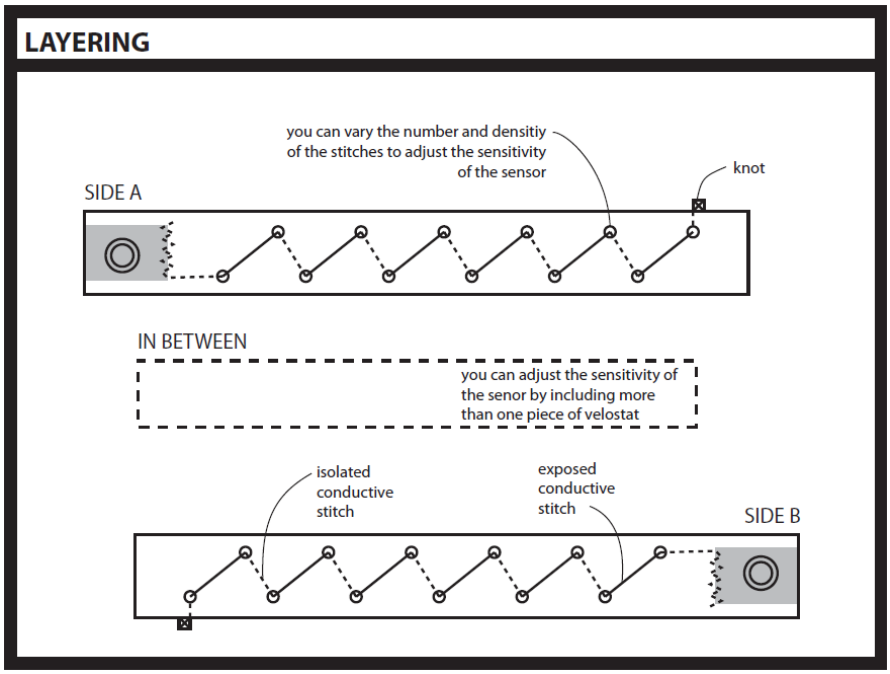

(Adapted from [44])

Figure 8.2: Layering Diagram for Neoprene Bend Sensor

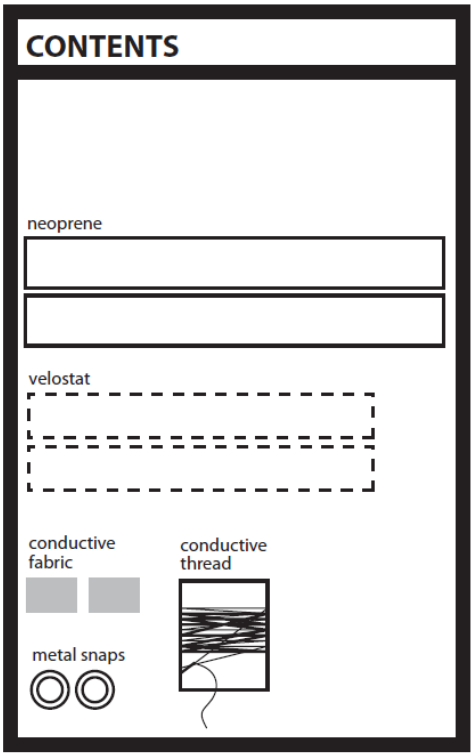

(Adapted from [44])

Figure 8.3: Contents of Neoprene Bend Sensor Kit

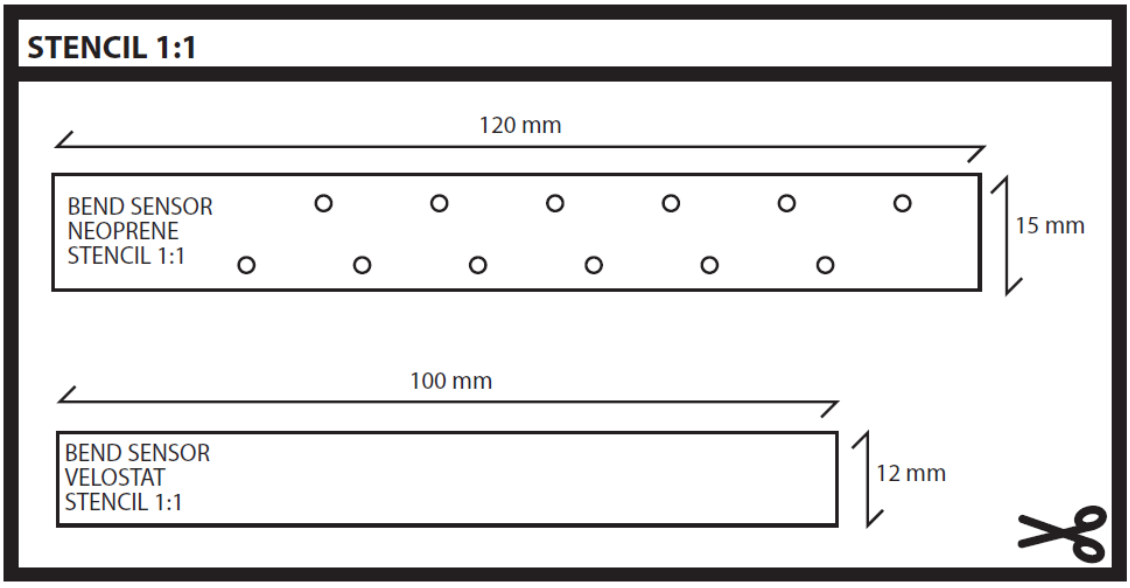

(Adapted from [44])

Figure 8.4: Stencil for Sewing Holes for Neoprene (Actual Size)

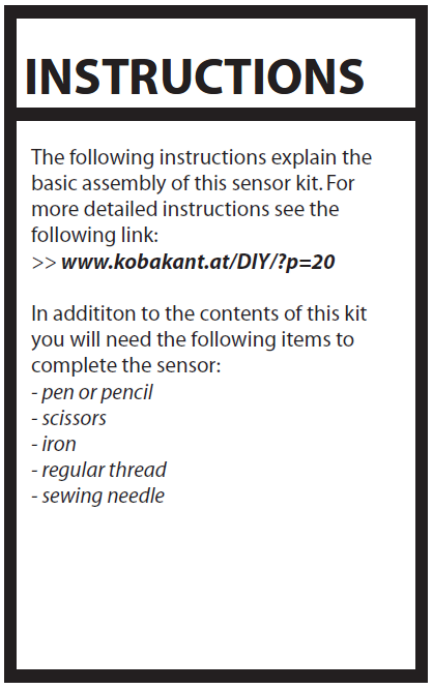

(Adapted from [44])

Figure 8.5: Introduction to Instructions for Neoprene Bend Sensor

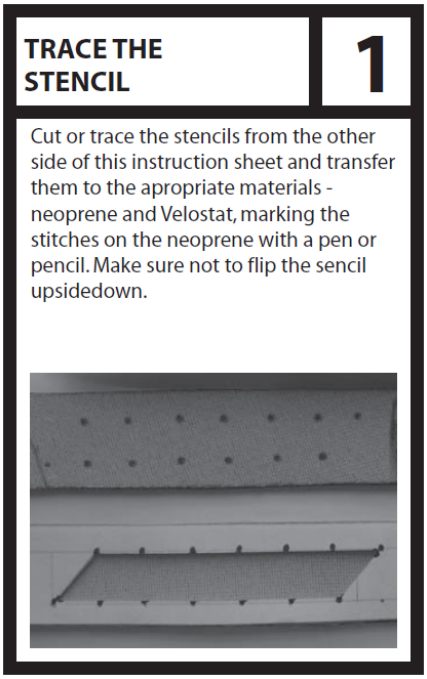

(Adapted from [44])

Figure 8.6: Neoprene Bend Sensor Instructions Part 1 – Trace the Stencil

(Adapted from [44])

Figure 8.7: Neoprene Bend Sensor Instructions Part 2 – Fuse Conductive Fabric

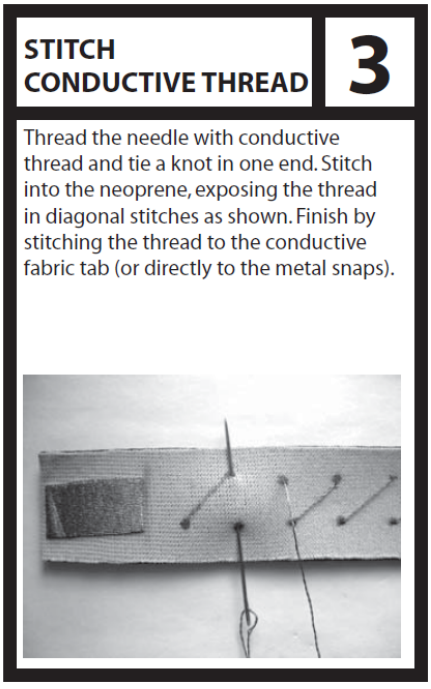

(Adapted from [44])

Figure 8.8: Neoprene Bend Sensor Instructions Part 3 – Stitch Conductive Thread

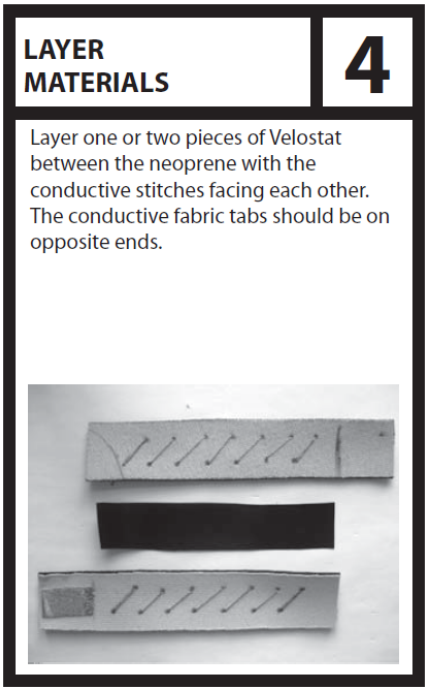

(Adapted from [44])

Figure 8.9: Neoprene Bend Sensor Instructions Part 4 – Layer Materials

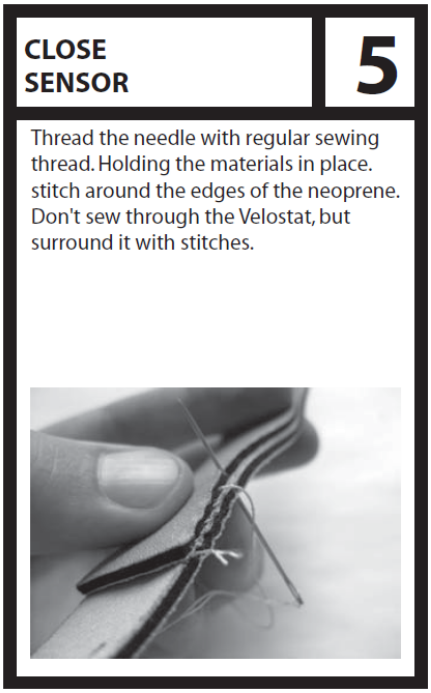

(Adapted from [44])

Figure 8.10: Neoprene Bend Sensor Instructions Part 5 – Close Sensor

(Adapted from [44])

Figure 8.11: Neoprene Bend Sensor Instructions Part 6 – Attach Snaps

(Adapted from [44])

Figure 8.12: Neoprene Bend Sensor Instructions Part 7 – Test Finished Sensor

D Loom Gear Setup

Table 8.4: Gearing Setups for Picanol PAT-A Airjet Loom

	Setup 1	Setup 2	Setup 3	Setup 4	Setup 5	Setup 6
	A – 17 **B – 68** **C – 21** **D – 42**	**A – 17** **B – 68** **C – 42** **D – 21**	**A – 43** **B – 43** **C – 21** **D – 42**	**A – 43** **B – 43** **C – 42** **D – 21**	**A – 68** **B – 17** **C – 21** **D – 42**	**A – 68** **B – 17** **C – 42** **D – 34**
Pick pinion E	**No. of picks/inch**	**No. of picks/inch**	**No. of picks/inch**	**No. of picks/inch**	**No. of picks/inch**	**No. of picks/inch**
49 t	277.60	138.76	69.40	34.68	17.36	8.68
50 t	283.20	141.60	70.80	35.40	17.68	8.84
51 t	288.88	144.44	72.20	36.12	18.04	9.04
52 t	294.52	147.28	73.64	36.80	18.40	9.20
53 t	300.20	150.12	75.04	37.52	18.76	9.40
54 t	305.88	152.92	76.44	38.24	19.12	9.56
55 t	311.52	155.76	77.88	38.92	19.44	9.72
56 t	317.20	158.60	**79.28**	39.64	19.84	9.92
57 t	322.84	161.44	80.72	40.36	20.16	10.08
58 t	328.56	164.28	82.12	41.08	20.52	10.28
59 t	334.20	167.12	83.44	41.76	20.92	10.44
60 t	339.84	169.92	84.96	42.48	21.24	10.60

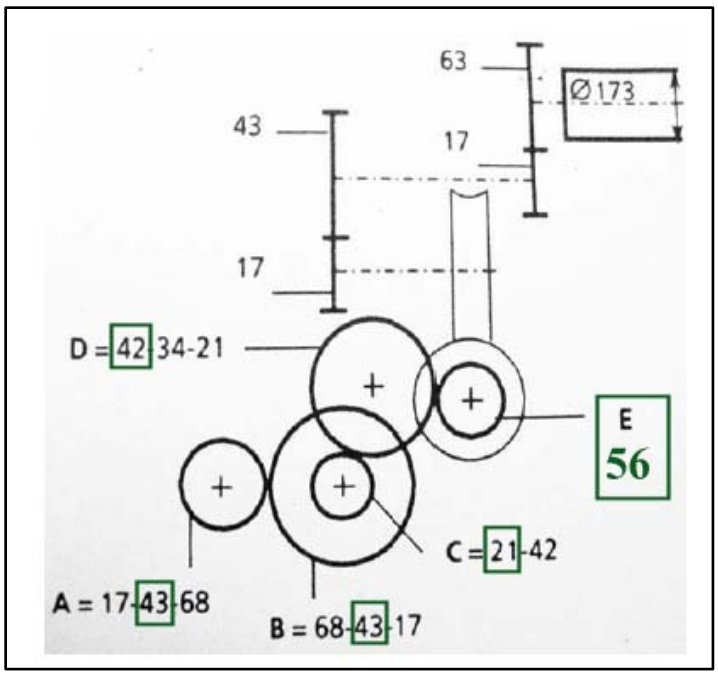

Figure 8.13: Gearing Diagram Setup for Prototype Fabric

E Chain Plan and Draw-in Draft for Weave Design

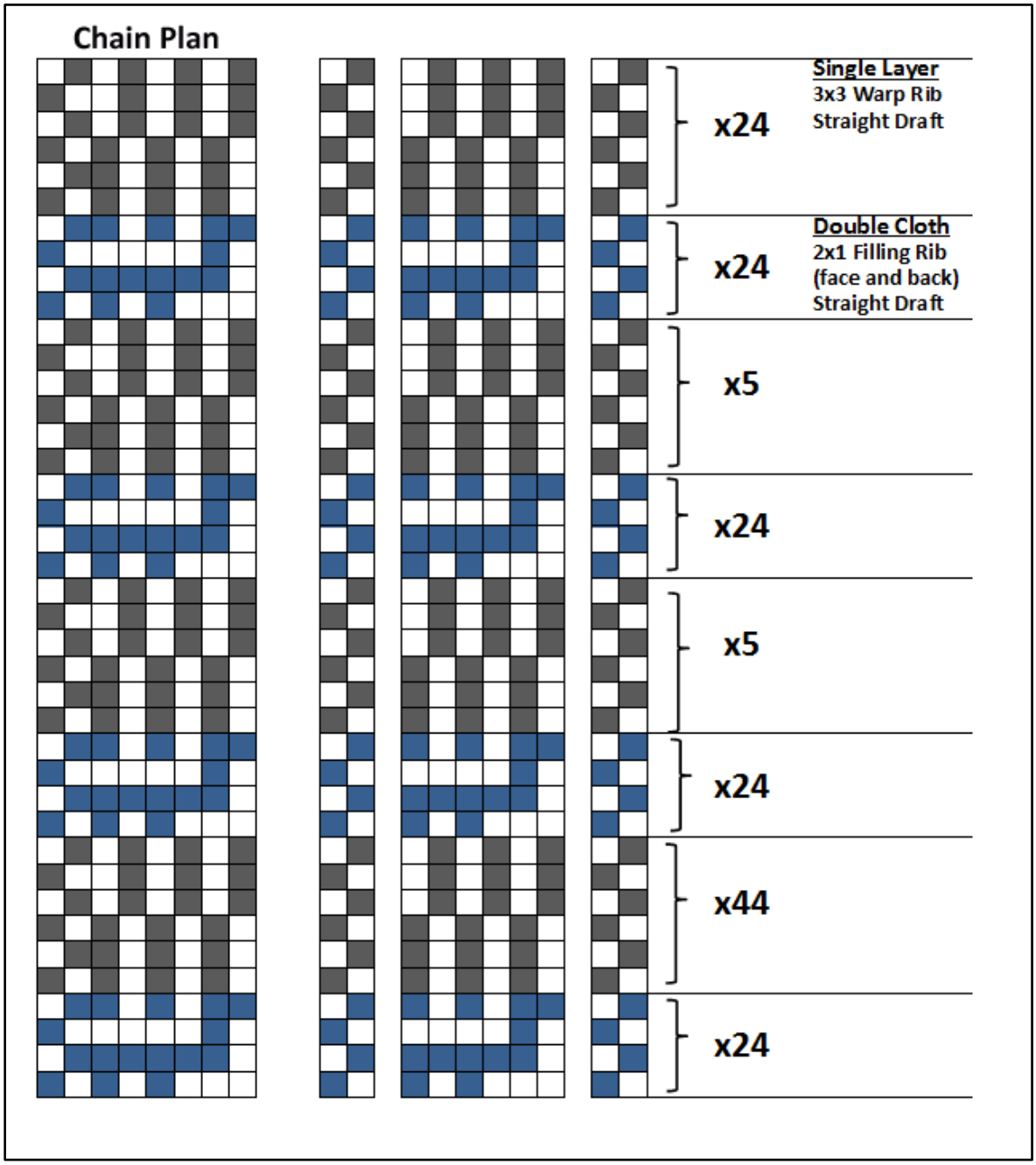

Figure 8.14: Chain Plan for Woven Fabric Design (1/5)

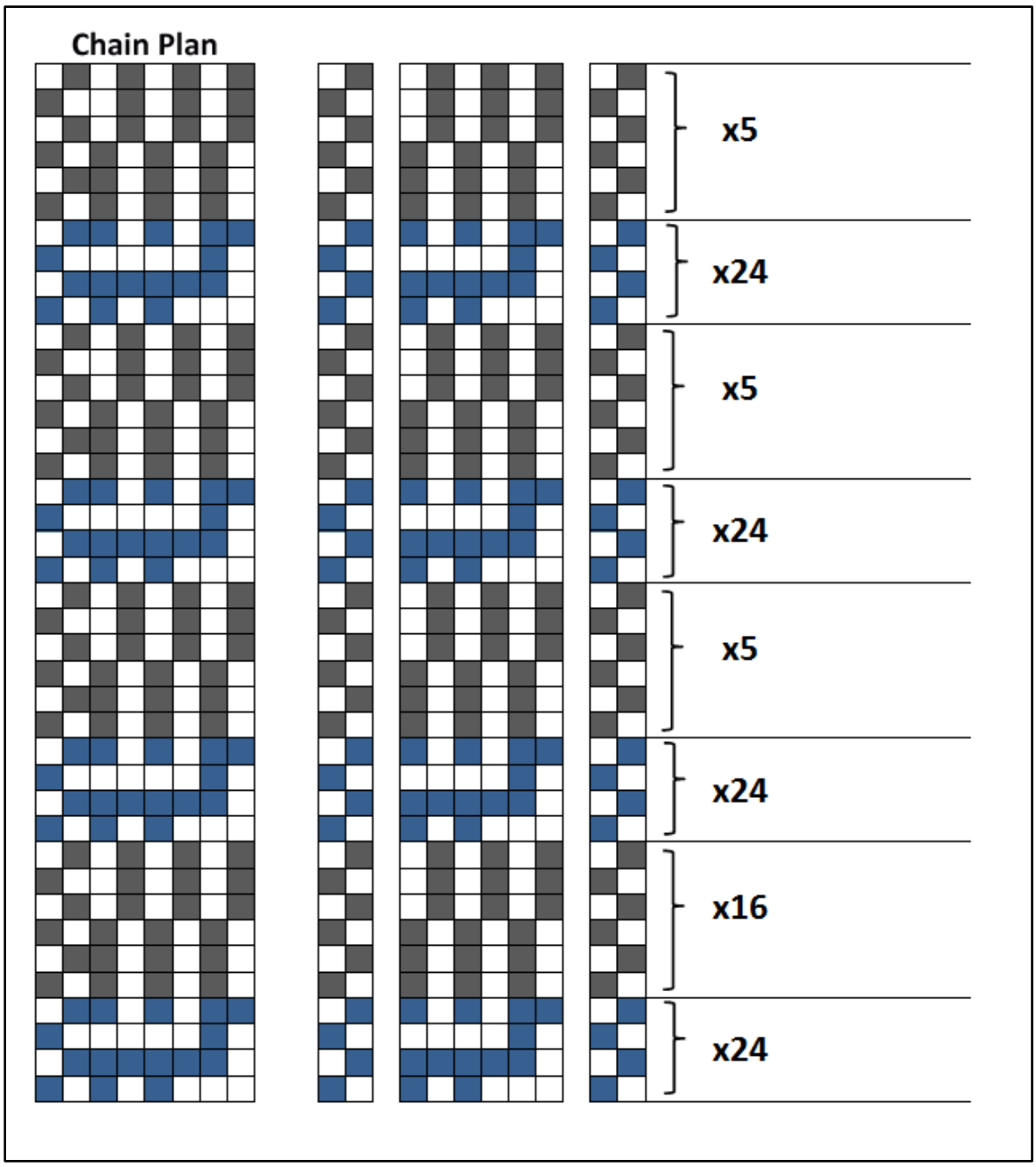

Figure 8.15: Chain Plan for Woven Fabric Design (2/5)

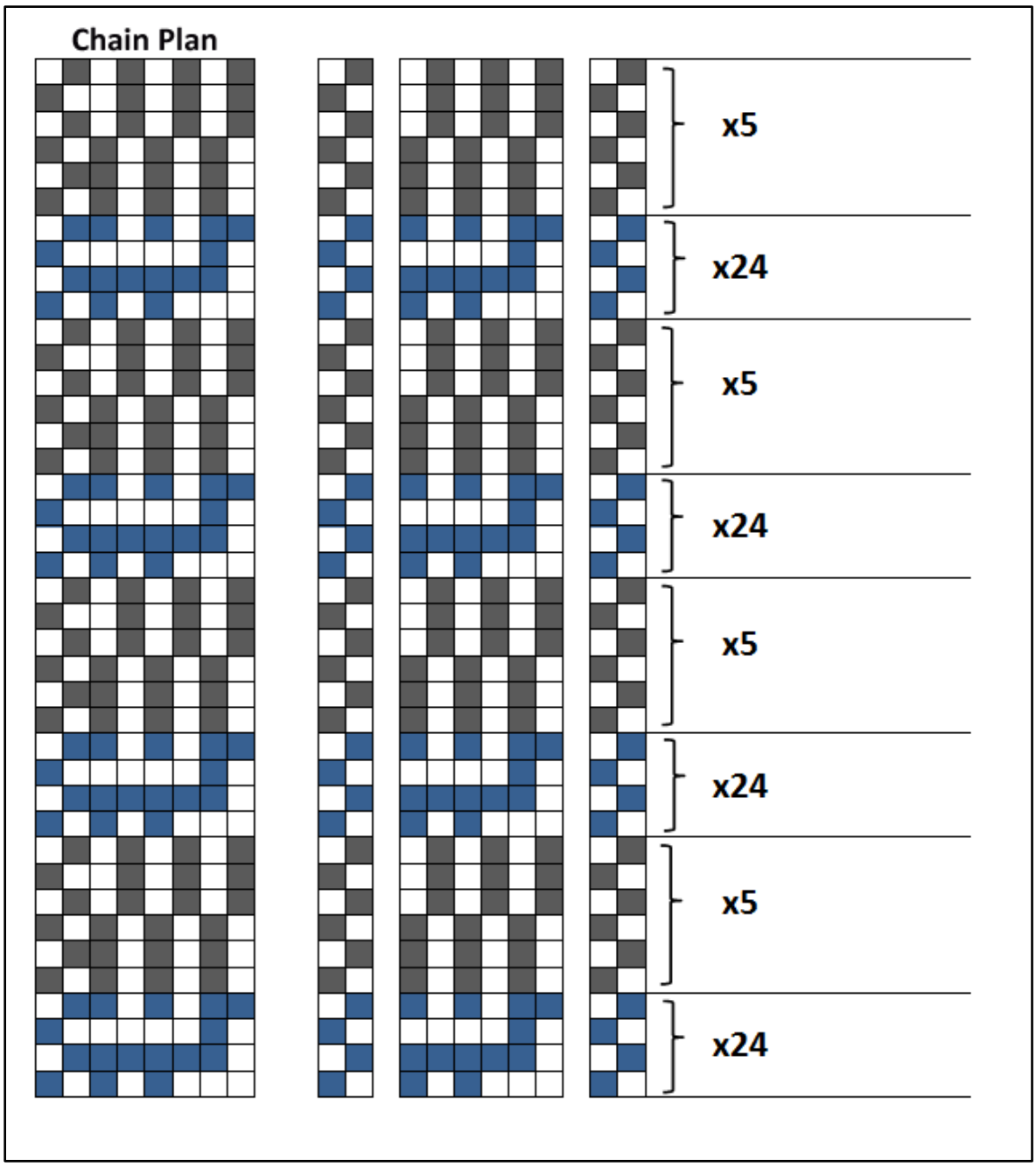

Figure 8.16: Chain Plan for Woven Fabric Design (3/5)

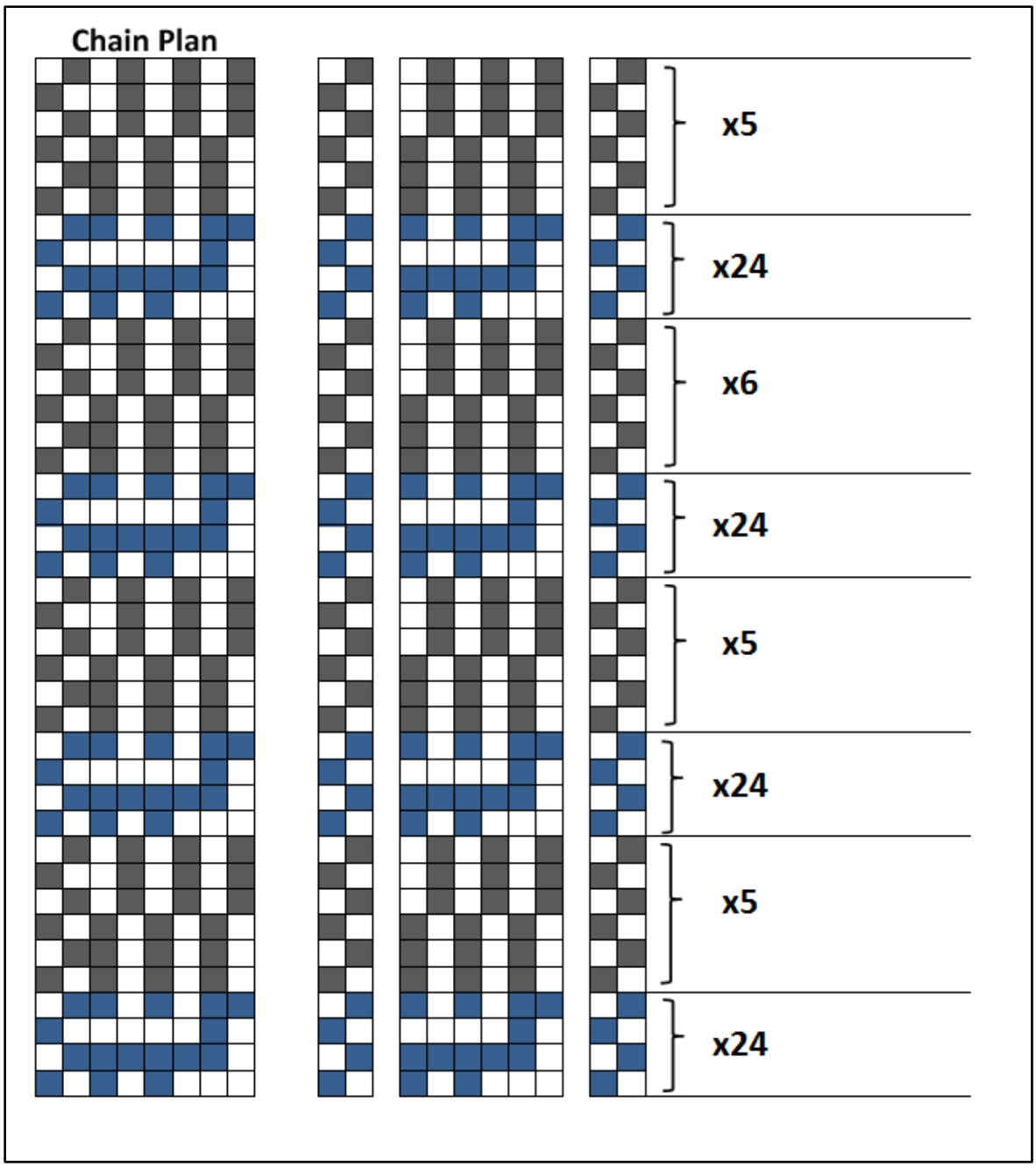

Figure 8.17: Chain Plan for Woven Fabric Design (4/5)

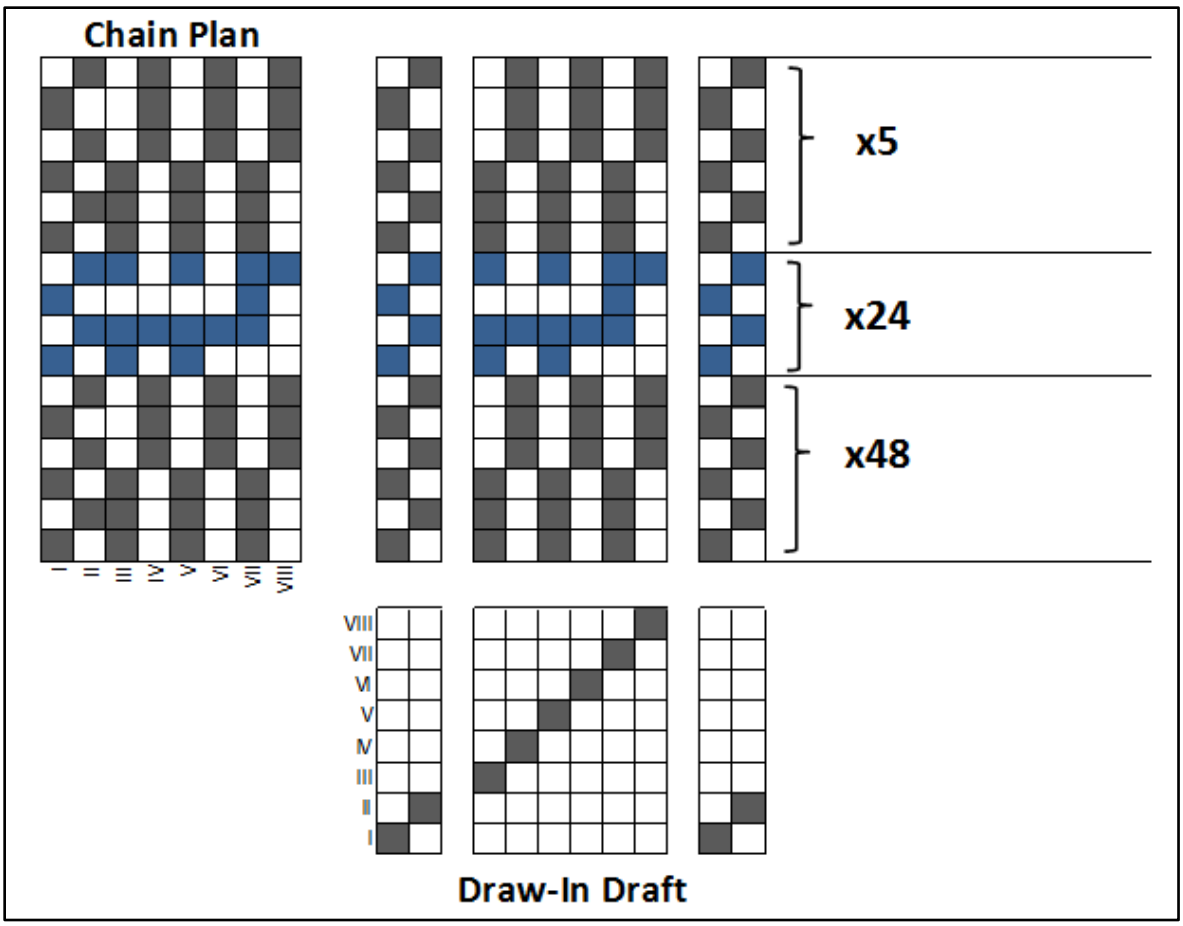

Figure 8.18: Chain Plan and Draw-in Draft for Woven Fabric Design (5/5)

F Choosing Shunt Resistor for Circuit

$$V_{OUT} = \frac{R_{VAR}}{R_{VAR} + R_{SHUNT}} \times V_{IN}$$

R-var1 represents one outer pressure point on the sensor
R-var2 represents the other outer pressure point on the sensor

R-var1 (kΩ)	0.1	1.5	2	2.5	3	3.5	4	4.5	5	5.5	6	6.5	7	7.5	8	8.5	9	9.9
R-shunt (kΩ)	10																	
V-in (V)	5																	
V-out1 (V)	0.05	0.65	0.83	1.00	1.15	1.30	1.43	1.55	1.67	1.77	1.88	1.97	2.06	2.14	2.22	2.30	2.37	2.487
R-var2 (kΩ)	9.9	8.5	8	7.5	7	6.5	6	5.5	5	4.5	4	3.5	3	2.5	2	1.5	1	0.1
R-shunt (kΩ)	10																	
V-in (V)	5																	
V-out2 (V)	2.487	2.30	2.22	2.14	2.06	1.97	1.88	1.77	1.67	1.55	1.43	1.30	1.15	1.00	0.83	0.65	0.45	0.05
Sensor Res. (kΩ)	10																	

Figure 8.19: Spreadsheet View – Choosing Shunt Resistance – 10 kΩ

$$V_{OUT} = \frac{R_{VAR}}{R_{VAR} + R_{SHUNT}} \times V_{IN}$$

R-var1 represents one outer pressure point on the sensor
R-var2 represents the other outer pressure point on the sensor

R-var1 (kΩ)	0.1	1.5	2	2.5	3	3.5	4	4.5	5	5.5	6	6.5	7	7.5	8	8.5	9	9.9
R-shunt (kΩ)	100																	
V-in (V)	5																	
V-out1 (V)	0.00	0.07	0.10	0.12	0.15	0.17	0.19	0.22	0.24	0.26	0.28	0.31	0.33	0.35	0.37	0.39	0.41	0.450
R-var2 (kΩ)	9.9	8.5	8	7.5	7	6.5	6	5.5	5	4.5	4	3.5	3	2.5	2	1.5	1	0.1
R-shunt (kΩ)	100																	
V-in (V)	5																	
V-out2 (V)	0.450	0.39	0.37	0.35	0.33	0.31	0.28	0.26	0.24	0.22	0.19	0.17	0.15	0.12	0.10	0.07	0.05	0.00
Sensor Res. (kΩ)	10																	

Figure 8.20: Spreadsheet View – Choosing Shunt Resistance – 100 kΩ

G Test 1 Screen Views

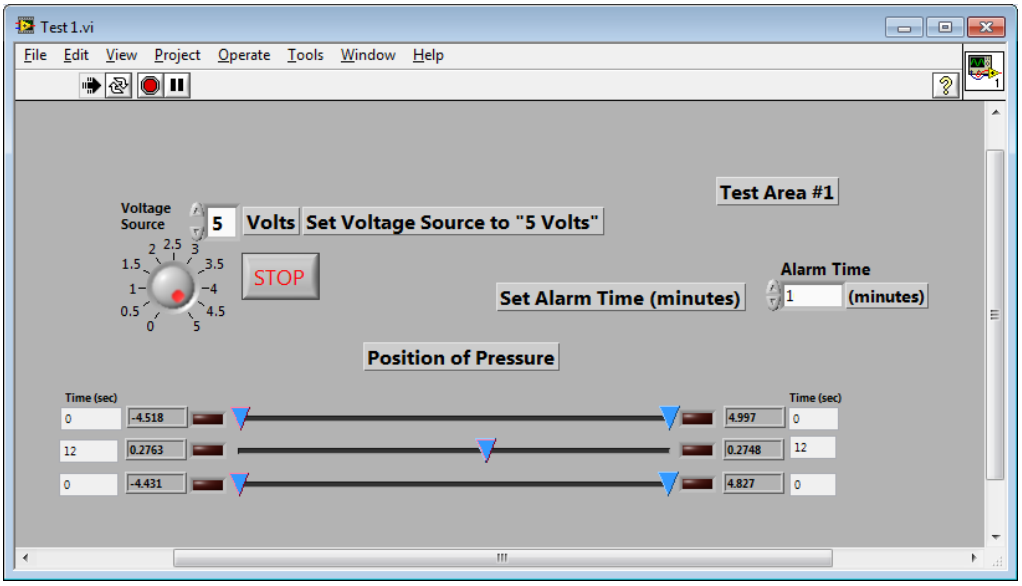

Figure 8.21: GUI, Test 1, Hard Surface, @ 12 Seconds

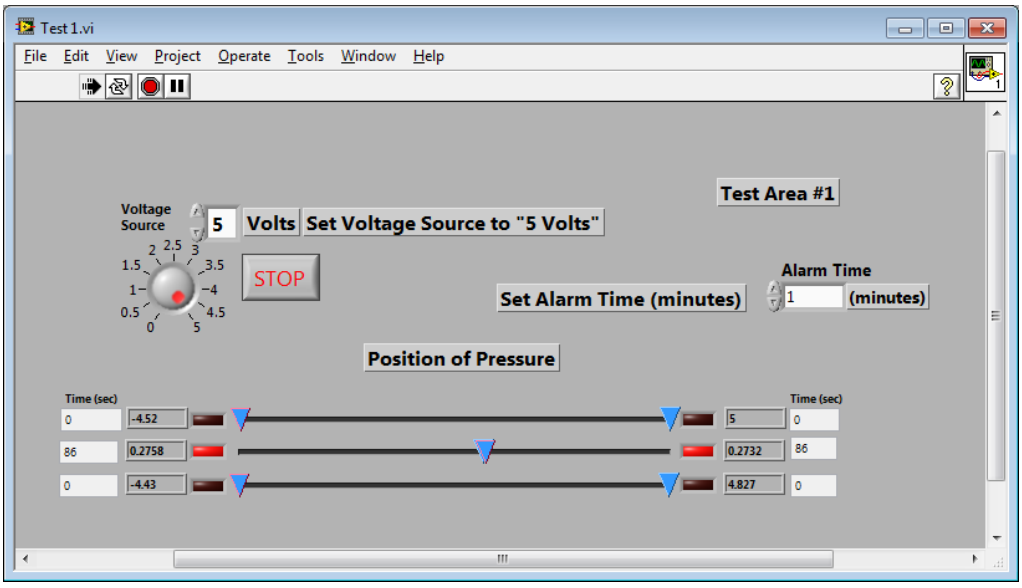

Figure 8.22: GUI, Test 1, Hard Surface, @ 86 Seconds with Alarm

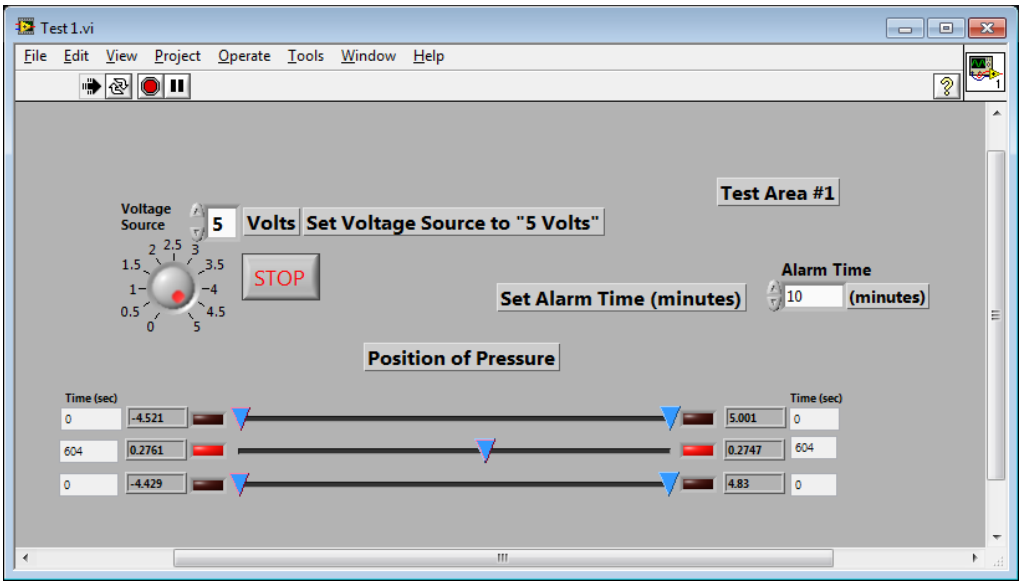

Figure 8.23: GUI, Test 1, Hard Surface, @ 604 Seconds with Alarm

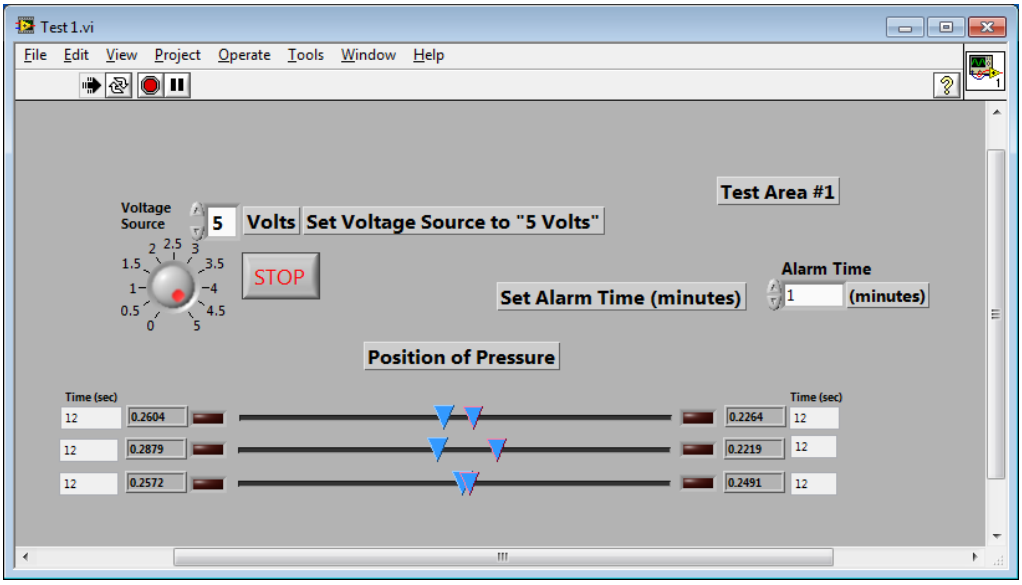

Figure 8.24: GUI, Test 1, Cushioned Surface, @ 12 Seconds

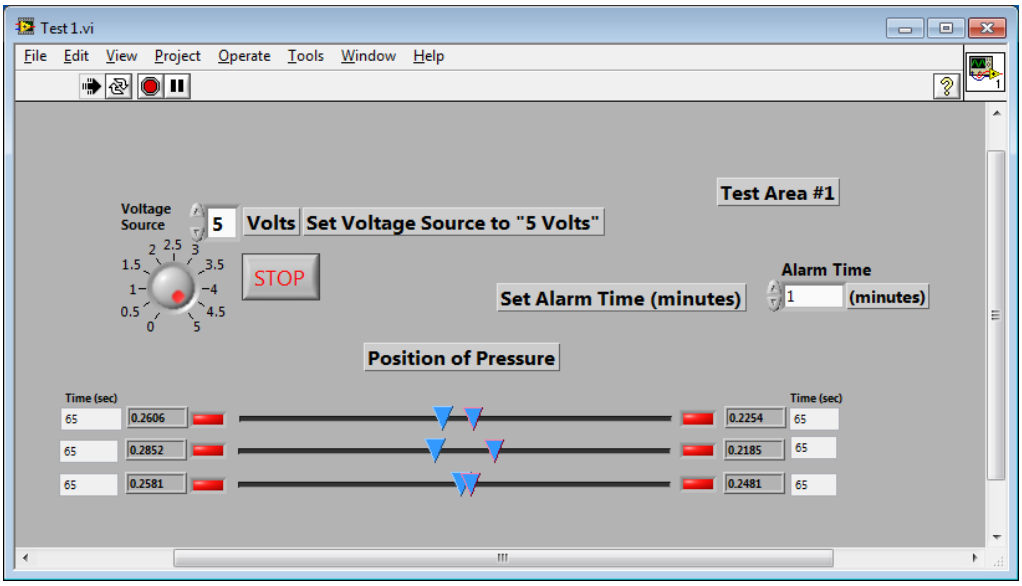

Figure 8.25: GUI, Test 1, Cushioned Surface, @ 65 Seconds with Alarm

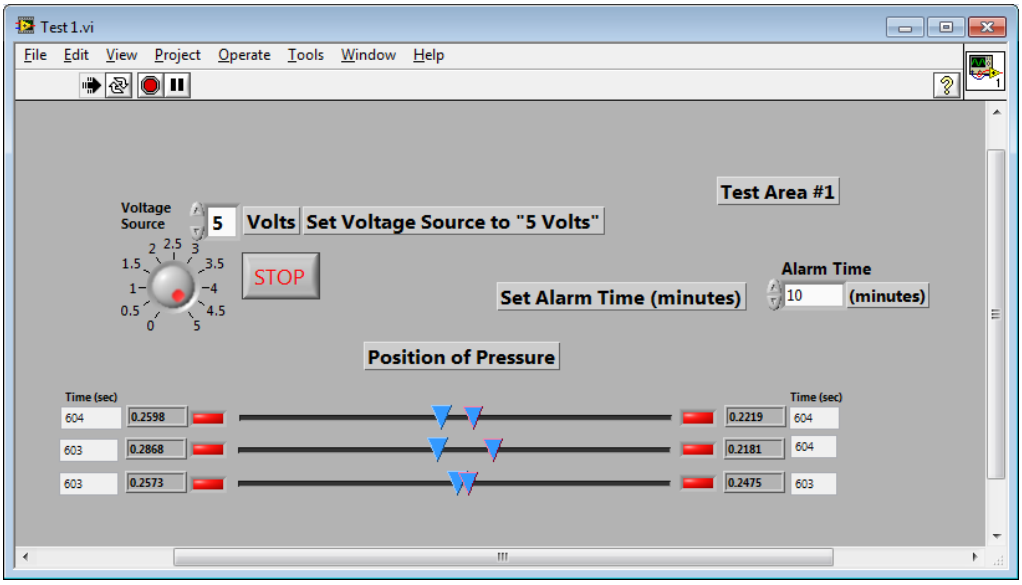

Figure 8.26: GUI, Test 1, Cushioned Surface, @ 604 Seconds with Alarm

H Test 2 Screen Views

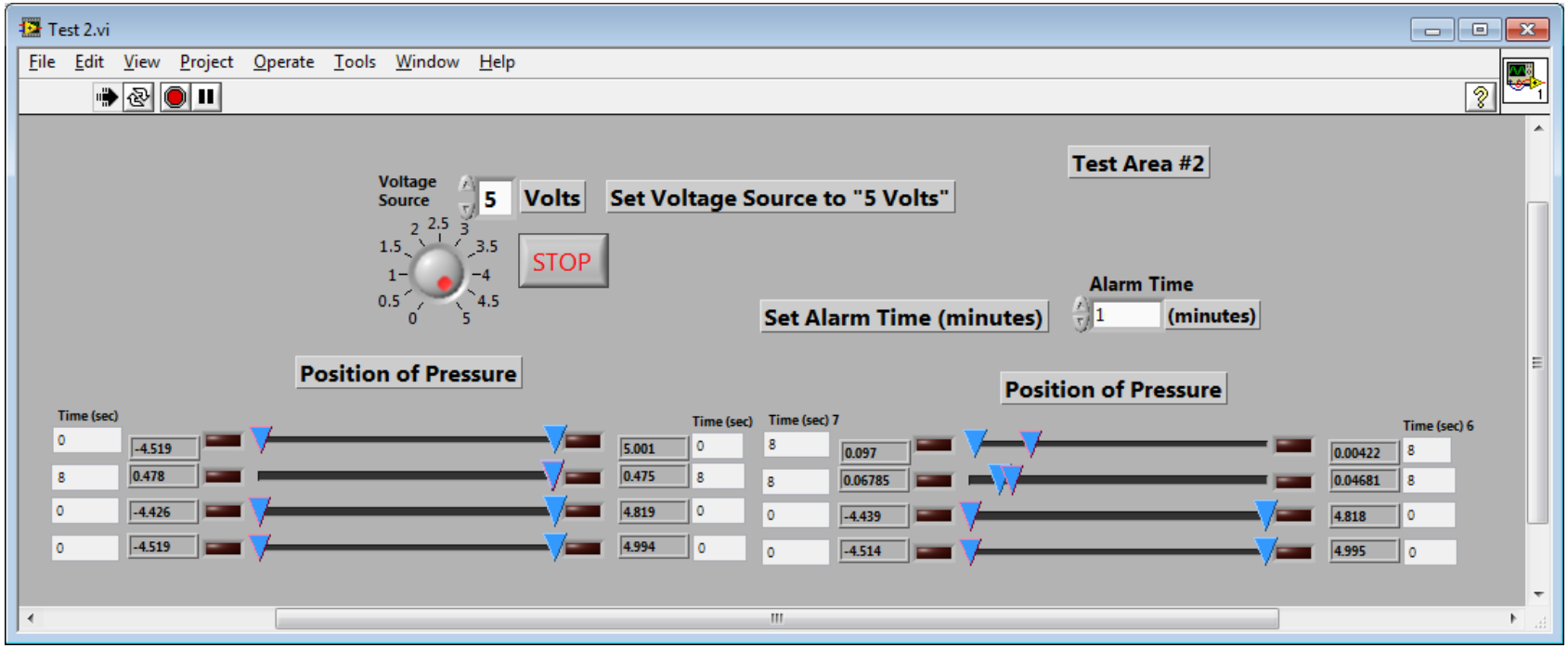

Figure 8.27: GUI, Test 2, Hard Surface, @ 8 Seconds

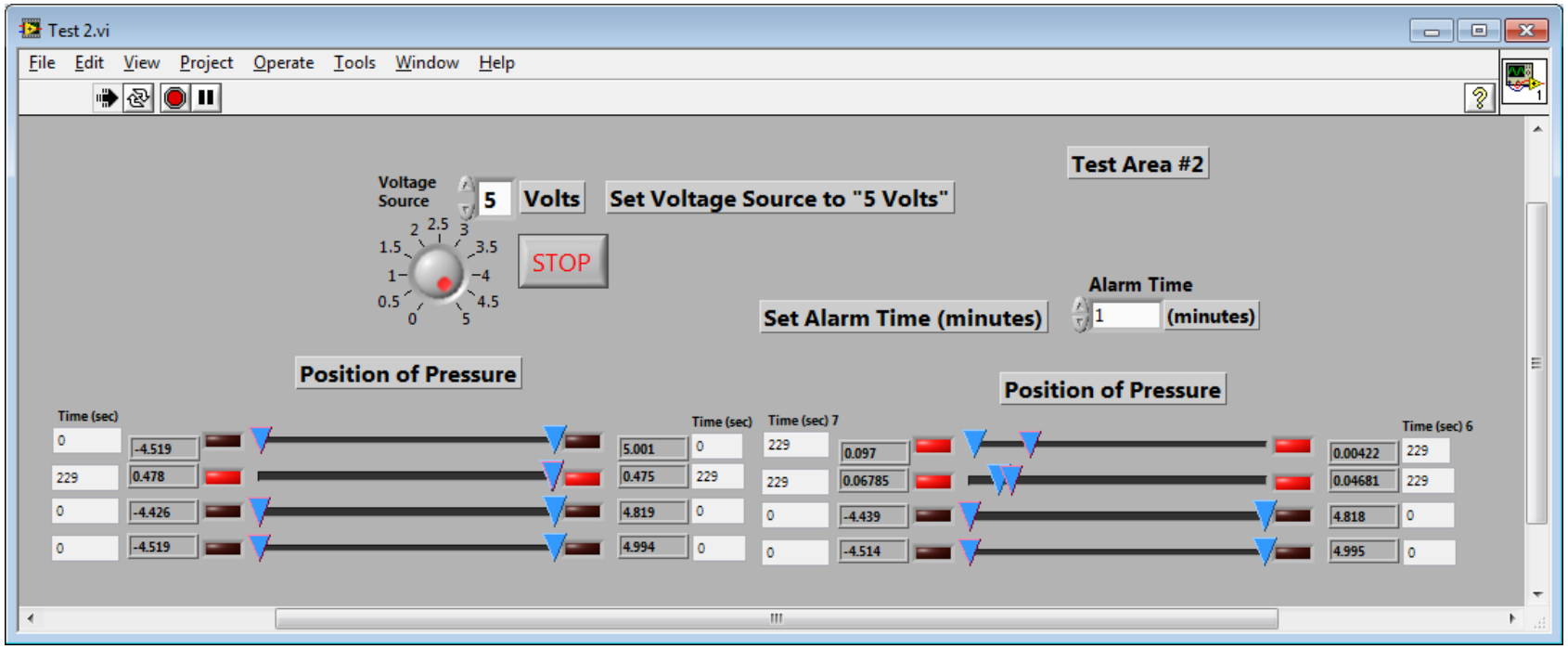

Figure 8.28: GUI, Test 2, Hard Surface, @ 229 Seconds with Alarm

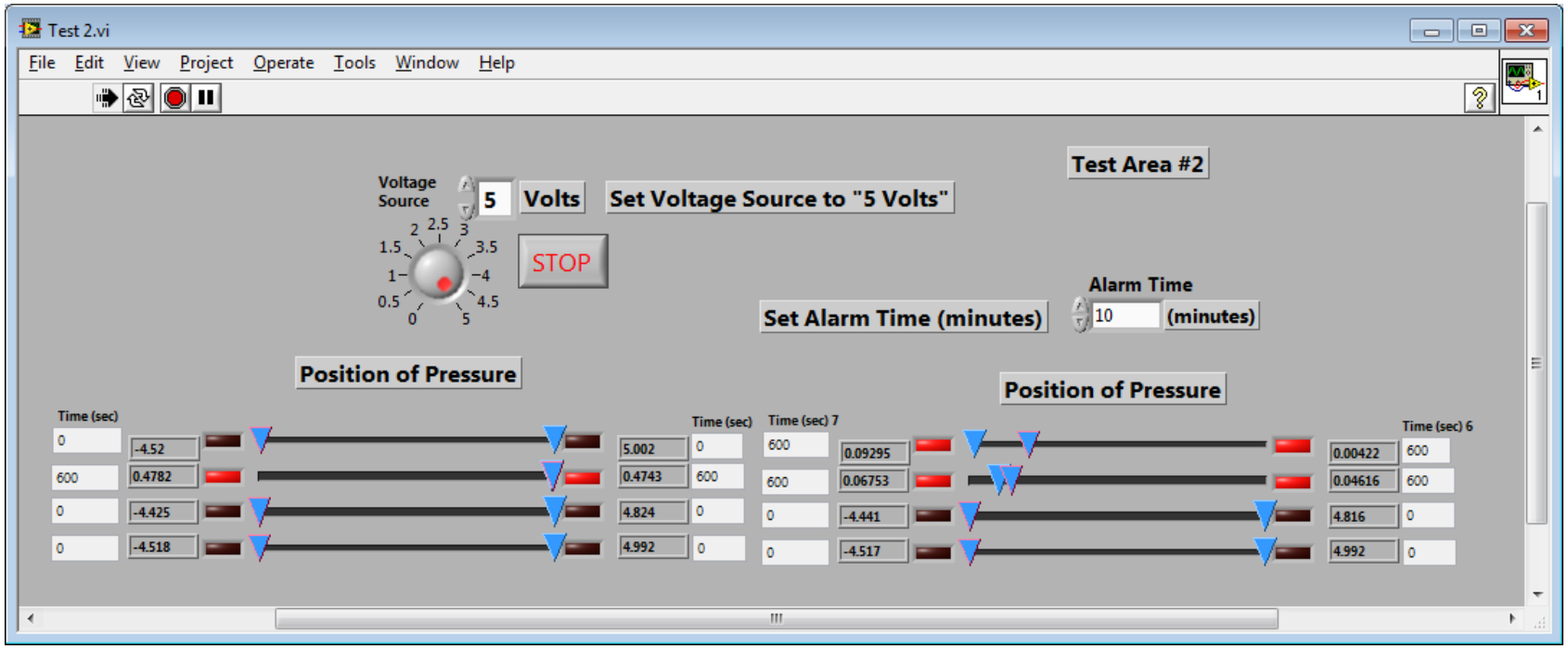

Figure 8.29: GUI, Test 2, Hard Surface, @ 600 Seconds with Alarm

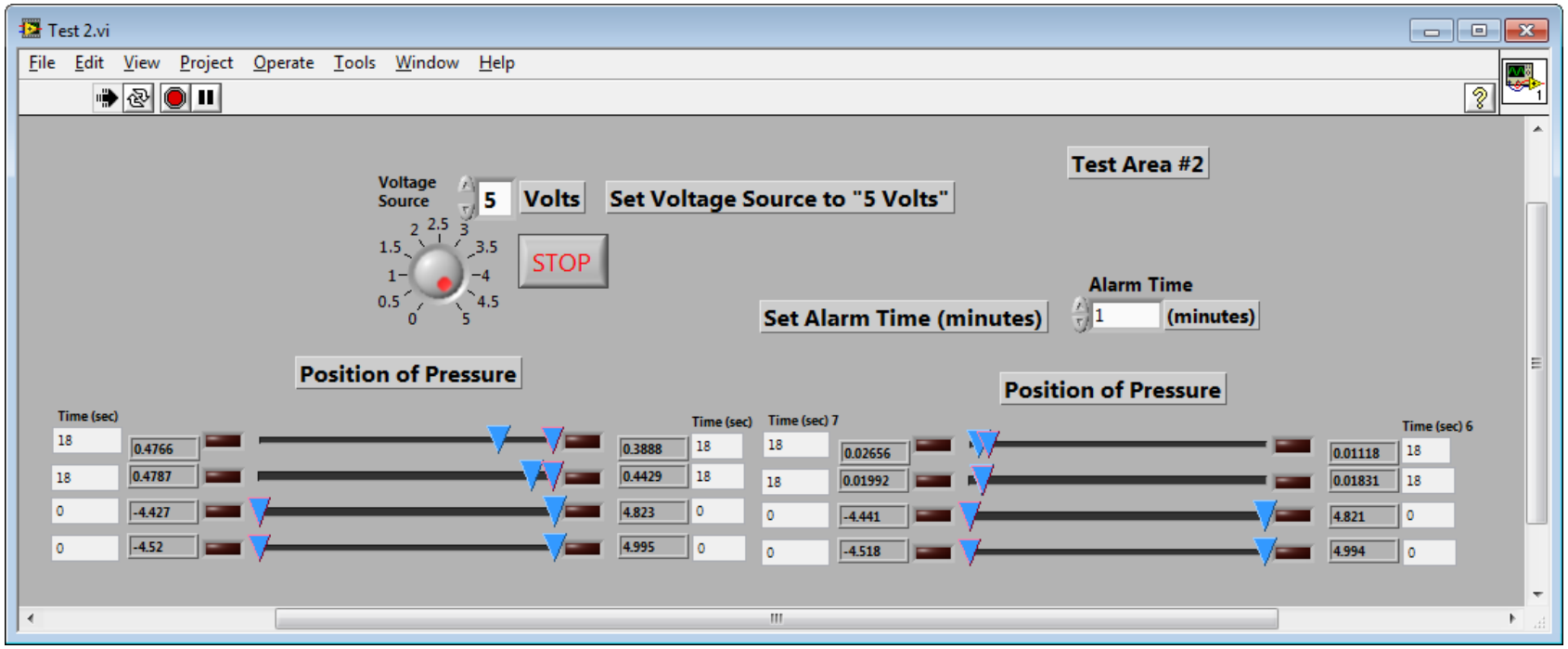

Figure 8.30: GUI, Test 2, Cushioned Surface, @ 18 Seconds

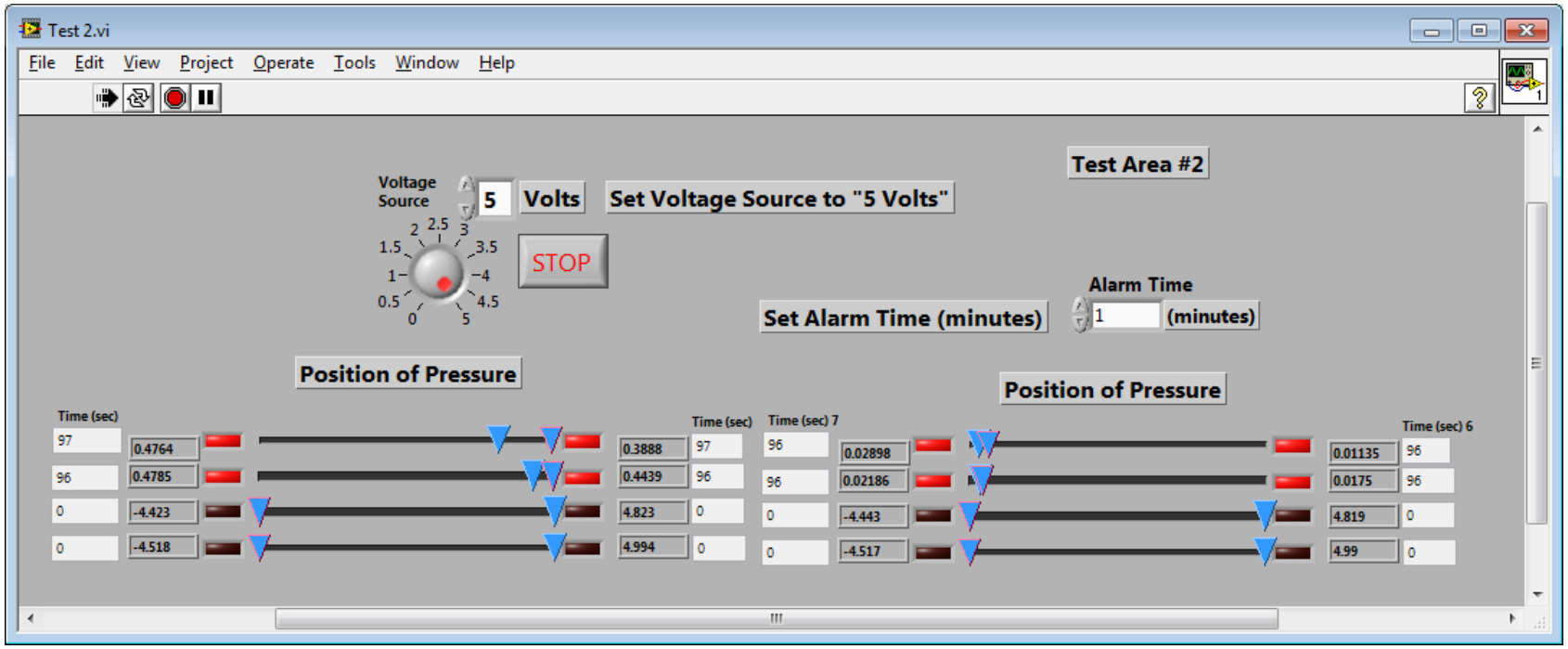

Figure 8.31: GUI, Test 2, Cushioned Surface, @ 96 Seconds with Alarm

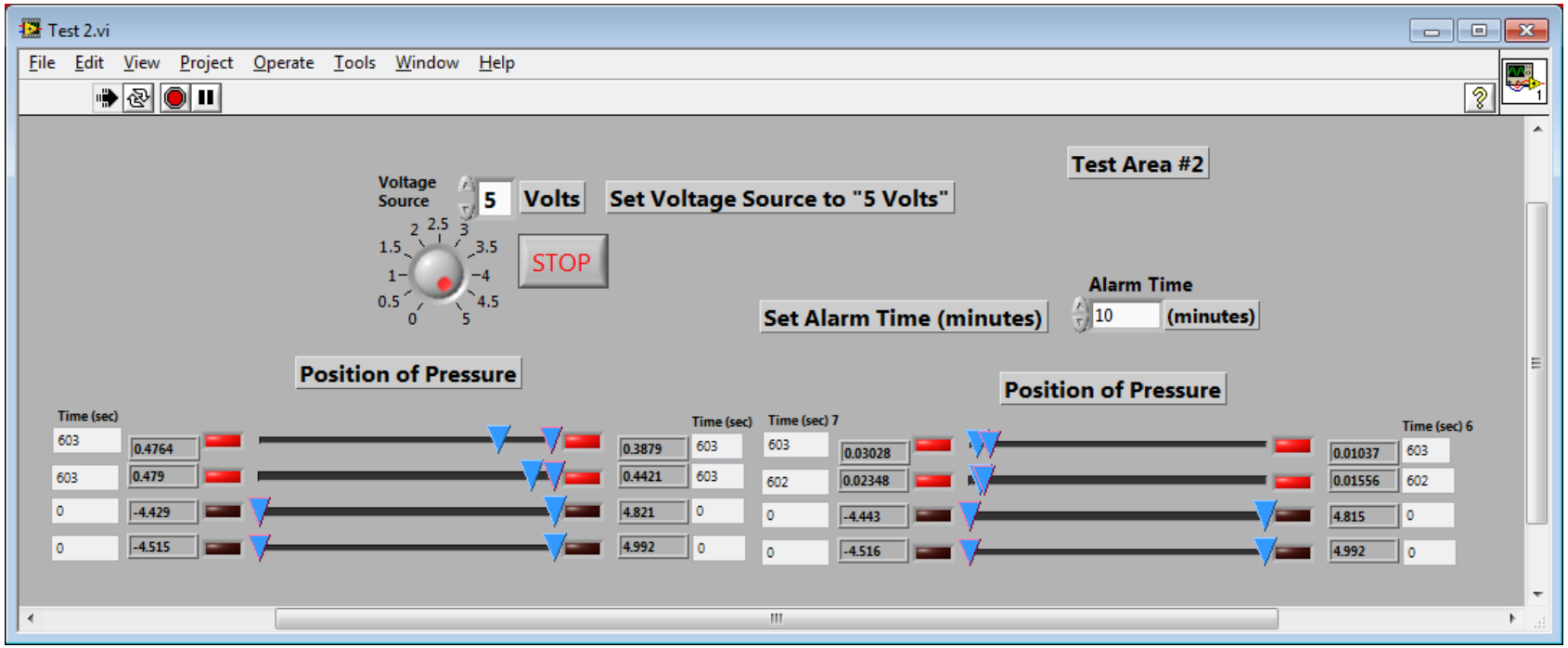

Figure 8.32: GUI, Test 2, Cushioned Surface, @ 603 Seconds with Alarm

I Test 3 Screen Views

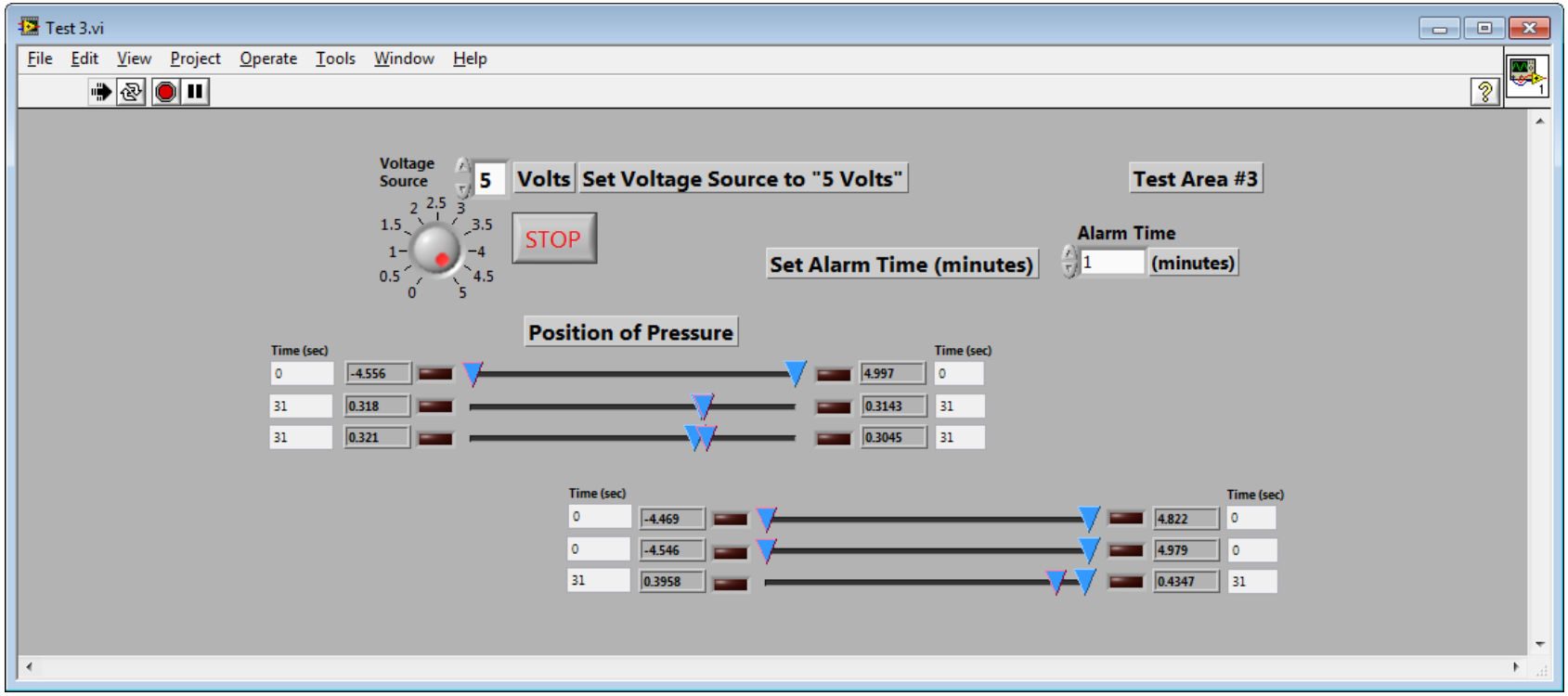

Figure 8.33: GUI, Test 3, Hard Surface, @ 31 Seconds

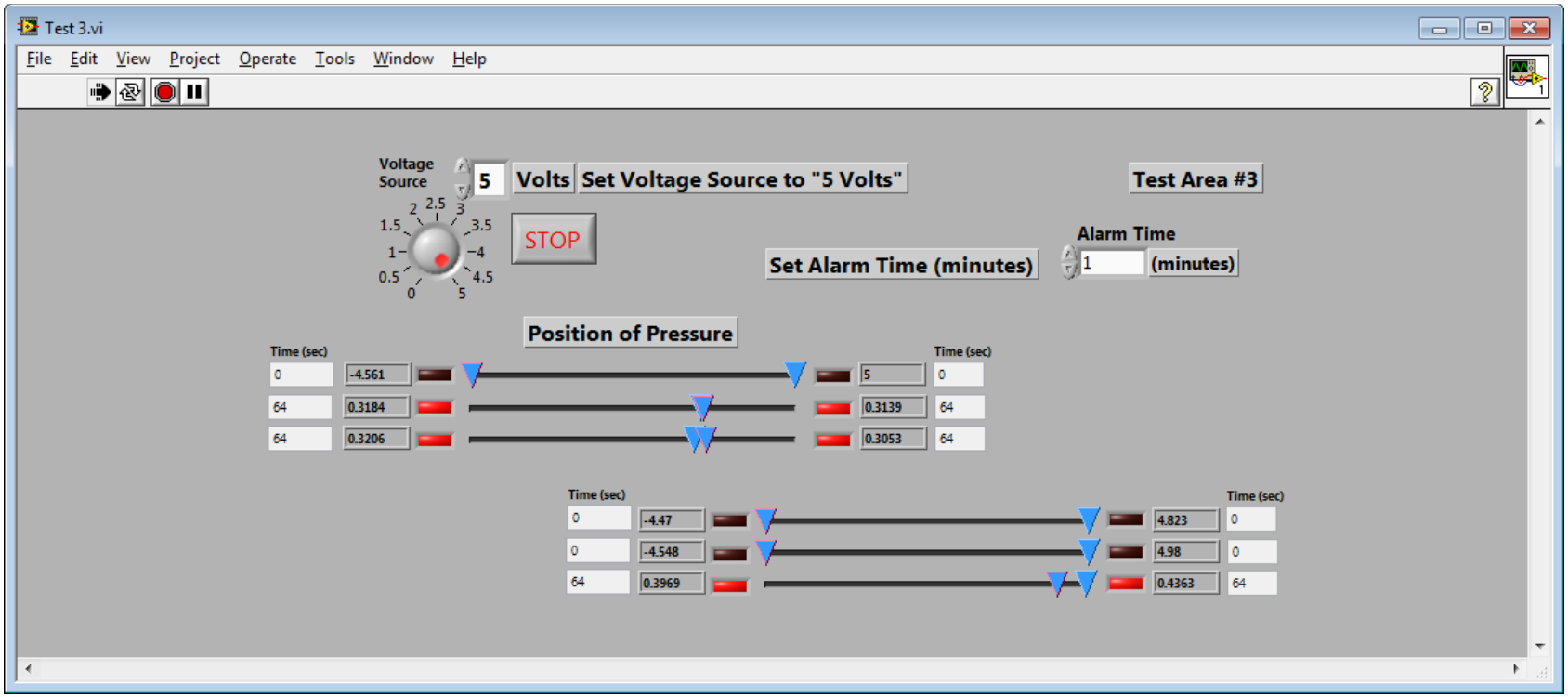

Figure 8.34: GUI, Test 3, Hard Surface, @ 64 Seconds with Alarm

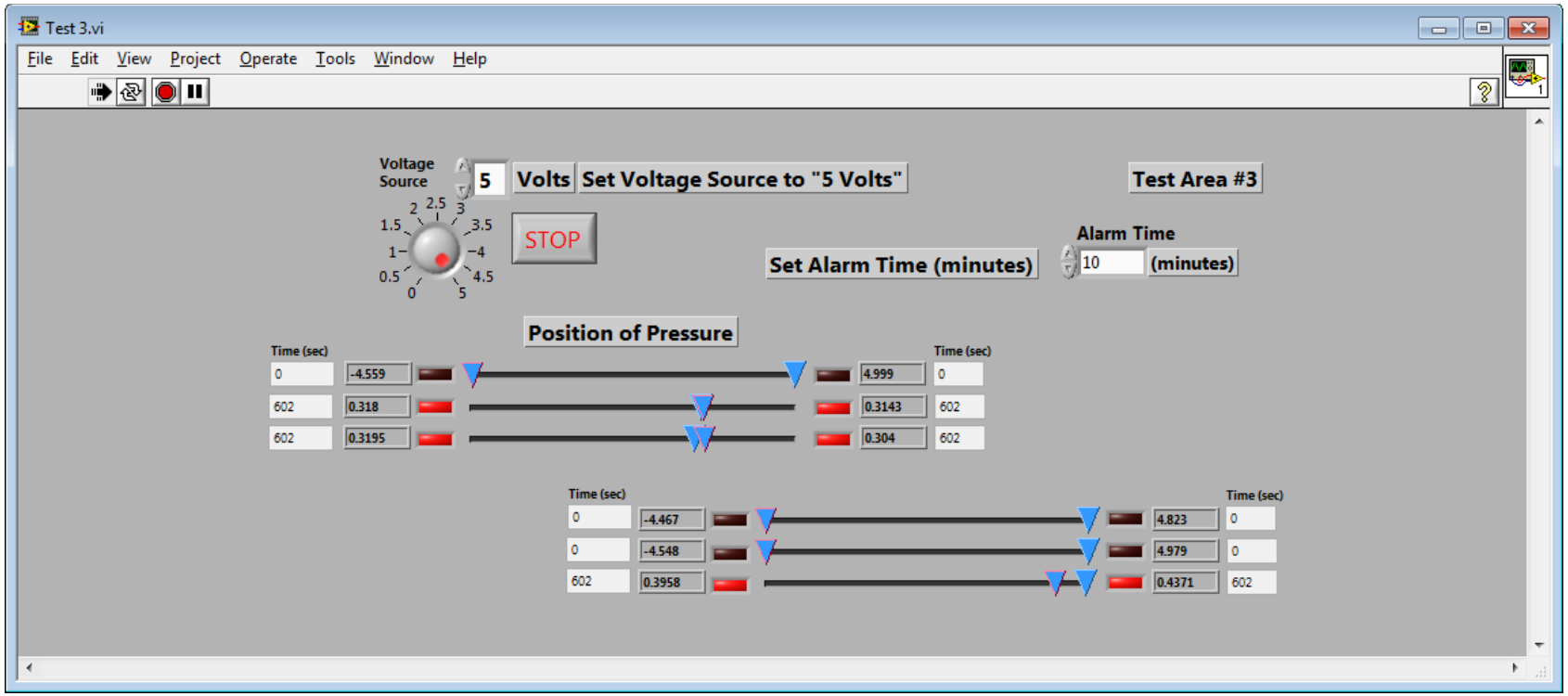

Figure 8.35: GUI, Test 3, Hard Surface, @ 602 Seconds with Alarm

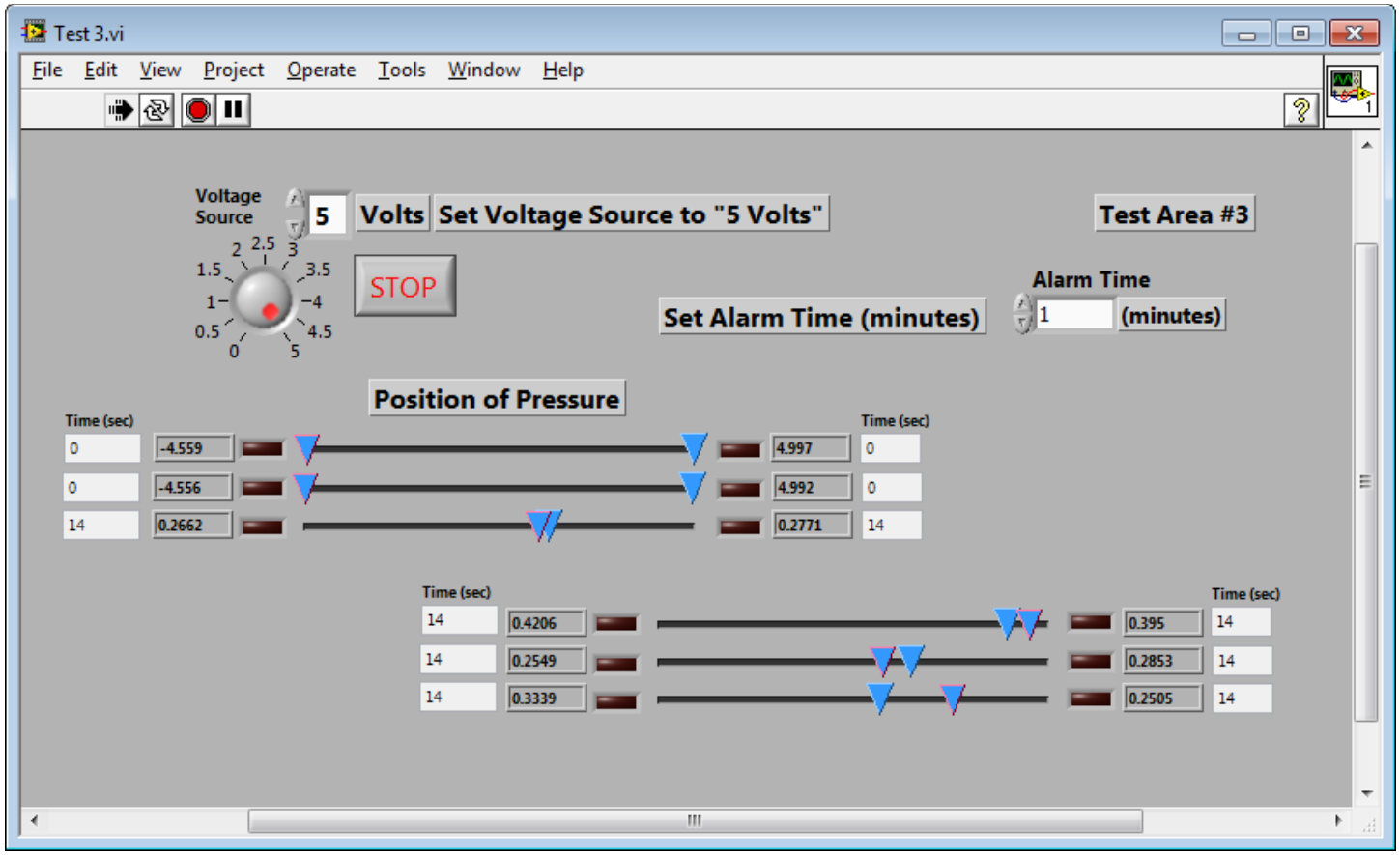

Figure 8.36: GUI, Test 3, Cushioned Surface, @ 14 Seconds

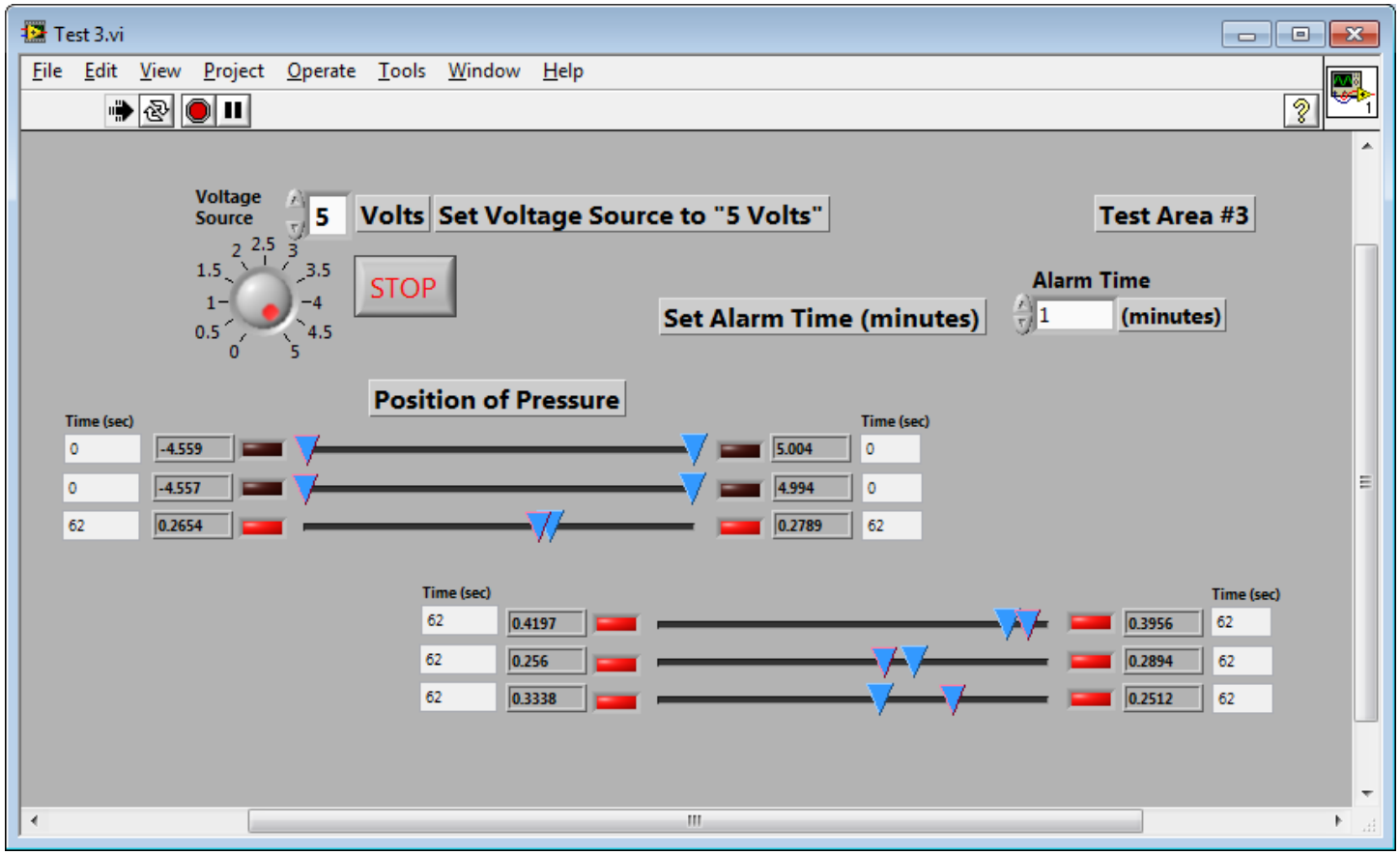

Figure 8.37: GUI, Test 3, Cushioned Surface, @ 62 Seconds with Alarm

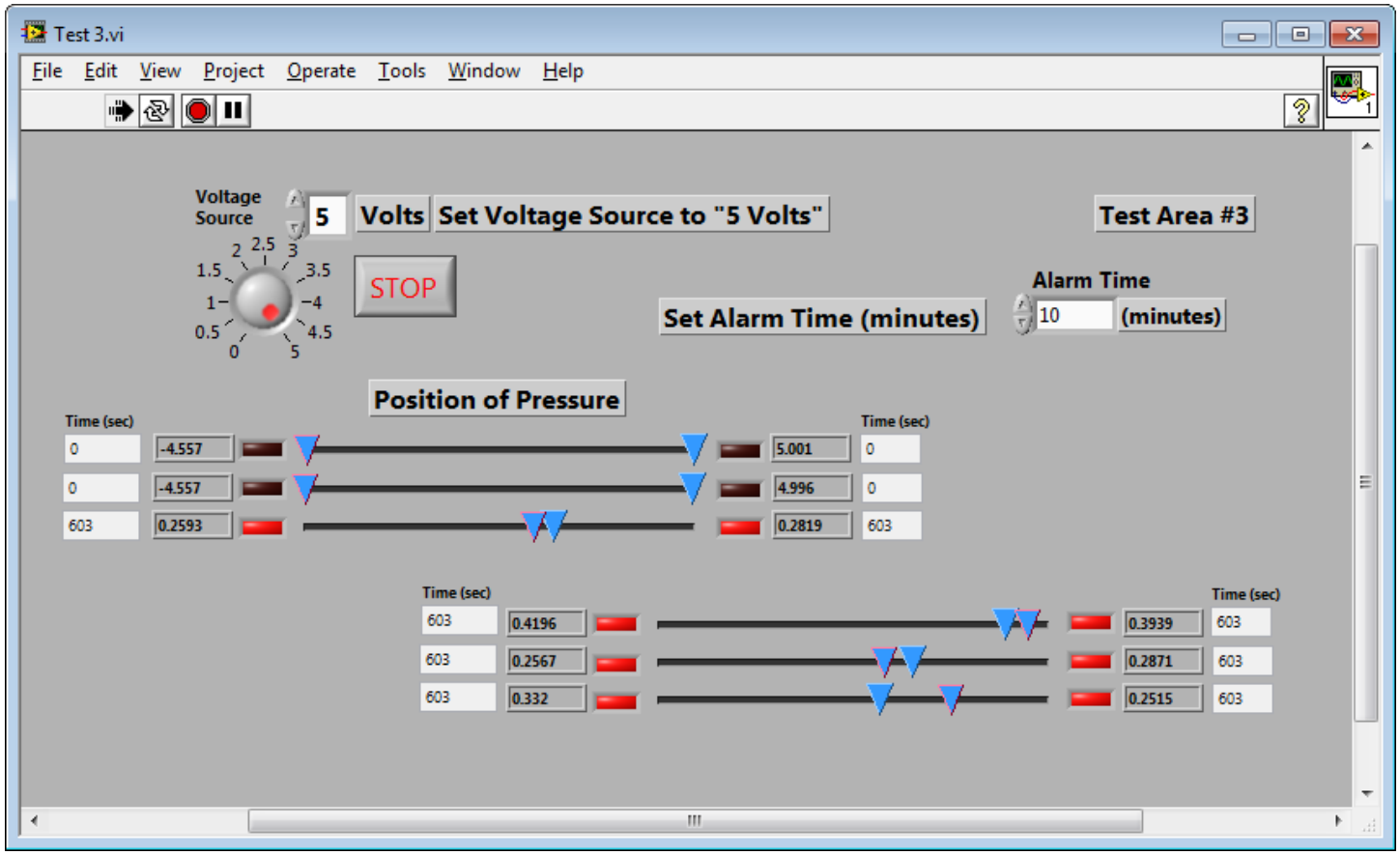

Figure 8.38: GUI, Test 3, Cushioned Surface, @ 603 Seconds with Alarm

J Test 4 Screen Views

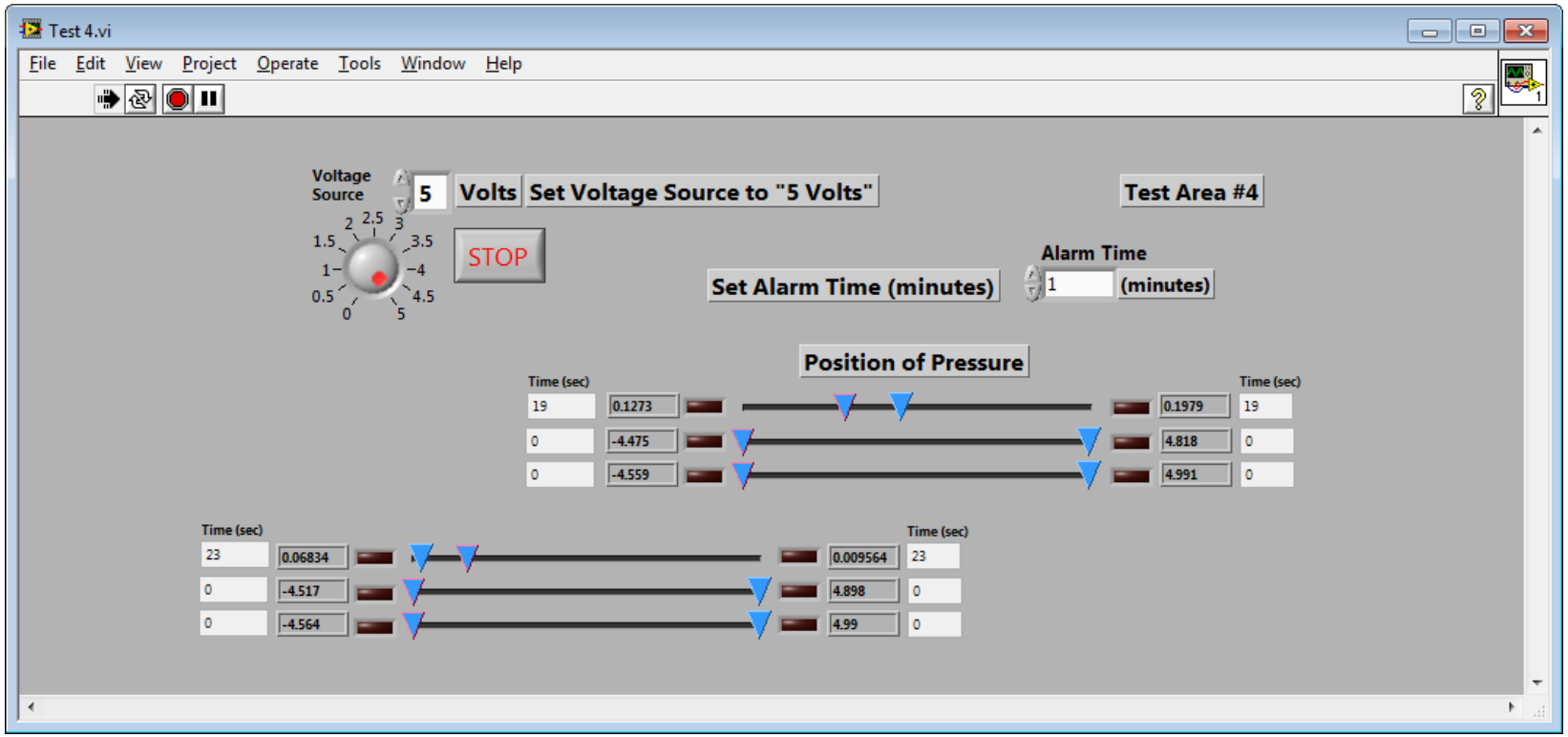

Figure 8.39: GUI, Test 4, Hard Surface, @ 23 Seconds

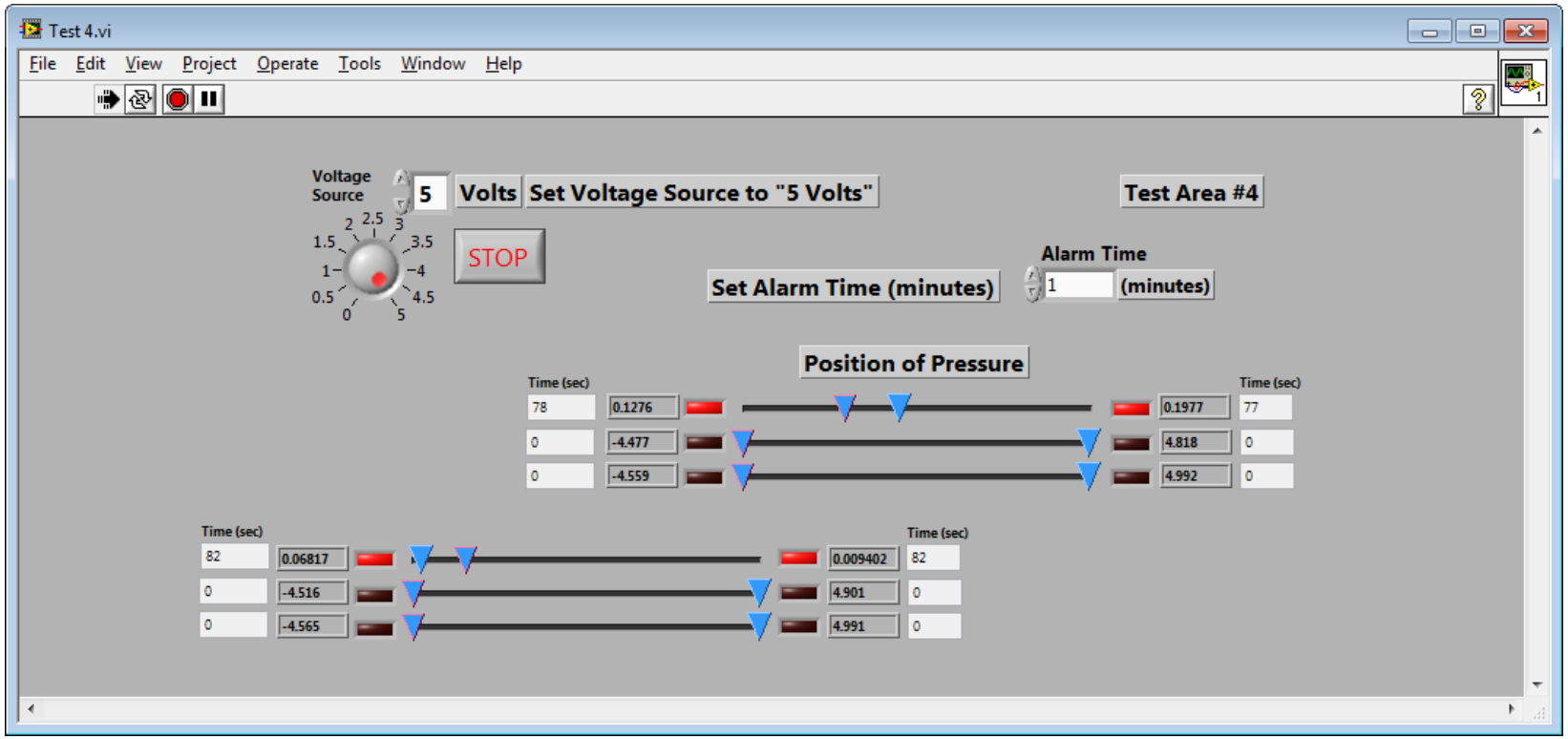

Figure 8.40: GUI, Test 4, Hard Surface, @ 82 Seconds with Alarm

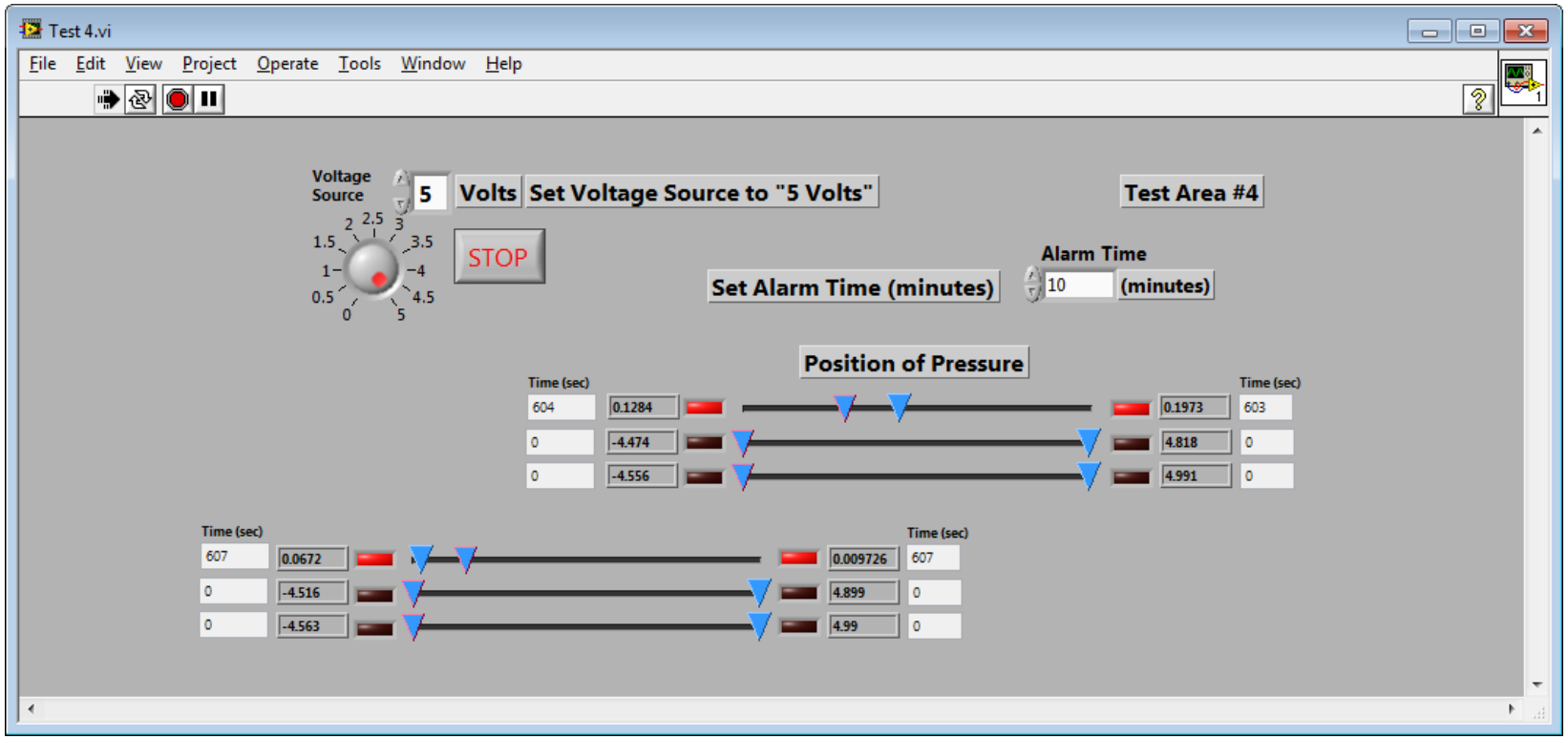

Figure 8.41: GUI, Test 4, Hard Surface, @ 607 Seconds with Alarm

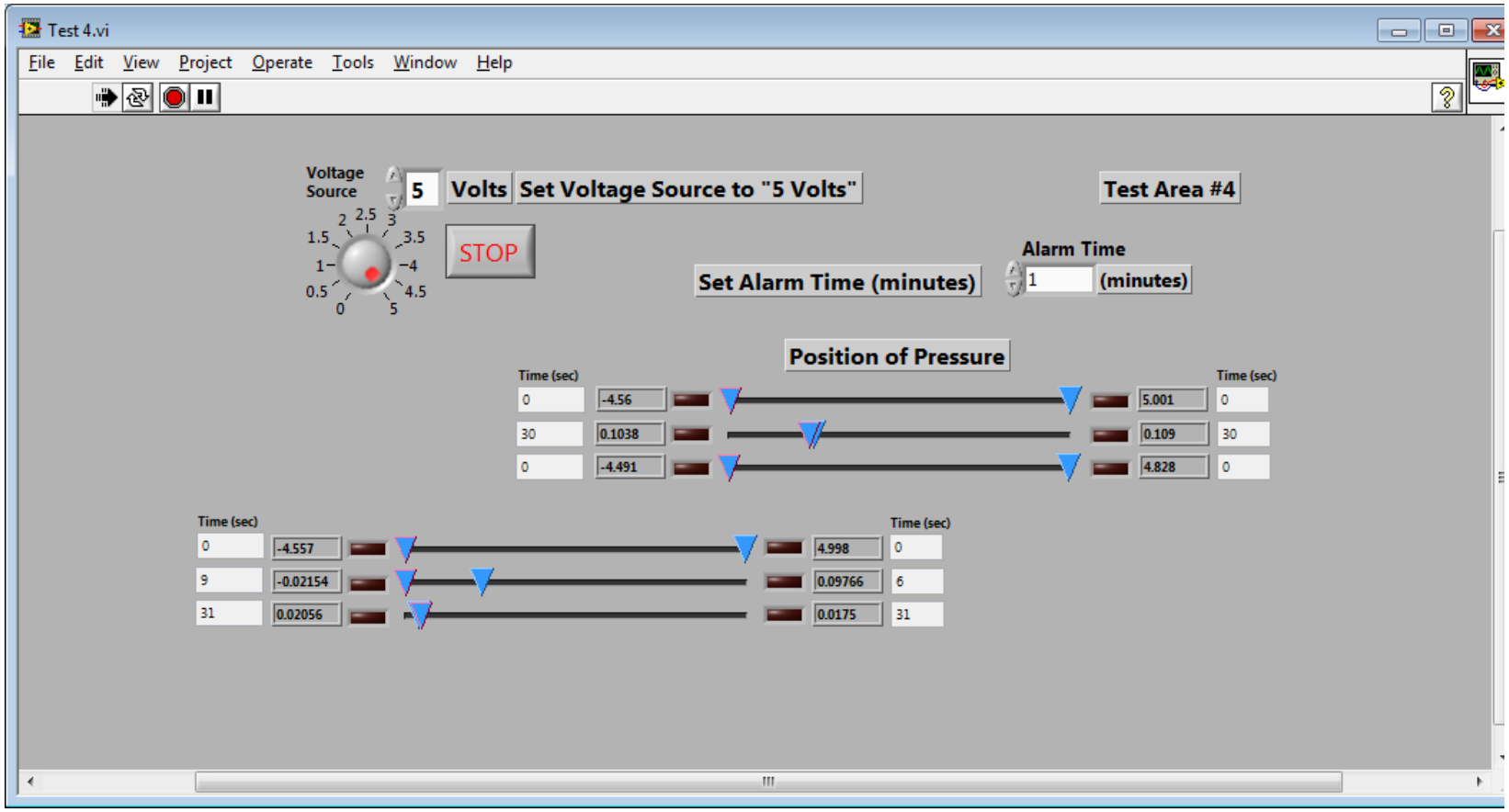

Figure 8.42: GUI, Test 4, Cushioned Surface, @ 31 Seconds

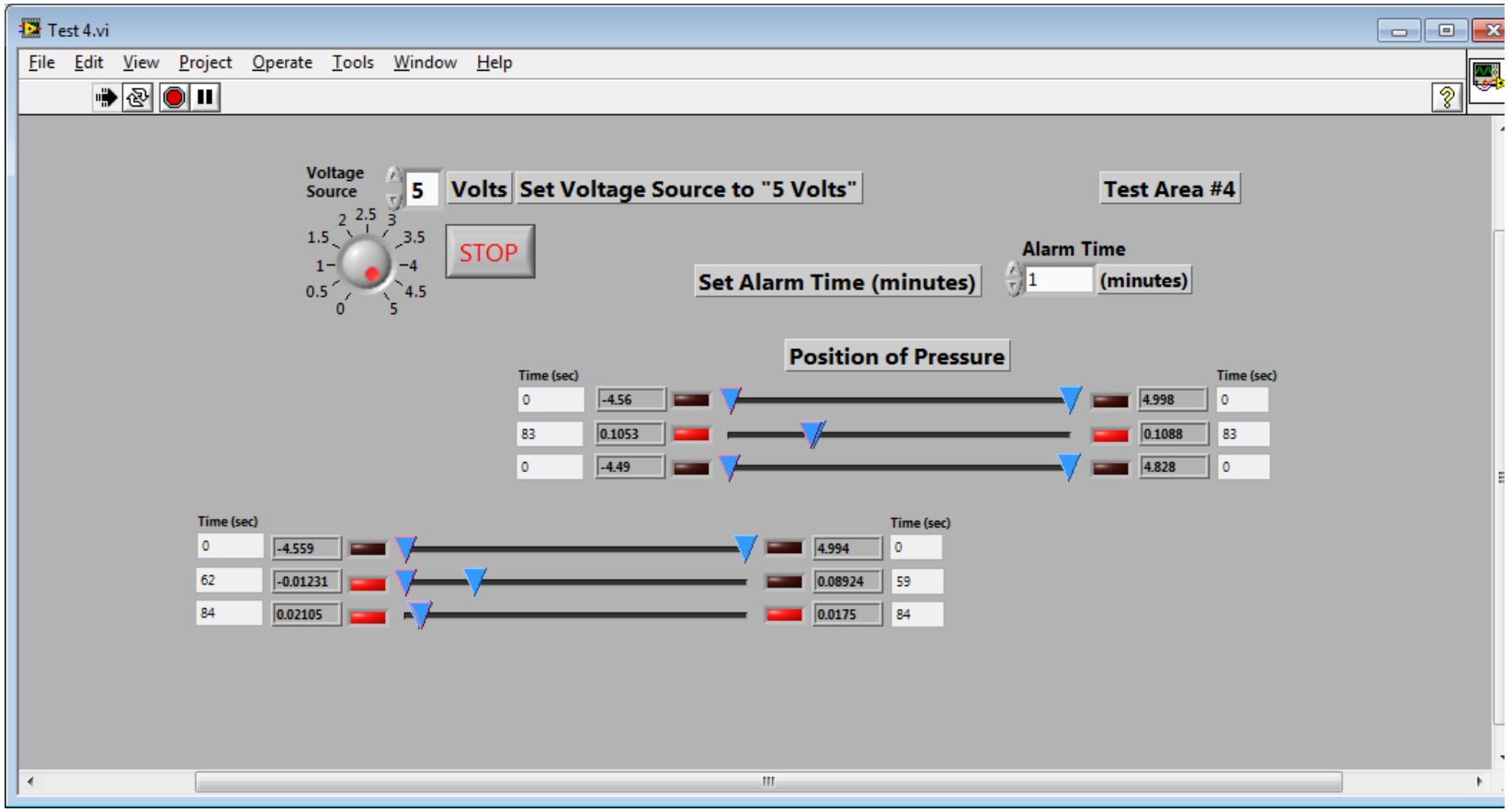

Figure 8.43: GUI, Test 4, Cushioned Surface, @ 84 Seconds with Alarm, with Sensor 22-Right Reset

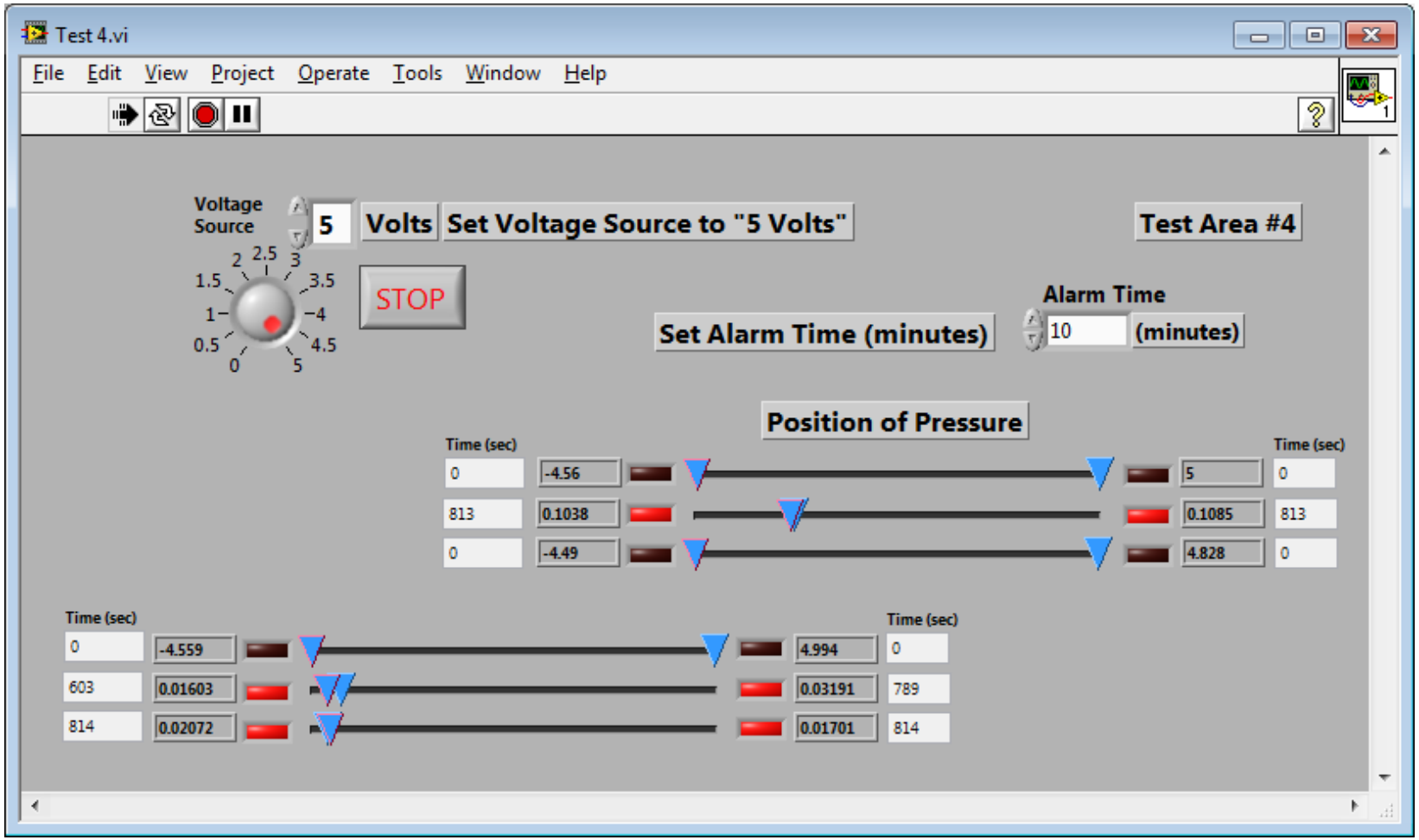

Figure 8.44: GUI, Test 4, Cushioned Surface, @ 814 Seconds with Alarm

K Test 5 Screen Views

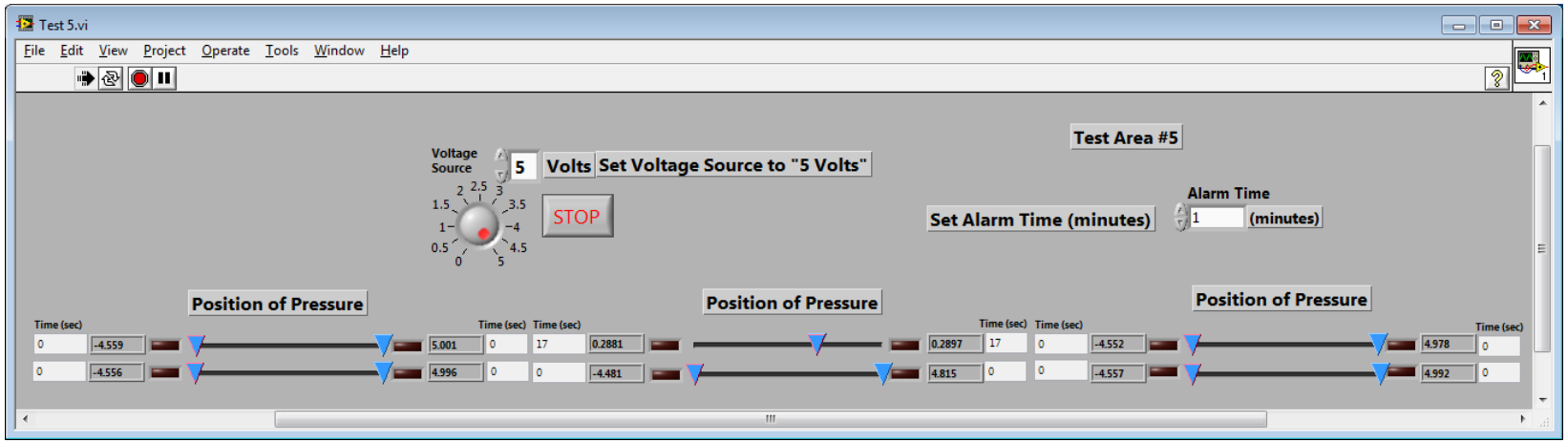

Figure 8.45: GUI, Test 5, Cushioned Surface, @ 17 Seconds

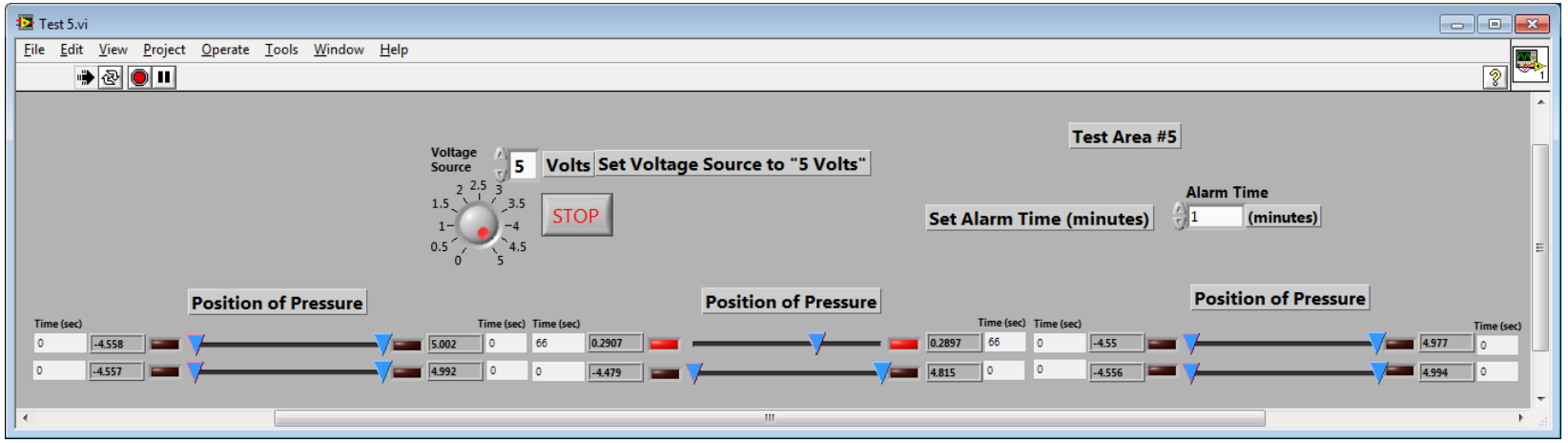

Figure 8.46: GUI, Test 5, Cushioned Surface, @ 66 Seconds with Alarm

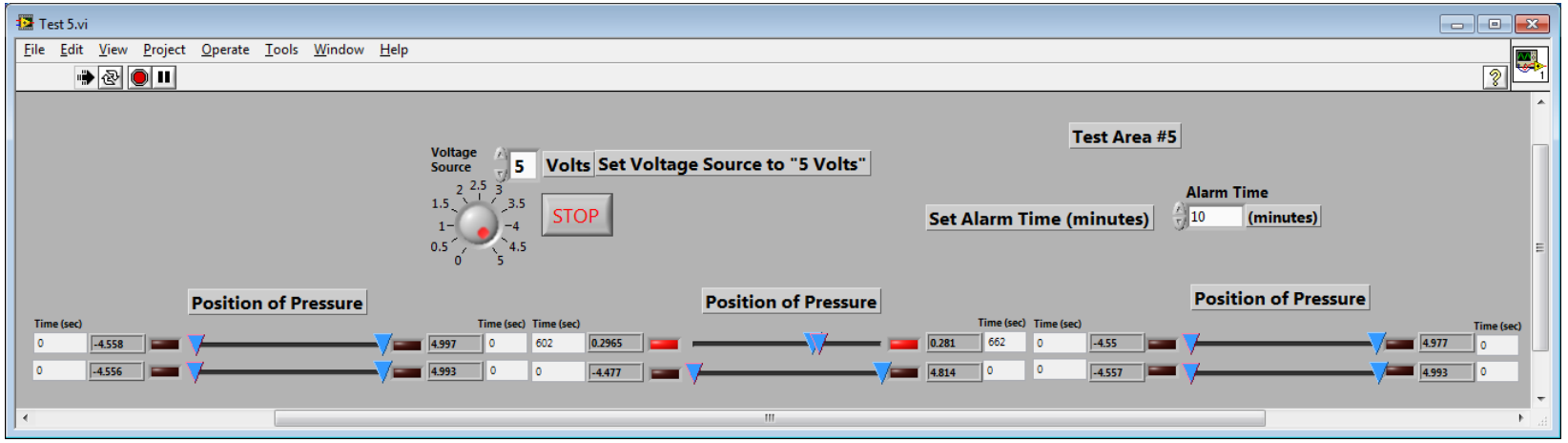

Figure 8.47: GUI, Test 5, Cushioned Surface, @ 662 Seconds with Alarm

L Test 6 Screen Views

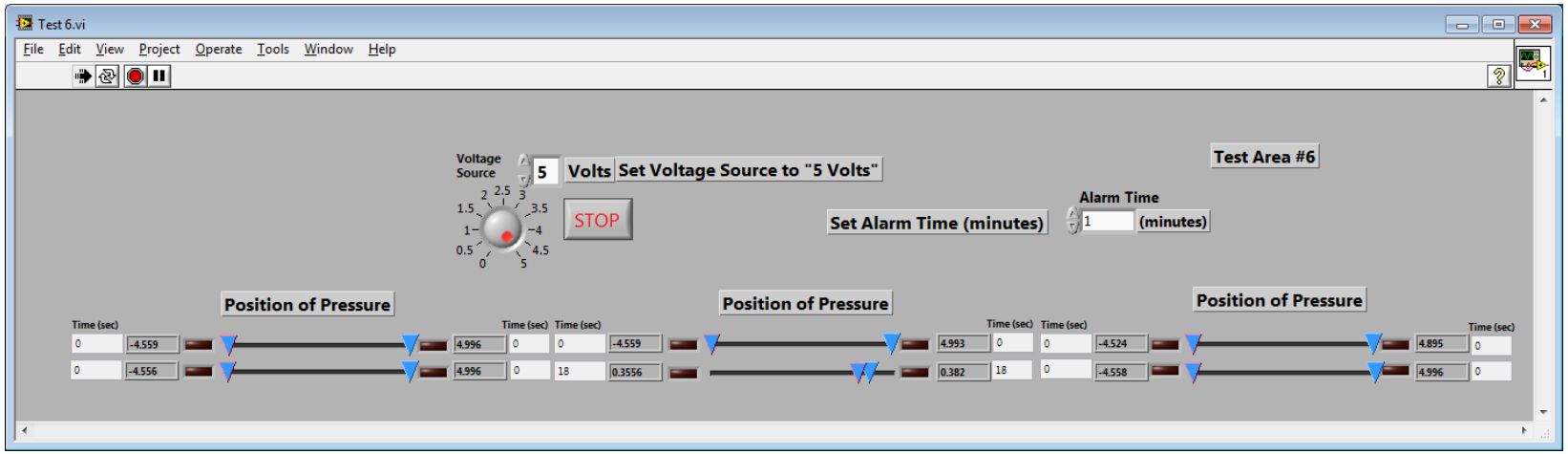

Figure 8.48: GUI, Test 6, Cushioned Surface, @ 18 Seconds

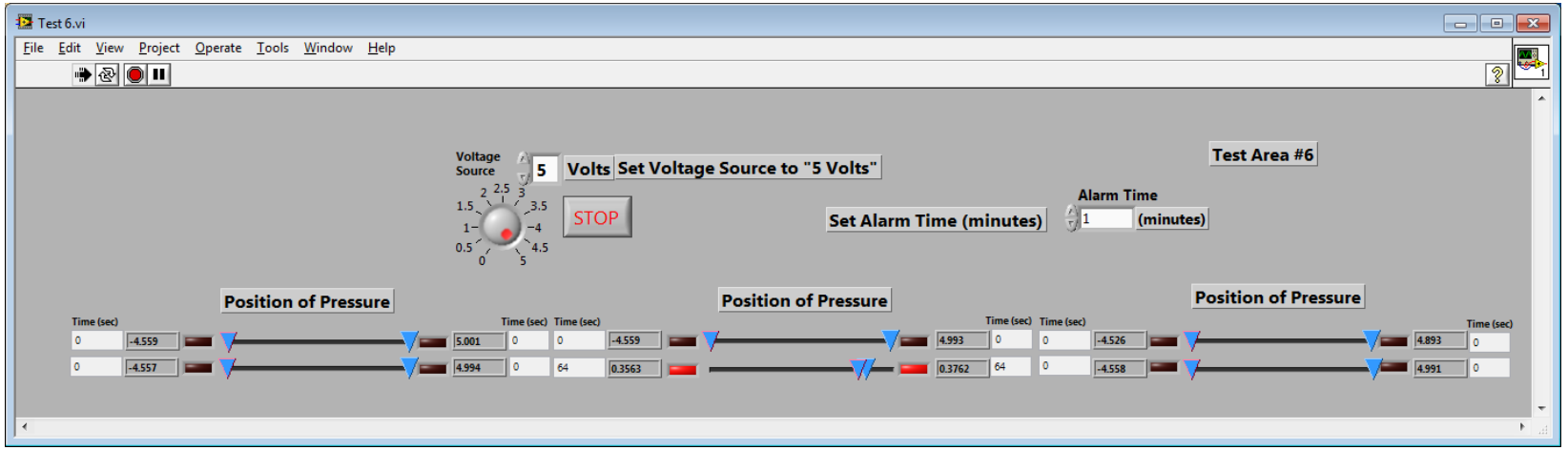

Figure 8.49: GUI, Test 6, Cushioned Surface, @ 64 Seconds with Alarm

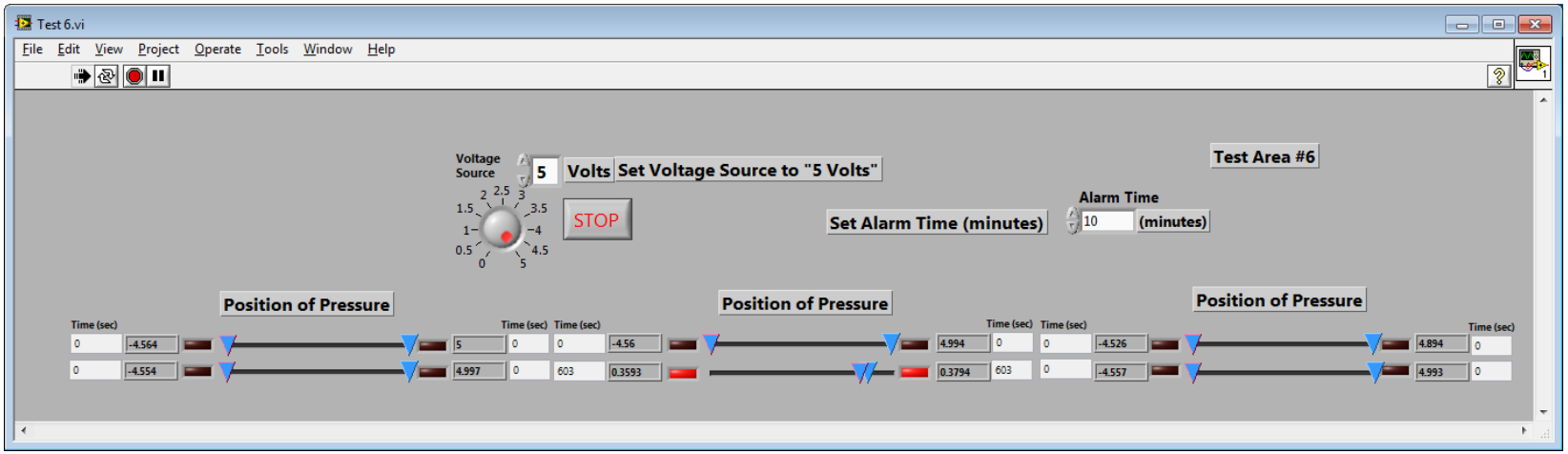

Figure 8.50: GUI, Test 6, Cushioned Surface, @ 603 Seconds with Alarm